AD NUMBER
AD333238
CLASSIFICATION CHANGES
TO: unclassified
FROM: confidential
LIMITATION CHANGES
TO: Approved for public release, distribution unlimited
FROM: Distribution authorized to U.S. Gov't. agencies and their contractors; Administrative/Operational Use; AUG 1962. Other requests shall be referred to Naval Ordnance Laboratory, White Oak, MD.
AUTHORITY
USNOL ltr, 29 Aug 1974; USNOL ltr, 29 Aug 1974

~~CONFIDENTIAL~~

NOLTR 62-25

TRANSITION, MINIMUM CRITICAL, MINIMUM TRANSITION, AND ROUGHNESS REYNOLDS NUMBERS, FOR SEVEN BLUNT BODIES OF REVOLUTION IN FLIGHT BETWEEN MACH NUMBERS OF 1.72 AND 15.1 (U)

RELEASED TO ASTIA
BY THE NAVAL ORDNANCE LABORATORY

- ☐ Without restrictions
- ☐ For Release to Military and Government Agencies Only.
- ☒ Approval by BuWeps required for release to contractors.
- ☐ Approval by BuWeps required for all subsequent release.

16 August 1962

NOL

UNITED STATES NAVAL ORDNANCE LABORATORY, WHITE OAK, MARYLAND

NOLTR 62-25

NOTICE: This material contains information affecting the national defense of the United States within the meaning of the Espionage Laws, Title 18, U.S.C. Sections 793 and 794, the transmission or revelation of which in any manner to an unauthorized person is prohibited by law.

DOWNGRADED AT 3 YEAR INTERVALS;
DECLASSIFIED AFTER 12 YEARS.
DOD DIR 5200.10

~~CONFIDENTIAL~~

Aerodynamics Research Report No. 173

TRANSITION, MINIMUM CRITICAL, MINIMUM TRANSITION, AND ROUGHNESS REYNOLDS NUMBERS, FOR SEVEN BLUNT BODIES OF REVOLUTION IN FLIGHT BETWEEN MACH NUMBERS OF 1.72 AND 15.1

by

Neal Tetervin

ABSTRACT: In the present investigation results of the stability theory for laminar flow were compared with transition locations determined from heat-transfer distributions obtained by previous investigators for seven blunt bodies of revolution in supersonic flight. The comparison shows that when transition occurred it took place even though the boundary layer was calculated to be very stable with respect to small disturbances for the entire region between the stagnation point and the transition location.

In every case transition occurred at a larger boundary-layer Reynolds number than the estimated minimum Reynolds number for transition. Consequently, no contradiction of the assumption that there is a minimum transition Reynolds number and no disagreement with the results of the method for estimating this Reynolds number is found.

Five of the seven cases considered contained useful transition data. A first examination of these five sets of data seems to indicate a connection between the boundary-layer Reynolds number at transition and the maximum roughness Reynolds number ahead of transition. A further examination, however, shows that the scatter of these data is too large to conclude statistically from only five sets of data that a connection really exists.

The boundary-layer transition Reynolds number was found to be influenced much more strongly by the maximum roughness Reynolds number ahead of the transition point than by the local wall temperature ratio at the transition point.

U. S. NAVAL ORDNANCE LABORATORY
WHITE OAK, MARYLAND

16 August 1962

NOLTR 62-25

Transition, Minimum Critical, Minimum Transition, and Roughness Reynolds Numbers, for Seven Blunt Bodies of Revolution in Flight Between Mach Numbers of 1.72 and 15.1

This report presents the results of an investigation of transition from laminar to turbulent boundary-layer flow on seven blunt bodies of revolution in flight in the Mach number range between 1.72 and 15.1. Mr. J. R. Katz programmed the required computations for the IBM 704 electronic computer.

This work was sponsored by the Re-Entry Body Section of the Special Projects Office, Bureau of Naval Weapons under the Applied Research Program in Aeroballistics, Task No. NOL-363.

R. E. ODENING
Captain, USN
Commander

K. R. ENKENHUS
By direction

CONTENTS

ILLUSTRATIONS

TABLES

SYMBOLS

$\bar{a}$	speed of sound
A	constant - equation (17)
b	constant - equation (53)
B	constant - equation (17)
$\bar{C}$	constant in Sutherland's formula for the viscosity
C_f	skin-friction coefficient, $C_f = \bar{\tau}_w/\rho_w \bar{u}_e^2$
C_p	pressure coefficient, $(\bar{p}_e/\bar{p}_o - \bar{p}_\infty/\bar{p}_o)$
$\bar{c}_p$	specific heat at constant pressure
d	constant in equation (54)
$\bar{h}$	enthalpy
H	ratio, (δ^*/θ)
$\bar{J}$	mechanical equivalent of heat, 778 ft-lbs per BTU
$\bar{k}$	height of roughness
k	$\bar{k}/\bar{L}$
$\bar{k}_s$	equivalent sand roughness height
K	$(3\gamma_E-1)/2(\gamma_E-1)$
l	dimensionless wall shear parameter, $(\bar{\theta}/\bar{u}_e)(\bar{t}_w/\bar{t}_e)(\partial\bar{u}/\partial\bar{y})_w$
$\bar{L}$	reference length
m	$(3-\gamma_E)/2(\gamma_E-1)$
M	Mach number
n	dimensionless correlation number, $-(\bar{\theta}^2/\bar{\nu}_w)(d\bar{u}_e/d\bar{x})(\bar{t}_w/\bar{t}_e)^2(\bar{t}_o/\bar{t}_e)$
N	momentum parameter, $2\left[n(H_{tr}+2)+l\right]$

Nu	Nusselt number (see eq. (39))
$\bar{p}$	static pressure
$p'(\bar{t}_o/\bar{t}_e)$	$-(1/M_e)dM_e/dx$
Pr	Prandtl number
q	heat transfer by conduction to surface per unit area per unit time $(\bar{\kappa}\ \partial\bar{t}/\partial\bar{y})_w$
r	recovery factor
$\bar{R}$	radius of cross section of body of revolution
R	$\bar{R}/\bar{L}$
Re_L	reference Reynolds number, $\bar{u}_M\bar{L}/\bar{\nu}_o$
Re_k	roughness Reynolds number, $\bar{u}_k\bar{k}/\bar{\nu}_k$
Re_θ	momentum thickness Reynolds number, $\bar{u}_e\bar{\theta}/\bar{\nu}_e$
$Re_{\theta,c}$	minimum critical Reynolds number of stability theory, based on momentum thickness
$Re_{\theta,m}$	minimum transition Reynolds number, based on momentum thickness
Re_x	Reynolds number, $\bar{u}_e\bar{x}/\bar{\nu}_e$
Re_w	Reynolds number, $\bar{u}_e\bar{x}/\bar{\nu}_w$
Re_∞	Reynolds number, $\bar{u}_\infty\bar{L}/\bar{\nu}_\infty$
St	Stanton number (see eqs. (43) and (46))
S_w	surface temperature ratio parameter, $(\bar{t}_w/\bar{t}_o - 1)$
$\bar{t}$	temperature
$\bar{u}$	velocity parallel to surface
$\bar{u}_M$	$\sqrt{2\bar{h}_o J}$
u	$\bar{u}/\bar{u}_M$
$\bar{x}$	distance along surface, measured from origin of boundary layer

x	$\bar{x}/\bar{L}$
$\bar{y}$	distance measured perpendicular from surface
α	exponent of Prandtl number in Reynolds analogy parameter (see eq. (40))
β	non-dimensional pressure gradient parameter
γ	ratio of specific heat at constant pressure to specific heat at constant volume
$\bar{\delta}$	full boundary-layer thickness
$\bar{\delta}*$	boundary-layer displacement thickness, $\int_0^\infty (1-\bar{\rho}\bar{u}/\bar{\rho}_e\bar{u}_e)d\bar{y}$
θ	boundary-layer momentum thickness, $\int_0^\infty \bar{\rho}\bar{u}/\bar{\rho}_e\bar{u}_e(1-\bar{u}/\bar{u}_e)d\bar{y}$
κ	thermal conductivity
λ	$\left(\bar{t}_o+\bar{C}/\bar{t}_w+\bar{C}\right)\sqrt{\bar{t}_w/\bar{t}_o}$
$\bar{\mu}$	dynamic viscosity
$\bar{\nu}$	kinematic viscosity
$\bar{\rho}$	mass density
$\bar{\tau}$	shear stress, $\bar{\mu}\left(\partial\bar{u}/\partial\bar{y}\right)$
ϕ	$\left[(\theta\sqrt{Re_L})^2/\lambda\right]\sqrt{(\gamma_E-1)/2}$

Subscripts

a	measured along axis of symmetry
e	local value at outer edge of boundary layer
E	effective value
f	value for $d\bar{p}/d\bar{x} = 0$
k	at distance $\bar{k}$ from surface

I	at standard sea level atmosphere
M	maximum value
o	at stagnation point
r	for zero heat transfer
T	at transition point
tr	associated transformed quantity
w	value at surface
∞	free-stream conditions, ahead of bow shock wave
$\overline{}$	all quantities with a "bar" are dimensional, all others are non-dimensional

INTRODUCTION

It is well known that the heat-transfer rate for a turbulent boundary layer is larger than for a laminar one and that the difference widens with increase in boundary layer Reynolds number. This difference in heat-transfer rate is often important enough to justify the effort to provide an extremely smooth surface in order to increase the probability of extensive regions of laminar flow. When all other factors are fixed, the extent of laminar flow usually increases with decrease in surface roughness if the extent is less than that for a perfectly smooth surface. Even for a perfectly smooth surface, however, the position at which the flow changes from laminar to turbulent cannot at present be calculated theoretically. Two positions related to the transition position can, however, be estimated. One is the position ahead of which transition cannot occur when the boundary layer is exposed to very small disturbances of a particular type. This position can be calculated by use of the results of the stability theory (ref. (1)). The other and more forward position is the one ahead of which transition cannot occur when the boundary layer is highly disturbed. A rough estimate of this position can be made by the method of reference (2).

Because all information that can lead to a more accurate prediction of the transition point is valuable, those two theoretically determined positions are compared with transition positions determined from heat-transfer distributions obtained by previous investigators for seven bodies of revolution in flight at supersonic speeds. The effect of roughness on transition is also considered.

ANALYSIS

Derivation of Differential Equation for Φ

In order to estimate the location at which the boundary layer first becomes unstable, and the location ahead of which transition is supposedly impossible, it is first necessary to calculate a number of laminar boundary-layer parameters. A convenient method is Cohen and Reshotko's (ref. (3)). The method was developed for a gas which is both thermally and calorically perfect and which has a Prandtl number of unity and a viscosity that varies directly with the temperature. Although $\bar{c}_p$ and γ are consequently both constant, their numerical values are not specified in the Cohen and Reshotko method.

The form of the boundary-layer momentum equation used in the present analysis is obtained from the herein corrected form of equation (B5) of reference (3). The correct form allows λ to depend on x and is

$$\frac{n}{P'\left(\frac{\bar{t}_o}{\bar{t}_e}\right)} = \frac{M_e}{\lambda R^2}\left(\frac{\bar{t}_o}{\bar{t}_e}\right)^K \int_0^{\frac{\bar{x}}{\bar{L}}} \frac{N\lambda R^2}{M_e\left(\frac{\bar{t}_o}{\bar{t}_e}\right)^K}\, d\frac{\bar{x}}{\bar{L}} \tag{1}$$

The value of γ that appears in the exponent K is an effective value. Its determination is discussed in the section entitled, "Calculation Procedure." From equation (1) there is obtained the differential equation

$$\frac{d}{dx}\left[\frac{n}{P'\left(\frac{\bar{t}_o}{\bar{t}_e}\right)}\right] = N + \frac{\left[\frac{n}{P'\left(\frac{\bar{t}_o}{\bar{t}_e}\right)}\right]}{\left[\frac{M_e\left(\frac{\bar{t}_o}{\bar{t}_e}\right)^K}{\lambda R^2}\right]}\ \frac{d}{dx}\left[\frac{M_e\left(\frac{\bar{t}_o}{\bar{t}_e}\right)^K}{\lambda R^2}\right] \tag{2}$$

All quantities in equation (2) are non-dimensional. From the definition (see eq. (34) of ref. (3)),

$$P' = -\frac{\bar{L}}{\bar{u}_e}\frac{d\bar{u}_e}{d\bar{x}} = -\frac{1}{u_e}\frac{du_e}{dx}$$

and the relations

$$u_e^2 = \frac{\frac{\gamma_E - 1}{2}M_e^2}{1 + \frac{\gamma_E - 1}{2}M_e^2} \tag{3}$$

and

$$\frac{\bar{t}_o}{\bar{t}_e} = 1 + \frac{\gamma_E - 1}{2}M_e^2 \tag{4}$$

it follows that

$$P'\left(\frac{\bar{t}_o}{\bar{t}_e}\right) = -\frac{1}{M_e}\frac{dM_e}{dx} \tag{5}$$

Moreover, the correlation number n, which is defined as,

$$n = -\frac{d\bar{u}_e}{d\bar{x}}\ \frac{\bar{\theta}^2}{\bar{\nu}_w}\left(\frac{\bar{t}_w}{\bar{t}_e}\right)^2\left(\frac{\bar{t}_o}{\bar{t}_e}\right) \qquad \text{(eq. (22), ref. (3))}$$

can be written as

$$n = -\frac{du_e}{dx} Re_L \theta^2 \frac{\bar{\nu}_o}{\bar{\nu}_w} \left(\frac{\bar{t}_w}{\bar{t}_e}\right)^2 \left(\frac{\bar{t}_o}{\bar{t}_e}\right) \tag{6}$$

The ratio $(\bar{\nu}_o/\bar{\nu}_w)$ can be placed in a more convenient form by noting that for a thermally perfect gas

$$\frac{\bar{\rho}_w}{\bar{\rho}_o} = \frac{\bar{p}_w}{\bar{p}_o} \frac{\bar{t}_o}{\bar{t}_w}$$

Because the static pressure in a boundary layer is independent of the distance normal to the surface, it follows that

$$\bar{p}_w = \bar{p}_e$$

The ratio $(\bar{\nu}_o/\bar{\nu}_w)$ can then be written as

$$\frac{\bar{\nu}_o}{\bar{\nu}_w} = \left(\frac{\bar{\mu}_o}{\bar{\mu}_w}\right)\left(\frac{\bar{p}_e}{\bar{p}_o}\right)\left(\frac{\bar{t}_o}{\bar{t}_w}\right) \tag{7}$$

From the assumption of isentropic flow at the outer edge of the boundary layer it follows that

$$\frac{\bar{p}_e}{\bar{p}_o} = \left[1 + \frac{\gamma_\epsilon - 1}{2} M_e^2\right]^{\frac{-\gamma_\epsilon}{\gamma_\epsilon - 1}} \tag{8}$$

The viscosity ratio $(\bar{\mu}_w/\bar{\mu}_o)$ is assumed to be given by the relation

$$\frac{\bar{\mu}_w}{\bar{\mu}_o} = \lambda\left(\frac{\bar{t}_w}{\bar{t}_o}\right) \tag{9}$$

(see eq. (4) of ref. (3))

where

$$\lambda = \left(\frac{\bar{t}_o + \bar{C}}{\bar{t}_w + \bar{C}}\right)\sqrt{\frac{\bar{t}_w}{\bar{t}_o}}$$

(see eq. (5) of ref. (3))

The viscosity at the wall is thus calculated by the Sutherland relation. By use of equations (8) and (9), equation (7) becomes

$$\frac{\overline{\nu_o}}{\overline{\nu_w}} = \frac{\left(\frac{\overline{t}_o}{\overline{t}_w}\right)^2}{\lambda\left[1+\frac{\gamma_E-1}{2}M_e^2\right]^{\frac{\gamma_E}{\gamma_E-1}}} \tag{10}$$

When the relation (10) is substituted into equation (6) and relation (4) is used, the result is

$$n = \frac{-\frac{du_e}{dx}\left(\theta\sqrt{Re_L}\right)^2}{\lambda\left[1+\frac{\gamma_E-1}{2}M_e^2\right]^{\frac{3-2\gamma_E}{\gamma_E-1}}}$$

which can also be written as

$$n = \frac{-\frac{dM_e}{dx}\sqrt{\frac{\gamma_E-1}{2}}\left(\theta\sqrt{Re_L}\right)^2}{\lambda\left[1+\frac{\gamma_E-1}{2}M_e^2\right]^{\frac{3-\gamma_E}{2(\gamma_E-1)}}} \tag{11}$$

when equation (3) is used.

By use of equations (5) and (11) the quantity $n/P'(\overline{t}_o/\overline{t}_e)$ that occurs in equation (1) can now be written as

$$\frac{n}{P'\left(\frac{\overline{t}_o}{\overline{t}_e}\right)} = \frac{\left(\theta\sqrt{Re_L}\right)^2\sqrt{\frac{\gamma_E-1}{2}}\,M_e}{\lambda\left[1+\frac{\gamma_E-1}{2}M_e^2\right]^m} \tag{12}$$

where

$$m = \frac{3-\gamma_E}{2(\gamma_E-1)}$$

Now introduce a quantity ϕ related to the non-dimensional momentum thickness, $\theta\sqrt{Re_L}$, by the definition

$$\phi = \frac{\left(\theta\sqrt{Re_L}\right)^2\sqrt{\frac{\gamma_E-1}{2}}}{\lambda} \tag{13}$$

Then

$$\frac{n}{P'\left(\frac{\overline{t}_o}{\overline{t}_e}\right)} = \frac{\phi M_e}{\left[1+\frac{\gamma_E-1}{2}M_e^2\right]^m} = \frac{\phi M_e}{\left(\frac{\overline{t}_o}{\overline{t}_e}\right)^m} \tag{14}$$

Equation (2) then becomes

$$\frac{d}{dx}\left[\frac{\phi M_e}{\left(\frac{\tilde{t}_o}{\tilde{t}_e}\right)^m}\right] = N + \frac{\left[\frac{\phi M_e}{\left(\frac{\tilde{t}_o}{\tilde{t}_e}\right)^m}\right]}{\left[\frac{M_e\left(\frac{\tilde{t}_o}{\tilde{t}_e}\right)^K}{\lambda R^2}\right]} \frac{d}{dx}\left[\frac{M_e\left(\frac{\tilde{t}_o}{\tilde{t}_e}\right)^K}{\lambda R^2}\right] \tag{15}$$

After some manipulation and the use of equation (4), equation (15) can be written as

$$\frac{d\phi}{dx} = \frac{N\left[1+\frac{\gamma_\epsilon-1}{2}M_e^2\right]^m}{M_e} + \phi\left[\frac{(\gamma_\epsilon+1)M_e\frac{dM_e}{dx}}{1+\frac{\gamma_\epsilon-1}{2}M_e^2} - \frac{2}{R}\frac{dR}{dx} - \frac{1}{\lambda}\frac{d\lambda}{dx}\right] \tag{16}$$

Equation (16) is the boundary-layer momentum equation in a form that contains the Cohen and Reshotko parameter N. All the quantities in equation (16) except Φ and N are obtainable from the given data. Then, if Φ and N are known at one value of x the value of Φ can be found at a slightly larger value of x by use of equation (16). This value of Φ, together with the given pressure and wall temperature distribution and equation (11), determines n. Because N depends only on n and $\tilde{t}_w/\tilde{t}_O$, the integration of equation (16) can then proceed. Once n and Φ are known all other boundary-layer quantities can be calculated.

Derivation of Integral for Determination of Φ Near Stagnation Point

The stagnation point, where M_e and R are zero, is a singular point of equation (16). When a numerical step-by-step solution of equation (16) is begun at the stagnation point the result is usually a variation of Φ with x that is highly oscillatory and diverging, at least for small values of x. One way to avoid this difficulty is to calculate Φ from an integral instead of from the differential equation, equation (16). This integral can be developed by noting that the wall temperature distribution is a symmetrical function of x for a body of revolution at zero angle of attack; all the bodies of the present investigation were supposedly at, or close to, zero angle of attack. Because the wall temperature is a symmetrical function of x about the stagnation point it follows that

$$\left(\frac{\partial \tilde{t}_w}{\partial x}\right)_{x=0} = 0$$

When the wall temperature is independent of x, Cohen and Reshotko (ref. (3)) suggest the approximation

$$N = A + Bn \quad ; \tag{17}$$

this approximation allows equation (16) to be integrated in closed form and so results in the desired integral. For a constant wall temperature, the term $d\lambda/dx$ in equation (16) is zero and so drops out. In the present case the wall temperature is assumed to be constant from x = 0 to a large enough value of x, say x_1, to allow the step-by-step integration of equation (16) to be started at x_1 without the difficulties usually found when the integration is begun at x = 0, the singular point of equation (16).

Upon use of the approximation given by equation (17) and the relation

$$n = -\phi \frac{\frac{dM_e}{dx}}{\left[1 + \frac{\gamma_E - 1}{2} M_e^2\right]^m} \quad , \tag{18}$$

which results when equations (11) and (13) are used, equation (16) becomes

$$\frac{d\phi}{dx} = \frac{\left[1 + \frac{\gamma_E - 1}{2} M_e^2\right]^m}{M_e} \left\{ A - \phi \frac{B \frac{dM_e}{dx}}{\left[1 + \frac{\gamma_E - 1}{2} M_e^2\right]^m} \right\} + \phi \left[\frac{(\gamma_E + 1) M_e \frac{dM_e}{dx}}{1 + \frac{\gamma_E - 1}{2} M_e^2} - \frac{2\left(\frac{dR}{dx}\right)}{R} \right] \tag{19}$$

Equation (19) is a linear first-order differential equation for ϕ. After integration the result is

$$\phi = \frac{A\left[1 + \frac{\gamma_E - 1}{2} M_e^2\right]^{\frac{\gamma_E + 1}{\gamma_E - 1}}}{M_e^B R^2} \int_0^x \frac{M_e^{B-1} R^2}{\left[1 + \frac{\gamma_E - 1}{2} M_e^2\right]^{\frac{3\gamma_E - 1}{2(\gamma_E - 1)}}} dx \tag{20}$$

for the condition, $M_e = 0$ at x = 0. In the present calculations the use of equation (20) from x = 0 to the value of x at which M_e is equal to .05 was found to be satisfactory. At the first few values of x very near zero, the values of ϕ computed by equation (20) usually do not form a smooth sequence of values, but this is not important because each value of ϕ is independent of its values at smaller x. Usually, the variation of ϕ with x becomes sufficiently smooth before x reaches the value at which M_e is equal to .05.

The values of A and B in equation (17) are found by making the line given by equation (17) tangent to the curve $N(n,S_w)$ at the stagnation point (see fig. 4 of ref. (3)). The value of B in equation (17) is then found from the relation

$$B = \left(\frac{\partial N}{\partial n}\right)_{n=n_o} \tag{21}$$

which follows from equation (17). Moreover, at the stagnation point of an axisymmetric body

$$N_o = -2n_o \tag{22}$$

(see page 14 of ref. (3)). Therefore, from equation (17) it follows that

$$A = -(B+2)n_o \tag{23}$$

Adaptation of Cohen and Reshotko Method for Calculation by Electronic Computer

In previous work at the Naval Ordnance Laboratory the Cohen and Reshotko method had been adapted so that calculations could be made by the IBM 704 computer. The adaptation consisted in expressing the Cohen and Reshotko parameters ℓ, $(C_f Re_w/Nu)_{Pr=1}$, H_{tr}, and $(\delta/\theta)_{M=0}$ in an analytic form by the use of "least-square" polynomials in the variables n and S_w. In the present work these polynomials were adjusted to eliminate slight discontinuities in ℓ and in $(C_f Re_w/Nu)_{Pr=1}$ at n = 0. Moreover, in order to handle cases with values of n less than -.7 or so, the polynomials for ℓ, $(C_f Re_w/Nu)_{Pr=1}$ and $(\delta/\theta)_{M=0}$ for $n < -.3$ were replaced by straight lines that had the same slope and value at n = -.3 as given by the polynomials. For the quantity H_{tr}, the modification consisted in the use of the value of H_{tr} at n = -.5 for $n < -.5$.

Value of n_o

In order to begin the computation the value of n_o must be known; this value is used in equation (23), and also to get the initial value of Φ and so of $(\theta\sqrt{Re_L})_o$ by use of equations (18) and (13). The present calculations are confined to bodies of revolution at zero angle of attack. For such bodies, the value of the non-dimensional pressure gradient parameter β is 1/2 at the stagnation point. Consequently, the correlation number n, which, in general, depends on both β and S_w, is, for a stagnation point, a function only of S_w. An analytic expression for this function was obtained by fitting a least-squares polynomial of the second degree to the values of n for $\beta = 1/2$ for all the S_w values given in table 2 of reference (3). This analytic expression was incorporated into the IBM 704 program.

Separation Criterion

Although the calculation of the separation point was not an objective of the present investigation a criterion to indicate the occurrence of a calculated separation point was incorporated into the calculation procedure. The criterion was obtained by noting that because the flows under consideration do not begin at a separation point the value of the shear parameter ℓ decreases as the pressure gradient parameter n increases (see fig. 2 of ref. (3)). That is, the friction coefficient decreases with increase in adverse pressure gradient. If n increases sufficiently there is eventually reached a value of ℓ such that a further decrease cannot occur unless n is decreased. For a decrease in adverse pressure gradient to cause a decrease in friction coefficient is, however, physically unrealistic for a flow that does not begin at a separation point. Consequently, only the upper branch of the curves of figure 2 of reference (3) seem physically allowable for the present computations. Because the correct criterion for separation, namely, $\ell = 0$, is thus not attainable, it was assumed that a fair estimate of the separation point can be obtained by assuming separation to occur at the smallest allowable value of ℓ. On each curve of ℓ against n for constant S_w, the smallest value of ℓ occurs at the largest value of n. These maximum values of n depend only on S_w; the analytic form of the separation criterion was therefore obtained by fitting a least-squares polynomial of the fourth degree to these maximum values of n. In the present computations separation was not indicated in any of the seven cases.

CALCULATION PROCEDURE

Given Data and Flight Parameters

The calculation procedure requires that the shape of the body R(x), the pressure distribution $\bar{p}_e/\bar{p}_o(x)$, and the wall temperature ratio $\bar{t}_w/\bar{t}_o(x)$, be given either in analytic or tabular form. In addition, all the quantities given in table 1, except $(\theta\sqrt{Re_L})_o$, were needed. The temperature $\bar{t}_\infty$, and the density $\bar{\rho}_\infty$, in the free stream ahead of the body were either part of the experimental data or else were obtained from tabulated properties of the standard atmosphere (ref. (4)). The temperature ratio $\bar{t}_o/\bar{t}_\infty$, and the pressure ratio $\bar{p}_o/\bar{p}_\infty$, were read from the charts of reference (5) when the velocity $\bar{u}_\infty$ was either greater than or only slightly less than 7000 ft/sec, the lower limit of the charts. For smaller values of $\bar{u}_\infty$, the tables of reference (6) were used.

<u>Re_∞</u>: The free-stream Reynolds number, Re_∞, was computed from its definition

$$Re_\infty = \frac{\bar{u}_\infty \bar{L}}{\bar{\nu}_\infty}$$

The velocity $\bar{u}_\infty$ and the kinematic viscosity $\bar{\nu}_\infty$ were either given explicity or else were obtained by calculation from other given quantities.

<u>Re_L</u>: The reference Reynolds number, Re_L, was computed from the definition

$$Re_L = \frac{\bar{u}_M \bar{L}}{\bar{\nu}_o}$$

where

$$\frac{\bar{u}_M}{\bar{u}_\infty} = \sqrt{\frac{1 + \frac{\gamma_\infty - 1}{2} M_\infty^2}{\frac{\gamma_\infty - 1}{2} M_\infty^2}} \qquad (24)$$

and

$$\bar{\nu}_o = \left(\frac{\bar{\mu}_o}{\bar{\mu}_\infty}\right)\left(\frac{\bar{\rho}_\infty}{\bar{\rho}_o}\right)\bar{\nu}_\infty$$

The ratio $\bar{\mu}_o/\bar{\mu}_\infty$ was calculated from Sutherland's formula

$$\frac{\bar{\mu}_o}{\bar{\mu}_\infty} = \left(\frac{\bar{t}_o}{\bar{t}_\infty}\right)^{\frac{1}{2}} \frac{1 + \frac{\bar{C}}{\bar{t}_\infty}}{1 + \frac{\bar{C}}{\bar{t}_\infty}\frac{\bar{t}_\infty}{\bar{t}_o}} \qquad \left(\bar{C} = 198.6^\circ R\right)$$

and the previously obtained value of $\bar{t}_o/\bar{t}_\infty$. The effect of dissociation on the ratio $\bar{\mu}_o/\bar{\mu}_\infty$ given by Sutherland's formula can be estimated by use of table 6 or figure 8 of reference (7). In most cases of the present investigation the correction to Sutherland's formula was less than ten percent. Because this correction is small and because a more inexact formula than Sutherland's is used in the Cohen and Reshotko method, namely, equation (4) of reference (3), the small correction for dissociation was not used. When the velocity $\bar{u}_\infty$ was either greater than or only slightly less than 7000 ft/sec, the ratio $\bar{\rho}_\infty/\bar{\rho}_o$ was read from the appropriate chart of reference (5). For smaller values of $\bar{u}_\infty$, this ratio was calculated from the relation for a perfect gas, namely,

$$\frac{\bar{\rho}_\infty}{\bar{\rho}_o} = \frac{\bar{p}_\infty}{\bar{p}_o} \frac{\bar{t}_o}{\bar{t}_\infty}$$

γ_E: In the present calculations the departure of air from perfect-gas behavior at high temperatures is partially accounted for by allowing the value of γ to have a value other than 1.4 in the relations involving this ratio. The value of γ used to obtain the relations between various flow quantities behind the nose shock is called γ_E and is assumed to be independent of x and y. For values of M_∞ less than about four, the value of γ_E was taken as 1.4. For larger values of M_∞, the value of γ_E was initially estimated by use of the charts of reference (5) by first locating the stagnation point conditions on the Mollier chart of reference (5) and then proceeding along a line of constant entropy. The values of log $\bar{p}/\bar{p}_I$ along this line of constant entropy were plotted against the corresponding values of log ρ/ρ_I. The result was approximately a straight line with slope γ_E.

Later, a simpler method for calculating γ_E was used. In this method the value of γ_E was chosen to give the correct value of the non-dimensional velocity gradient, (du_e/dx), at the stagnation point. This value of γ_E was obtained by noting that from the equation of motion for the flow outside the boundary layer,

$$\bar{\rho}_e \bar{u}_e \frac{d\bar{u}_e}{d\bar{x}} = -\frac{d\bar{p}_e}{d\bar{x}}$$

it follows, after use of L'Hospital's rule, that

$$\left(\frac{d\bar{u}_e}{dx}\right)_o = \sqrt{-\frac{\bar{p}_o}{\bar{\rho}_o}\left[\frac{d^2}{dx^2}\left(\frac{\bar{p}_e}{\bar{p}_o}\right)\right]_o} \qquad (25)$$

Moreover, from equations (3) and (8) a different expression can be obtained for $(d\bar{u}_e/dx)_o$. This expression contains γ_E and is,

$$\left(\frac{d\bar{u}_e}{dx}\right)_o = \bar{u}_M \sqrt{\frac{1-\gamma_E}{2\gamma_E}\left[\frac{d^2}{dx^2}\left(\frac{\bar{p}_e}{\bar{p}_o}\right)\right]_o} \tag{26}$$

The value of $\bar{u}_M$, the maximum attainable velocity, is equal to $\sqrt{2\bar{h}_o J}$, where $\bar{h}_o$ is the stagnation enthalpy. The value of γ_E is now defined to be that which makes the value of $(d\bar{u}_e/dx)_o$ calculated from equation (26) equal to the value calculated from equation (25). Thus, after equating equations (26) and (25), the result for γ_E is

$$\gamma_E = \left[1 - \frac{\bar{p}_o}{\bar{\rho}_o \bar{h}_o \bar{J}}\right]^{-1} \tag{27}$$

Experience showed that γ_E could be calculated more quickly by use of equation (27) than by the procedure involving the use of the Mollier chart of reference (5). Moreover, the value of γ_E obtained by use of equation (27) was close to that calculated by the use of the Mollier chart.

$\underline{\bar{h}_o}$: The value of the stagnation enthalpy, $\bar{h}_o$, was calculated by use of the relation

$$\bar{h}_o = \bar{C}_p \bar{t}_\infty \left(1 + \frac{\gamma_\infty - 1}{2} M_\infty^2\right) \tag{28}$$

The value of C_p was taken as 7.725 BTU/slug/deg Rankine and γ_∞ was taken equal to 1.4

$\underline{dM_e/dx}$: In order to integrate the momentum equation, equation (16), the quantity dM_e/dx is needed. By differentiating equation (8) there is obtained the relation

$$\frac{dM_e}{dx} = -\frac{1}{\gamma_E}\sqrt{\frac{\gamma_e-1}{2}}\;\frac{\frac{d}{dx}\left(\frac{\bar{p}_e}{\bar{p}_o}\right)}{\left(\frac{\bar{p}_e}{\bar{p}_o}\right)^{\frac{3\gamma_E-1}{2\gamma_E}}\left[1-\left(\frac{\bar{p}_e}{\bar{p}_o}\right)^{\frac{\gamma_E-1}{\gamma_E}}\right]^{1/2}} \tag{29}$$

In some cases the data were given as the pressure coefficient ratio $C_p/C_{p_o}(x)$ rather than as $\bar{p}_e/\bar{p}_o(x)$. In these cases $\bar{p}_e/\bar{p}_o$ was obtained from C_p/C_{p_o} by the relation that follows from the definition of C_p, namely,

$$\frac{\bar{p}_e}{\bar{p}_o} = \frac{\bar{p}_\infty}{\bar{p}_o} + \left(1-\frac{\bar{p}_\infty}{\bar{p}_o}\right)\frac{C_p}{C_{p_o}} \tag{30}$$

$(dM_e/dx)_o$: At the stagnation point dM_e/dx is needed in order to calculate $(\theta\sqrt{Re_L})_o$. Note, however, that it is not needed there for the integration of equation (16) because this equation is not used until a larger value of x. Because $\bar{p}_e/\bar{p}_o$ is a symmetric function of x, the derivative $d\left(\frac{\bar{p}_e}{\bar{p}_o}\right)/dx$ is zero at $x = 0$. Consequently, relation (29) is indeterminate there. In order to obtain an expression for $(dM_e/dx)_o$, L'Hospital's rule was applied to equation (29) with the result

$$\left(\frac{dM_e}{dx}\right)_o = \sqrt{-\frac{1}{\gamma_E}\left[\frac{d^2}{dx^2}\left(\frac{\bar{p}_e}{\bar{p}_o}\right)\right]_o} \tag{31}$$

$d^2/dx^2(p_e/p_o)_o$: The value of $d^2/dx^2(p_e/p_o)_o$ or of $d^2/dx^2(C_p/C_{p_o})_o$, for use in equation (31) was obtained either from an analytic expression for C_p/C_{p_o} or from tabular data obtained by smoothing the values of $(\bar{p}_e/\bar{p}_o)$ read from a graph. When smoothed tabular data were used, the value of $d^2/dx^2(C_p/C_{p_o})_o$ was obtained by one of two methods. In the first, values of C_p/C_{p_o} were read at equal intervals in x near $x = 0$, a difference table constructed, and the second derivative obtained by use of Newton's forward difference formula, namely,

$$\left[\frac{d^2}{dx^2}\left(\frac{C_p}{C_{p_o}}\right)\right]_o = \frac{1}{(\Delta x)^2}\left[\Delta^2\left(\frac{C_p}{C_{p_o}}\right) - \Delta^3\left(\frac{C_p}{C_{p_o}}\right) + \frac{11}{12}\Delta^4\left(\frac{C_p}{C_{p_o}}\right)\right] \tag{32}$$

This formula is obtainable by differentiating equation (5), page 192 of reference (8).

When this method was used for the "1/10th-Power" Nose Shape and for the Elliptical-Nose Cylinder the values of both $(\theta\sqrt{Re_L})_o$ and $\bar{q}_o$ did not form a "smooth" extension of their values for larger x. It was found, however, that the values of $(\theta\sqrt{Re_L})_o$ and $\bar{q}_o$ did fair smoothly into their values at larger x when the C_p/C_{p_o} distribution for small x was represented by the parabola

$$\frac{C_p}{C_{p_o}} = 1 - ax^2 \tag{33}$$

The value of "a" was calculated for the "1/10th-Power" Nose Shape by making the parabola given by equation (33) give the smoothed value of (C_p/C_{p_o}) at $x = .1$. For the Elliptical-Nose Cylinder the corresponding value of x was .05 instead of .1.

Smoothing of Data

By experience it was found that in order to obtain sufficiently smooth calculated distributions of the heat transfer $\bar{q}$ and some of the other boundary-layer parameters with x, the $\bar{p}_e/\bar{p}_o$ data had to be "smooth." When $\bar{p}_e/\bar{p}_o(x)$ was given in the form of a mathematical expression, the smoothness requirement was satisfied. When $\bar{p}_e/\bar{p}_o(x)$ was given in the form of a graph, $\bar{p}_e/\bar{p}_o$ was read at convenient intervals in x to produce a table. These tabular values were then smoothed by a fivefold application of formula (1) on page 276 of reference (8). This is a five-point, third-degree, least-squares smoothing formula. Although it was not certain that the smoothing procedure was necessary it was also applied to the radius distribution R(x), and the wall temperature distribution $\bar{t}_w(x)$. The smoothing procedure often produced a slight change in the original data distribution.

Formulas for Boundary-Layer Quantities

Re_θ: One of the boundary-layer quantities of interest is the boundary-layer momentum thickness Reynolds number Re_θ, defined as

$$Re_\theta = \frac{\bar{u}_e \bar{\theta}}{\bar{\nu}_e}$$

By introducing the reference Reynolds number Re_L, Re_θ can be written as

$$Re_\theta = u_e \theta Re_L \frac{\bar{\nu}_o}{\bar{\nu}_e}$$

or, after use of the perfect-gas law and equations (3), (4), and (8) as

$$\frac{Re_\theta}{\sqrt{Re_L}} = \frac{\sqrt{\frac{\gamma_E - 1}{2}}\, M_e \left(\theta \sqrt{Re_L}\right)}{\left[1 + \frac{\gamma_E - 1}{2} M_e^2\right]^{\frac{\gamma_E + 1}{2(\gamma_E - 1)}}} \frac{\bar{\mu}_o}{\bar{\mu}_e} \qquad (34)$$

The value of Re_θ in the present analysis was calculated by using the Sutherland viscosity formula for the ratio $\bar{\mu}_o/\bar{\mu}_e$.

$Re_k/k^2 Re_L^{3/2}$: Often of interest is the roughness Reynolds number, defined as

$$Re_k = \frac{\bar{u}_k \bar{k}}{\bar{\nu}_k}$$

A convenient expression for Re_k for small values of $(\bar{k}/\bar{\delta})$ can be obtained by expanding the velocity $\bar{u}$ and the kinematic viscosity $\bar{\nu}$ in a series in $\bar{y}$ and keeping only the first power of $\bar{y}$. To the first order in $\bar{y}$, the expression for Re_k becomes

$$Re_k = \frac{\bar{k}^2 \left(\frac{\partial \bar{u}}{\partial \bar{y}}\right)_w}{\bar{\nu}_w} \qquad (35)$$

The expression (35) is expected to be sufficiently accurate when $\bar{k}$ is not much larger than $\bar{\theta}$. In the present investigation the measured values of $\bar{k}$ on all the bodies were always less than $(\bar{\delta}/7)$.

When the relation

$$\left(\frac{\partial \bar{u}}{\partial \bar{y}}\right)_w = \eta \frac{\bar{u}_e}{\bar{\theta}} \frac{\bar{t}_e}{\bar{t}_w} , \qquad (36)$$

which is equation (21) of reference (3), is used together with the perfect-gas law and the approximation that $\bar{p}_e = \bar{p}_w$, equation (35) can be written as

$$R_{e_K} = \frac{K^2 R_{e_L} l\, u_e \left(\frac{\bar{t}_e}{\bar{t}_o}\right)\left(\frac{\bar{p}_e}{\bar{p}_o}\right)\left(\frac{\bar{t}_o}{\bar{t}_w}\right)^3}{\theta \lambda} \tag{37}$$

When equations (3), (4), and (8) are used, equation (37) becomes

$$\frac{R_{e_K}}{K^2 R_{e_L}^{3/2}} = \frac{\sqrt{\frac{\gamma_\varepsilon - 1}{2}}\, M_e\, l \left(\frac{\bar{t}_o}{\bar{t}_w}\right)^3}{\lambda \left(\theta \sqrt{R_{e_L}}\right)\left[1 + \frac{\gamma_\varepsilon - 1}{2} M_e^2\right]^{\frac{5\gamma_\varepsilon - 3}{2(\gamma_\varepsilon - 1)}}} \tag{38}$$

The computations made by the IBM 704 machine gave the quantity $Re_k/k^2Re_L^{3/2}$. From this quantity, the roughness Reynolds number Re_k was calculated for the desired value of k.

<u>(Nu/x)</u>: The heat transfer by conduction per unit area of surface per unit time is given by

$$\bar{q} = \bar{K}_w \left(\frac{\partial \bar{t}}{\partial \bar{y}}\right)_w = \frac{\bar{K}_w}{\bar{c}_{p_w}} \left(\frac{\partial \bar{h}}{\partial \bar{y}}\right)_w$$

The Nusselt number is defined as

$$N_u = \frac{\bar{x} \left(\frac{\partial \bar{t}}{\partial \bar{y}}\right)_w}{\bar{t}_r - \bar{t}_w}$$

in reference (3). In the present analysis this definition is generalized to

$$N_u = \frac{\bar{x} \left(\frac{\partial \bar{h}}{\partial \bar{y}}\right)_w}{\bar{h}_r - \bar{h}_w} = \frac{\bar{x}\, \bar{c}_{p_w}\, \bar{q}}{\bar{K}_w (\bar{h}_r - \bar{h}_w)} \tag{39}$$

because of the high temperatures in some of the cases analyzed. In order to calculate Nu, the relation

$$\frac{N_u}{\sqrt{R_{e_w}}} = \frac{C_f \sqrt{R_{e_w}}}{\left(\frac{C_f R_{e_w}}{N_u}\right)_{P_r = 1}} P_r^{\alpha} \tag{40}$$

which is equation (38) of reference (3), is used. Upon use of the definition of C_f, of Re_w, and the relation

$$\bar{\tau}_w = \bar{\mu}_w \left(\frac{\partial \bar{u}}{\partial \bar{y}}\right)_w$$

and equation (36), it follows that

$$C_f Re_w = 2 l \frac{\bar{x}}{\bar{\theta}} \frac{\bar{t}_e}{\bar{t}_w} \tag{41}$$

When equations (4) and (41) are used, equation (40) becomes

$$\frac{Nu}{x} = 2 \frac{l}{\left(\frac{C_f Re_w}{Nu}\right)_{P_r=1}} \frac{\left(\frac{\bar{t}_o}{\bar{t}_w}\right)}{\theta\left(1+\frac{\gamma_e-1}{2}M_e^2\right)} P_r^{\alpha} \tag{42}$$

The value of the Prandtl number was read from figure 11 of reference (7) for the average temperature and pressure on the surface of the body. The value of α was taken as .4, the value suggested in reference (3).

St: Also of interest is the Stanton number, St_∞, defined as

$$St_\infty = \frac{\bar{q}}{\bar{\rho}_\infty \bar{u}_\infty (\bar{h}_r - \bar{h}_w)} \tag{43}$$

The Stanton number can be expressed in terms of the Nusselt number by eliminating $\bar{q}$ from relations (39) and (43). Upon use of the definition of the Prandtl number, the result is

$$St_\infty = \frac{Nu}{x} \frac{1}{P_{r_w}} \frac{\bar{\mu}_w}{\bar{\rho}_\infty \bar{u}_\infty} \tag{44}$$

When equation (9) is used, equation (44) becomes

$$St_\infty = \frac{Nu}{x} \frac{\lambda}{P_{r_w} Re_\infty} \left(\frac{\bar{t}_w}{\bar{t}_o}\right)\left(\frac{\bar{\mu}_o}{\bar{\mu}_\infty}\right) \tag{45}$$

The value of Pr_w used in equation (45) was the same as that in equation (42).

The Stanton number can also be based on local gas properties at the outer edge of the boundary layer. In this case the Stanton number is denoted by St_e and is defined as

$$St_e = \frac{\bar{q}}{\bar{\rho}_e \bar{u}_e (\bar{h}_r - \bar{h}_w)} \tag{46}$$

By eliminating $\bar{q}$ between equations (40) and (46), using $\bar{\rho}_e \bar{u}_e$ to form Re_θ, and then using equation (34) for Re_θ, the result, after using equation (9), is

$$St_e = \frac{Nu}{X} \lambda \left(\frac{\bar{t}_w}{\bar{t}_o}\right) \frac{1}{Pr_w} \frac{\left(1 + \frac{\gamma_E - 1}{2} M_e^2\right)^{\frac{\gamma_E + 1}{2(\gamma_E - 1)}}}{Re_L \sqrt{\frac{\gamma_E - 1}{2}}\, M_e} \tag{47}$$

Here, again, the value of Pr_w is the same as in equation (42).

$\bar{q}$: The heat transfer was calculated by use of equation (43) written as

$$\bar{q} = St_\infty \bar{\rho}_\infty \bar{u}_\infty \bar{h}_o \left(\frac{\bar{h}_r}{\bar{h}_e} \frac{\bar{h}_e}{\bar{h}_o} - \frac{\bar{h}_w}{\bar{h}_o}\right) \tag{48}$$

The ratio $\bar{h}_e/\bar{h}_o$ is calculated from the relation for the conservation of energy outside the boundary layer, namely,

$$\frac{\bar{h}_e}{\bar{h}_o} = \frac{1}{1 + \frac{\bar{u}_e^2}{2\bar{h}_e}}$$

The gas is assumed to be thermally and calorically perfect with a constant effective value of γ called γ_E. For such a gas the relation between $\bar{h}_e$ and the speed of sound, $\bar{a}_e$, is

$$\bar{h}_e = \frac{\bar{a}_e^2}{\gamma_E - 1} \tag{49}$$

When this relation is used in the relation for $\bar{h}_e/\bar{h}_o$ the result is

$$\frac{\bar{h}_e}{\bar{h}_o} = \frac{1}{1 + \frac{\gamma_E - 1}{2} M_e^2} \tag{50}$$

The ratio $\bar{h}_r/\bar{h}_e$ is calculated from the relation

$$\frac{\bar{h}_r}{\bar{h}_e} = 1 + r\frac{\bar{u}_e^2}{2\bar{h}_e}$$

where r is the recovery factor, taken equal to $\sqrt{Pr_w}$.

This relation becomes

$$\frac{\bar{h}_r}{\bar{h}_e} = 1 + r\frac{\gamma_E - 1}{2}M_e^2 \tag{51}$$

when equation (49) is used. Upon the use of equations (50) and (51), equation (48) becomes

$$\bar{q} = St_\infty \bar{\rho}_\infty \bar{u}_\infty \bar{h}_o \left(\frac{1 + r\frac{\gamma_E - 1}{2}M_e^2}{1 + \frac{\gamma_E - 1}{2}M_e^2} - \frac{\bar{h}_w}{\bar{h}_o} \right) \tag{52}$$

In order to partially account for the fact that $\bar{h}_w/\bar{h}_o$ is not necessarily equal to $\bar{t}_w/\bar{t}_o$, without increasing the length of the computation, the ratio $\bar{h}_w/\bar{h}_o$ was approximated by the expression

$$\frac{\bar{h}_w}{\bar{h}_o} = b\frac{\bar{t}_w}{\bar{t}_o} \tag{53}$$

An expression for b was constructed by imposing two conditions. The first was that at the stagnation point

$$\bar{h}_w = \bar{h}_{w_o}$$

Therefore b is given the value $(\bar{h}_{w_o}/\bar{h}_o)/(\bar{t}_{w_o}/\bar{t}_o)$ when $\bar{t}_w = \bar{t}_{w_o}$. The second condition was that

$$\bar{h}_w = \bar{h}_o$$

where

$$\bar{t}_w = \bar{t}_o$$

Therefore b is given the value unity when $\bar{t}_w = \bar{t}_o$. The two conditions then are

$$b = \frac{\left(\frac{\bar{h}_{w_o}}{\bar{h}_o}\right)}{\left(\frac{\bar{t}_{w_o}}{\bar{t}_o}\right)} \qquad \text{for} \quad \bar{t}_w = \bar{t}_{w_o}$$

and

$$b = 1 \quad \text{for} \quad \bar{t}_w = \bar{t}_o$$

For other values of $\bar{t}_w$, b is assumed to vary linearly with $\bar{t}_w$. The result for b then is

$$b = \frac{1-d}{1-\frac{\bar{t}_{w_o}}{\bar{t}_o}} \left(\frac{\bar{t}_w}{\bar{t}_o} - \frac{\bar{t}_{w_o}}{\bar{t}_o} \right) + d \tag{54}$$

where

$$d = \frac{\left(\frac{\bar{h}_{w_o}}{\bar{h}_o}\right)}{\left(\frac{\bar{t}_{w_o}}{\bar{t}_o}\right)}$$

Because the wall temperature usually fell with increase in distance from the stagnation point, more accurate calculated values for $\bar{q}$ would have resulted if b had been made equal to unity at $\bar{t}_w = \bar{t}_{oo}$ instead of at $\bar{t}_w = \bar{t}_o$. This change in b would have increased $\bar{h}_w/\bar{h}_o$ in equation (52) and so would have reduced the calculated values of $\bar{q}$.

In every case the appropriate calculated quantity, namely, either St_{oo}, St_e, or $\bar{q}$, was compared with the distribution along the surface obtained from the experimental temperature data and presented in references (9) to (16). For these seven cases the calculated and experimentally obtained quantities were close enough together to indicate that the method used to calculate the characteristics of the laminar boundary layer is sufficiently accurate for the purposes of the present investigation.

$\underline{\delta^*/\theta,\ \delta/\theta}$: The boundary-layer thickness ratios δ^*/θ and δ/θ were also calculated. The expression for δ^*/θ is

$$\frac{\delta^*}{\theta} = H_{tr} + \frac{\gamma_E - 1}{2} M_e^2 \left(H_{tr} + 1 \right) \tag{55}$$

and the expression for δ/θ is

$$\frac{\delta}{\theta} = \frac{\delta_{tr}}{\theta_{tr}} + \frac{\gamma_E - 1}{2} M_e^2 \left(H_{tr} + 1 \right) \tag{56}$$

Equations (55) and (56) are equations (40) and (41) respectively of reference (3) with γ replaced by γ_E.

$\bar{\tau}_w/\bar{\rho}_e\bar{u}_e^2$: The local friction coefficient, $\bar{\tau}_w/\bar{\rho}_e\bar{u}_e^2$, is often of interest. The relation

$$\frac{\bar{\tau}_w}{\bar{\rho}_e\bar{u}_e^2} = \frac{\left(\bar{\mu}\frac{\partial\bar{u}}{\partial\bar{y}}\right)_w}{\bar{\rho}_e\bar{u}_e^2}$$

is used with relations (36), (9), (8), (4), and (3) to obtain

$$\frac{\bar{\tau}_w}{\bar{\rho}_e\bar{u}_e^2} = \frac{\lambda l}{\theta\sqrt{Re_L}} \frac{\left[1+\frac{\gamma_E-1}{2}M_e^2\right]^{\frac{3-\gamma_E}{2(\gamma_E-1)}}}{\sqrt{\frac{\gamma_E-1}{2}}\sqrt{Re_L}\,M_e} \tag{57}$$

β: In order to estimate the value of Re_θ below which the stability theory (ref. (1)) predicts that all small two-dimensional disturbances decay, the tables of reference (17) were used. In order to use these tables it is necessary to know the value of the non-dimensional pressure gradient parameter β. The computations by use of the Cohen and Reshotko method (ref. (3)) result, however, in the non-dimensional pressure gradient parameter n instead of β. The parameter β is a function of n and the non-dimensional wall temperature parameter S_w. This function is shown in figure 4 of reference (17). In the present investigation β was expressed as a function of n and S_w by a least-squares polynomial of the fourth degree in both n and S_w and the values of β were calculated from this polynomial.

$Re_{\theta,c}$: The minimum critical Reynolds number, $Re_{\theta,c}$ is the Reynolds number below which all small two-dimensional disturbances are damped. Once the value of β, of M_e, and of S_w was known at a value of x, the corresponding value of $Re_{\theta,c}$ was obtained from the tables of reference (17). Because the values of β, M_e, and S_w usually did not correspond exactly to an entry in the tables of reference (17) it was necessary to interpolate. A sufficiently accurate method of interpolation was first to change the tables to tables of $\log_{10}Re_{\theta,c}$ instead of $Re_{\theta,c}$. A linear interpolation procedure in β, M_e, and S_w was then used to find the value of $Re_{\theta,c}$ for given values of β, M_e, and S_w. This interpolation was part of the calculation routine and was made by the IBM 704 electronic computer.

$Re_{\theta,m}$: The minimum transition Reynolds number $Re_{\theta,m}$ is the value of Re_θ below which transition supposedly cannot begin. The value of $Re_{\theta,m}$ was estimated for each value of x by first constructing a table of $Re_{\theta,m,f}$ against M_e from the curve for $Re_{\theta,m,f}$ for an insulated surface given in figure 2 of reference (2) and then interpolating to find the local value of $Re_{\theta,m,f}$ for the local value of M_e. For reasons given in the "Discussion" and in reference (2) only the curve for an insulated surface was used even though the surfaces were not insulated. The value of $Re_{\theta,m}$ was then obtained by the relation

$$Re_{\theta,m} = Re_{\theta,m,f}\left(\frac{Re_{\theta,m}}{Re_{\theta,m,f}}\right)$$

where the ratio $(Re_{\theta,m})/(Re_{\theta,m,f})$ was obtained from the curve marked "equation (67)" of figure 5 of reference (2). This curve was first converted to a table of $(Re_{\theta,m})/(Re_{\theta,m,f})$ for equal increments in β and an interpolation was made to find the value for a required value of β.

Method of Integration of Differential Equations

In order to calculate the value of the integral in equation (20), the integral, called I, was calculated from the equation

$$\frac{dI}{dx} = \frac{M_e^{B-1}\, R^2}{\left[1+\frac{\gamma_E-1}{2}M_e^2\right]^{\frac{3\gamma_E-1}{2(\gamma_E-1)}}} \qquad (I(0)=0) \qquad (58)$$

This differential equation was integrated by a procedure that was already coded on the IBM 704 electronic computer (ref. (18)). The procedure consisted in using the fourth order Runge-Kutta method for the first two steps in x and then using the fourth order Adams-Moulton predictor-corrector method. The same procedure was used to integrate equation (16) from the first point at which it replaced equation (20) to the end of the range of x. For the present computations the IBM 704 electronic computer used eight significant figures in all the calculations and the results were printed out to five significant figures. The step size in x was .001 for all the calculations. By trial, this interval was found to be sufficiently small so that a doubling of the interval in a few test cases affected, at most, only the fifth significant figure in one or two of the boundary-layer parameters at a few values of x.

BODY DATA AND CALCULATED RESULTS IN TABULAR FORM

Table 2: Table 2 indicates how the pressure distribution, the wall temperature distribution, and the radius distribution were obtained for each of the seven bodies.

Table 3: In table 3 are given the "surface roughness" data for the seven bodies. Also given are the roughness heights that were used in the calculation of the roughness Reynolds number Re_k.

Table 4: The quantities listed in table 4 were calculated by the methods described in the sections entitled, "Analysis," and "Calculation Procedure." The included range of x is equal to, or slightly greater than, the range for which the flow was judged to be laminar. From the listed quantities any other quantity for which a formula is given in the section entitled, "Calculation Procedure," can be computed. To get H_{tr} and δ_{tr}/θ_{tr} for use in equations (55) and (56) it is necessary to use figures 7 and 8, respectively, of reference (3).

SOME FREE-FLIGHT DATA AND CALCULATED STABILITY AND TRANSITION RESULTS

In figures 1 to 7 is shown the calculated variation with x of Re_θ, $Re_{\theta,m}$, Re_k, and M_e at the largest Mach number at which data were available for each of the seven bodies. Also shown is the calculated minimum critical Reynolds number, $Re_{\theta,c}$, and the measured wall temperature distribution.

29° Hemisphere-Cone: In figure 1a is shown the variation of the boundary-layer Reynolds number Re_θ and the minimum transition Reynolds number $Re_{\theta,m}$ with the non-dimensional distance x from the stagnation point for a hemisphere-cone with an included angle of 29° (ref. (9)). Also shown is the range of values of $Re_{\theta,c}$. Transition occurred somewhere between x = .6632 and x = .7850, that is, between 38° and 45° from the stagnation point, at a value of Re_θ between 642 and 742. In this region of the body, $Re_{\theta,c}$ was more than 100 times as large as Re_θ. Ahead of the transition region, this ratio was still larger. Transition therefore occurred even though the boundary layer was estimated to be very stable with respect to the small two-dimensional disturbances used in the stability theory. It is apparent from the figure that Re_θ exceeded $Re_{\theta,m}$ beyond about 3.2° from the stagnation point.

In figure 1b is shown the variation of the local Mach number, M_e, the local ratio of the surface to stagnation temperature, T_w/T_o, and the local roughness Reynolds number Re_k. In the transition region, M_e lay between about .8 and 1.0. The wall temperature ratio, T_w/T_o, varied from about .565 at the stagnation point to about .515 at x = .7850. The maximum value of the roughness Reynolds number was .0157 near x = .60; this roughness Reynolds number is based on a roughness height of three microinches (see table 3).

The data given in table 4 for the lower Mach numbers for this body also show that transition occurred where $Re_{\theta,c}$ was very much larger than Re_θ. It is noted that at Mach numbers of 2.32 and 2.47 there was a region of the body, roughly between x = 1.5 and x = 1.9, in which $Re_{\theta,c}$ was less than Re_θ. In both of these cases transition occurred further back, where $Re_{\theta,c}$ was larger than Re_θ.

<u>50° Hemisphere-Cone</u>: In figure 2a is shown the variation of Re_θ, $Re_{\theta,m}$, and $Re_{\theta,c}$ with x for a hemisphere-cone with an included angle of 50° (ref. (10)). Transition began somewhere between x = .3379 and x = .5222, that is, between 19.3° and 29.9° from the stagnation point. In this region, Re_θ lay between 303 and 436. The critical Reynolds number, $Re_{\theta,c}$, was more than 100 times as large as Re_θ ahead of, and in the first part of the transition region. Transition is supposedly impossible ahead of about 3.3° from the stagnation point, the region in which Re_θ was less than $Re_{\theta,m}$. At the lowest Mach number, namely at 2.5, the data in table 4 indicate that this point moves back to about 4.3°.

In figure 2b is shown the variation of M_e, T_w/T_o, and Re_k. The local Mach number, M_e, in the region in which transition began was between .40 and .63. The local wall temperature ratio fell slightly from .46 at the stagnation point and then rose to .57 near the 30° station where the flow was definitely in transition. The maximum value of Re_k was equal to about 11.1 and occurred at about x = .36, just beyond the last thermocouple at which the flow definitely was laminar. The values of Re_k were calculated by use of a roughness height of 70.7 microinches. This number was obtained by multiplying the measured rms values of 25 microinches by $\sqrt{8}$ in order to obtain the peak height; the factor, $\sqrt{8}$, follows from the assumption that the roughness can be approximated by a "sine-wave" shape (ref. (19)). The value, 25 microinches, was obtained by use of a profilometer before the surface was oxidized to stabilize the emissivity. The oxidation probably increased the roughness height and so the actual maximum roughness height might easily have been larger than 70.7, the value used to calculate Re_k.

Just as for a flight Mach number of 4.7, transition at the lower Mach numbers occurred between $x = .3379$ and $x = .5222$ (see table 4). In the region in which transition began, the critical Reynolds number, $Re_{\theta,c}$, is more than 60 times greater than Re_θ for all five Mach numbers for which data are given in table 4.

Hemisphere-Cylinder

In figure 3a is shown the variation of Re_θ, $Re_{\theta,m}$, and $Re_{\theta,c}$ with x for a hemisphere-cylinder (ref. (11)). The results from this flight do not allow transition to be more precisely defined than to say that it occurred somewhere between the stagnation point and the 11 1/2° location ($x = .2008$). Consequently, transition occurred at a value of Re_θ less than 220. Transition occurred even though $Re_{\theta,c}$ was more than 1700 times as great as Re_θ. The data in table 4 indicate that for all five Mach numbers, $Re_{\theta,c}$ was at least 800 times as large as Re_θ. Transition is supposedly impossible ahead of about 2.8° from the stagnation point. Transition therefore occurred not more than about 9° behind the most forward possible point. At the lowest Mach number, namely 3.0, the data in table 4 indicate that the most forward possible transition point moved back to about 4.3° from the stagnation point.

In figure 3b is shown the distribution of M_e, $\bar{t}_w/\bar{t}_o$, and Re_k. Transition occurred in a region in which the local Mach number was less than .24. The wall temperature ratio was equal to .24 at the stagnation point. The roughness of the body was stated to be about three to five microinches near the stagnation point and about five microinches further back. Scratches of the order of 15 microinches existed behind the stagnation region. These numbers were obtained by use of an interferometer microscope, not on the body itself, but on a sample of the body metal polished in the same way as the body. In reference to the early transition in this test, the original investigators (ref. (11)) suggest that perhaps irregularities other than the five microinch surface roughness caused the early transition.

"1/10th-Power" Nose Shape

In figure 4a is shown the calculated data for a body, (ref. (12)), whose nose shape is defined by the equation given in table 2. At $x = .416$ the flow was laminar but at $x = .611$ transition was already well along toward completion. Transition therefore began at a value of Re_θ between 277 and 417. At the lower Mach numbers transition occurred further back. In fact, at the lowest Mach number transition had not occurred at $x = 1.920$, the location of the rearmost thermocouple.

When transition did occur, $Re_{\theta,c}$ was more than 250 times larger than Re_θ for the entire length of laminar flow for all Mach numbers. The indication from figure 4a is that the value of Re_θ was less than $Re_{\theta,m}$ for $x < .1$. At the lowest Mach number, namely, 1.72, the corresponding region was that for $x < .15$. The information in figure 4b indicates that transition occurred between a local Mach number of about .3 and .8. The wall temperature ratio varied from about .26 at the stagnation point to about .40 at x = .611. The maximum roughness Reynolds number in the region in which the flow definitely was laminar was equal to 1.8.

Flat-Face Cone-Cylinder

In figure 5a is shown the variation of Re_θ, $Re_{\theta,m}$ and $Re_{\theta,c}$ with x for a body consisting of a flat face followed by a cone which is followed by a cylinder (ref. (13)). The last thermocouple on the cone, at x = 4.493, indicated laminar flow. A calculation of the heat-transfer rate at x = 5.290 under the assumption that the flow was turbulent results in a heat-transfer rate of about 44 BTU/sq ft/sec. The calculated value for laminar flow is about five BTU/sq ft/sec and the value given in reference (13) is about 38 BTU/sq ft/sec. Consequently the flow not only was not laminar, but probably was completely turbulent. It is remarked that the value of x for station (13) in reference (13) should be 5.290 instead of 4.77, the value given in reference (13). At x = 4.906 the calculated value is about 44 BTU/sq ft/sec for turbulent flow, about five for laminar flow, and the value given in reference (13) is about 78. Therefore, although the flow may not have been completely turbulent at x = 4.906, it does not appear to have been laminar. Transition therefore occurred between x = 4.493 and x = 4.906. Similar calculations for flight Mach numbers of 13 and 10 lead to the same conclusion, namely, that transition began between x = 4.493 and x = 4.906. Transition thus occurred near the intersection of the cone and the cylinder, the region in which Re_θ increased rapidly by a factor that varied between about 3.2 at a flight Mach number of 14.5 to about 2.2 at a Mach number of 10. Consequently transition occurred at a value of Re_θ that was in the neighborhood of 500 even though $Re_{\theta,c}$ was infinite. Beyond the first 43 percent of the front face, Re_θ exceeded $Re_{\theta,m}$.

In figure 5b is shown the distribution of M_e, τ_w/τ_o, and Re_k. The maximum value of Re_k is about 1.7 and occurs on the radius of the nose corner. A smaller local maximum occurs at the cone-cylinder junction; its value is about .23. The wall temperature ratio was about .18 near the stagnation point and fell to about .10 at the end of the conical portion of the body.

Spherical-Segment Nose

In figure 6a is shown the variation of Re_θ, $Re_{\theta,m}$, and $Re_{\theta,c}$ with x for a body made up of a spherical segment followed by a cylinder (ref. (14)). The flow appeared to be laminar over the spherical face and over the cylinder at least as far back as x = .716, the location of the rearmost thermocouple. Note that Re_θ was small over the entire body. The maximum calculated value is about 170 just beyond the face-cylinder junction. The value of Re_θ then dropped rapidly to a minimum near 20 and then increased slowly to the rear. The values of Re_θ were so small that although they exceeded $Re_{\theta,m}$ at about 8° from the stagnation point they were never more than about 2 1/2 times as large as $Re_{\theta,m}$. Moreover, over the cylindrical portion of the body $Re_{\theta,m}$ exceeded Re_θ. It is noted that these values of $Re_{\theta,m}$ are calculated for an insulated surface and so may be too large because the ratio τ_w/τ_o is very low in the present case. Even if the values of $Re_{\theta,m}$ were only half of those shown, Re_θ would still be less than $Re_{\theta,m}$ over most of the cylindrical portion of the body and not much larger over the face. In the present case the boundary layer remained laminar where stability theory predicted it should.

In figure 6b is shown the distribution of M_e, τ_w/τ_o, and Re_k. Note the low values of τ_w/τ_o; this ratio was not greater than .12 over the entire body. Some data indicate that when the ratio τ_w/τ_o is small, of the order of .25 or so, transition occurs far forward on the body (refs. (20) and (21)). In this and in the previous case, where the wall temperature ratio was also near .12, laminar flow existed in spite of the low value of this ratio. It is noted, however, that although a large portion of the body was covered by laminar flow, the maximum values of Re_θ for the laminar flow were small. Also to be noted is that in the present and in the previous case the Reynolds number per foot, which, in reference (21), is stated to be important in the "transition-reversal" problem, was low.

Elliptical-Nose Cylinder

In figure 7a is shown the variation of Re_θ, and $Re_{\theta,m}$ with x for a body with an elliptical nose followed by a cylinder. This body is called "3-204-1" in references (15) and (16). The smallest value of $Re_{\theta,c}$ over the region of laminar flow is also listed. For this body, calculations were made for two meridian sections. Along section ABCEA' the measured surface roughness height was 1/2 microinch, root-mean-square. Along section ALM the measured roughness height was 1/2 microinch, rms up to x = .3491; for x > .3491 the roughness was 45 microinches, rms.

Along section ABCEA', the smooth section, transition began near x = 1.815. The nose-cylinder junction is at x = 1.115; consequently, laminar flow covered the face and a portion of the cylindrical afterbody equal in length to .7 of the cylinder radius. Transition began at a value of Re_θ of about 1080. Here again, transition began in a region in which $Re_{\theta,c}$ was very much larger than Re_θ. Transition was supposedly impossible ahead of x = .086, the region in which $Re_\theta < Re_{\theta,m}$.

In figure 7b is shown the distribution of local Mach number M_e, the ratio of the local wall temperature to the stagnation temperature $\mathfrak{t}_w/\mathfrak{t}_o$, and the local roughness Reynolds number, Re_k, for the smooth section, section ABCEA'. The peak in the distribution of M_e, at x = 1.2, was introduced by the procedure for smoothing the pressure distribution data. A small change in the pressure distribution near the face-cylinder junction is not believed to affect significantly any conclusions which depend on the values of Re_θ or Re_k further downstream.

The values of $\mathfrak{t}_w/\mathfrak{t}_o$ were low; they varied from about .2 near the stagnation point to about .13 near x = 1.858. The largest value of Re_k was about .0182 and occurred at x = .955. In the region in which transition began the value of Re_k was about .0004.

In figure 7c is shown the distribution of Re_k for section ALM. At the edge of the roughness patch, at x = .3491, the roughness Reynolds number jumped from about .0030 to about 24.5. Transition began somewhere between x = .4190 and x = .6290, not far from the start of the roughness patch.

DISCUSSION

Because the boundary-layer Reynolds number is zero at the stagnation point, the flow is always laminar there. Moreover, any disturbance of the laminar boundary layer will, because of the smallness of the Reynolds number near the stagnation point, die out as it proceeds downstream with the flow. Consequently, transition cannot occur very close to the stagnation point. Further back, however, the local boundary-layer Reynolds number usually becomes large enough for disturbances to the laminar flow to either cause transition almost immediately if they are large enough, or to grow as they proceed downstream. The disturbances that grow as they move downstream usually result in transition somewhere downstream of the location of initial amplification.

Comparison with Results of Stability Theory

Although the location where very small disturbances begin to grow can be calculated by the stability theory (ref. (1)), the transition position cannot be calculated because the disturbances soon become too large for the stability theory to apply. The stability theory is at present limited to wave-like disturbances whose amplitude is small enough to allow the equations of motion and energy to be linearized. In the present investigation the results of the stability theory are used to estimate the distribution of the critical Reynolds number, $Re_{\theta,c}$, along the body and thus also the point at which Re_θ exceeds $Re_{\theta,c}$. The critical Reynolds number of the present analysis is the Reynolds number below which all small two-dimensional wave-like disturbances die out. Above this Reynolds number, disturbances with the proper frequency can grow. Consequently, if Re_θ exceeds $Re_{\theta,c}$, disturbances can grow and the flow is unstable. Although Dunn and Lin (ref. (1)) have, in their stability theory for compressible flow, also treated disturbances that travel at an angle to the main stream, the present investigation estimates $Re_{\theta,c}$ only for disturbances that travel in the direction of the main flow. It is not clear just what sort of a spiral path a disturbance traveling at an angle to the main flow would take on a body of revolution.

Although the stability theory is derived for the flow over an infinite plane it is applied in the present investigation to the flow over a body of revolution. About 20 years ago, Pretsch showed that if the boundary-layer thickness over a body of revolution is a small fraction of the radius of curvature of the surface, the stability theory gives the same critical Reynolds number for the flow over a body of revolution as for the flow over an infinite plane (ref. (22)). Pretsch derived his result for incompressible flow. It is assumed that the same result is valid for compressible flow.

In the present analysis the values of $Re_{\theta,c}$ were obtained from the tables of reference (17). These values were calculated by use of Lees' formula for the rapid estimation of $Re_{\theta,c}$ (ref. (1)). Lees' formula is approximate and is probably a useful approximation only when the local Mach number outside the boundary layer is less than or not much larger than unity. It is remarked that for Mach numbers greater than about two, even the exact method of calculation of $Re_{\theta,c}$ appears still to be under development. For certain conditions Lees' formula predicts that $Re_{\theta,c}$ is infinite. It turns out that the formula provides a good estimate of these conditions (ref. (1)).

It is clear from the data in figures 1 to 7 and from the data in table 4 that transition not only occurred at values of Re_θ less than $Re_{\theta,c}$ but also occurred where $Re_{\theta,c}$ was infinite. Moreover, except for the 29° hemisphere-cone at $M_\infty = 2.32$ and at 2.47, transition, when it occurred, occurred even though $Re_{\theta,c}$ was much larger than Re_θ for the entire region between the stagnation point and the transition region. Consequently, it is concluded that for laminar flow to exist it is not sufficient that Re_θ be less than $Re_{\theta,c}$. Moreover, it is also concluded that the probable reason for the occurrence of transition even though Re_θ was less than $Re_{\theta,c}$, is that transition was not caused by the growth of the small two-dimensional wave-like disturbances imposed at one instant as assumed in the theory for the calculation of $Re_{\theta,c}$. Because the values of $Re_{\theta,c}$ are approximate, they may be too large. It is believed, however, that they are not sufficiently greater than the correct values to affect these conclusions.

Comparison with Calculated Minimum Transition Reynolds Numbers

When the disturbances to the laminar flow are large enough, transition can occur even though Re_θ is less than $Re_{\theta,c}$ (see for example, ref. (2) and ref. (23)). An attempt was previously made to estimate the smallest Reynolds number at which transition can begin (ref. (2)) and led to the result that this Reynolds number, called $Re_{\theta,m}$, is the value of Re_θ at which the local laminar and turbulent friction coefficients are equal. Consequently, in order to calculate the value of $Re_{\theta,m}$ at an arbitrary value of M_e and $\bar{t}_w/\bar{t}_o$ it is first necessary to calculate the effect of M_e and $\bar{t}_w/\bar{t}_o$ on the laminar and turbulent friction coefficients. This effect was calculated by use of the reference enthalpy method (ref. (24)). Because, however, of some uncertainty in the ability of the reference enthalpy method to predict the turbulent friction coefficient for cold walls, $Re_{\theta,m}$ was calculated under the assumption that a good estimate for $Re_{\theta,m}$ is the value for an insulated wall, even if the wall is colder (see ref. (2)). The use of the reference enthalpy method causes a decrease in the estimated value of $Re_{\theta,m}$ as the wall temperature is lowered. For example, the value of $Re_{\theta,m}$ at x = .7204 on the body designated as "spherical-segment-nose" cylinder, where $\bar{t}_w/\bar{t}_o$ is about .27 and M_e is 4.064, is slightly less than 50, whereas the value given in table 4 for an insulated wall and shown in figure 6a is 95.4. Consequently, for the bodies with cold walls the values of $Re_{\theta,m}$ given in table 4 may be as much as double the values that would have been calculated for the actual wall temperature ratios. This fact, however, does not change the conclusion illustrated in figure 8, namely, that the values of Re_θ at transition, called $Re_{\theta,T}$, were in all cases much larger than the values of $Re_{\theta,m}$ at transition. The value of $Re_{\theta,T}$ is taken at the last thermocouple at which the flow was laminar. Therefore, the transition point values of Re_θ are actually somewhat larger than those given in figure 8. Because all the values of $Re_{\theta,T}$ were larger than the values of $Re_{\theta,m}$ at transition, the present data show no contradiction of the concept or of the method for estimating $Re_{\theta,m}$.

Roughness Reynolds Number

The roughness Reynolds number, Re_k, was calculated because it is known to be a significant measure of the ability of roughness to cause transition. For example, investigators have found that the average value of Re_k needed to produce transition at a 1/4-inch wide strip of sandpaper-type roughness in subsonic flow is about 400 (see for example ref. (25)). Moreover, reference (25) states that the transition Reynolds number based on $\overline{x}$, decreases to 95 percent of its value without roughness when Re_k for a 1/4-inch wide strip of sandpaper is between 178 and 330.

For the bodies of revolution considered in the present investigation, Re_k begins at zero at the stagnation point and then increases; it may have one or more local maxima on the body. For the cases analyzed in the present investigation the maximum values of Re_k fall between .0082, calculated for the 29° hemisphere-cone at M_∞ = 2.32 and the value 30.80 calculated for section ALM of the Elliptical-Nose Cylinder. These values of Re_k are much smaller than the values of Re_k for which strips of sandpaper-type roughness first affect transition. For example, the largest value, 30.80, is about 1/6th of the smallest value, 178, reported for a 1/4-inch wide strip of sandpaper (ref. (25)).

In order to see whether or not there is any relation between the largest value of Re_k in the laminar boundary layer on a body of revolution and $Re_{\theta,T}$, the values of $Re_{\theta,T}$ were plotted against the largest value of Re_k ahead of transition for five of the seven cases analyzed (fig. 9). (See also Table 5) Two of the cases do not appear on figure 9 because for one of them, the Hemisphere-Cylinder, the flow was already turbulent at the first thermocouple located at 11 1/2° from the nose. Consequently, the last and only thermocouple that indicated laminar flow was the one at the nose. The original investigators (ref. (11)) suggest that perhaps irregularities other than the five-microinch surface roughness caused the early transition. The other case of the seven that does not appear in figure 9 is that for the Spherical-Segment-Nose Cylinder. In this case transition did not occur on the portion of the body containing thermocouples and so values of $Re_{\theta,T}$ could not be calculated.

The maximum value of Re_k ahead of transition, called $Re_{k,M}$, rather than its value at transition, was used because for a surface with continuously distributed roughness, $Re_{k,M}$ rather than $Re_{k,T}$, is a measure of the largest disturbance introduced into the boundary layer by the roughness and so is probably a better measure of the effect of roughness on transition than $Re_{k,T}$. The use of $Re_{k,M}$ is analogous to the use of Re_k when transition is caused by a roughness strip. Thus, when transition occurs downstream of the roughness strip, $Re_{k,T}$ is zero and the relation is between $Re_{\theta,T}$ and $Re_{k,M}$. Actually, a better criterion than either $Re_{k,M}$ or $Re_{k,T}$ is probably one that depends on the distribution of Re_k in the entire region upstream of transition.

It may be of interest to note that the data for a surface completely covered with sand roughness (ref. (26) and page 450 of ref. (22)) show that the transition point is first affected by roughness when $\bar{u}_e \bar{k}_s / \bar{\nu}_e$ reaches about 120, or about 60 when the nominal height $\bar{k}$ is substituted for the equivalent sand roughness $\bar{k}_s$. The associated value of $Re_{x,T}$ is about $.664 \times 10^6$. For these data transition is therefore first affected when $Re_{k,M}$ is near 60. On the other hand, a calculation of $Re_{k,T}$ for these data results in a value of about 1.5. This number is obtained from the definition

$$Re_K = \frac{\bar{u}_K \bar{K}}{\bar{\nu}} \qquad \text{(incompressible flow)}$$

where

$$u_K = \left(\frac{\partial \bar{u}}{\partial \bar{y}}\right)_w K \qquad \left(\frac{\bar{K}}{\bar{\delta}} \text{ small}\right)$$

and the relation,

$$\left(\frac{\partial \bar{u}}{\partial \bar{y}}\right)_w = \frac{\bar{\tau}_w}{\bar{\mu}}$$

Then

$$Re_K = \left(\frac{\bar{u}_e \bar{K}}{\bar{\nu}}\right)^2 \frac{\bar{\tau}_w}{\bar{\rho}\, \bar{u}_e^2}$$

but

$$\frac{\tau_w}{\bar{\rho} \bar{u}_e^2} = \frac{.332}{\sqrt{Re_x}}$$

for the zero pressure gradient data of reference (26). Therefore

$$Re_K = \frac{.332}{\sqrt{Re_x}} \left(\frac{\bar{u}_e \bar{K}}{\bar{\nu}} \right)^2$$

For

$$Re_x = .664 \times 10^6 \quad \text{and} \quad \left(\frac{\bar{u}_e \bar{K}}{\bar{\nu}} \right) = 60$$

the result is

$$Re_K = 1.47$$

That is, the value of $Re_{k,T}$ when transition first begins to move forward on a surface with continously distributed roughness is much less than values of Re_k previously quoted for the first effect of roughness strips on transition (ref. (25)). Note, however, that values of $Re_{k,T}$ not far from 1.47 have previously appeared in the literature. For example, in reference (27) a value of $Re_{k,T}$ as low as 7.35 is given. Moreover, in reference (19) a still lower value of $Re_{k,T}$, namely, about two is given. In this case the value of Re_k at the location where $\bar{k}$ is equal to $\bar{\delta}$ is about 400; this value is thus equal to $Re_{k,M}$. Consequently, it appears that for surfaces completely covered with roughness the value of $Re_{k,T}$ can be near unity where transition is first affected by the roughness. The smallest value of $Re_{k,M}$ previously given in the literature, seems, however, to be that of reference (26), that is, a value near 60.

The data in figure 9 cover a range of $Re_{k,M}$ from about .008 to about 31, that is, from about 1/7000 to about 1/2 of the value 60. The largest value, 30.8, occurred on a patch of roughness that caused $Re_{\theta,T}$ to drop from about 1082 to about 177 on the Elliptical-Nose Cylinder. Consequently, transition is affected when $Re_{k,M}$ is as low as 30.8. Moreover, the data in figure 9 indicate that the two points for the Elliptical-Nose Cylinder, namely, the points for $Re_{k,M}$ of 30.8 and .01825, are consistent with the variation between $Re_{\theta,T}$ and $Re_{k,M}$ indicated by the other four sets of data. It is emphasized that all the data of figure 9 are for blunt bodies of revolution in supersonic flight with $Re_{\theta,c}$ much larger than Re_θ.

The line drawn through the data in figure 9 is a least-squares line for log $Re_{\theta,T}$ against log $Re_{k,M}$. Its equation is

$$Re_{\theta,T} = \frac{424}{Re_{K,M}^{\;.188}}$$

Although the equation of the line is given, it is not concluded that figure 9 establishes a connection between $Re_{\theta,T}$ and $Re_{k,M}$. The reason is that an application of the information in reference (28) shows that the scatter of the data around the least-squares line is too large to allow the conclusion to be drawn from only five sets of data that figure 9 establishes a relation between $Re_{\theta,T}$ and $Re_{k,M}$ for blunt bodies of revolution in supersonic flight with $Re_{\theta,c}$ much greater than Re_{θ}.

On the other hand, even if there really were a relation between $Re_{\theta,T}$ and $Re_{k,M}$ somewhat like that shown by the least-squares line of figure 9, some scatter of the data would still be expected. The reasons are: first, the values of $Re_{\theta,T}$ were computed for the rearmost thermocouple at which the flow was laminar. Because transition often began between two thermocouples, its precise location and, consequently, the precise value of $Re_{\theta,T}$, could not be found. Second, the value of the surface roughness was not obtained in the same way in all the tests (see Table 3). Consequently, some of the roughness Reynolds numbers probably are not directly comparable. Note that Re_k is proportional to the roughness height squared. Third, the surfaces were not all finished by the same process and so two surfaces with the same measured roughness height can affect transition differently (see ref. (29)). The fourth reason is that not every part of the surface of the bodies could be examined with a microscope. Fifth, these roughness data are for the bodies before flight. Because the bodies could not be examined after flight the conditions of their surfaces when transition occurred are not really known. These reasons would probably be sufficient to cause a fairly large amount of scatter even if there were a strong connection between $Re_{\theta,T}$ and $Re_{k,M}$. In spite of these reasons for the data to scatter, it is probably not correct to conclude anything more from figure 9 than that the previous impression, namely, "the smoother the surface the greater the likelihood of extensive regions of laminar flow," is re-enforced by these data.

It is remarked that a plot of $Re_{\theta,T}$ against $(\bar{t}_w/\bar{t}_e)_T$, shown in figure 10, (see also Table 5) indicates a very much weaker connection between $Re_{\theta,T}$ and $(\bar{t}_w/\bar{t}_e)_T$ than indicated in figure 9 between $Re_{\theta,T}$ and $Re_{k,M}$. Note the large amount of scatter. The line drawn in figure 10 is a least-squares line for log $Re_{\theta,T}$ against log $(\bar{t}_w/\bar{t}_e)_T$ and has the equation

$$Re_{\theta,T} = 650\left(\frac{\bar{t}_w}{\bar{t}_e}\right)^{.415}$$

SUMMARY

Because of the importance of aerodynamic heating at high speeds and because the rate of heat transfer is much greater for a turbulent than for a laminar boundary layer it is important to be able to estimate the location at which the flow changes from laminar to turbulent. The main result of previous theoretical work is a theory that can be used to estimate the location at which the laminar boundary layer becomes unstable once the necessary parameters of the laminar boundary layer are known. In the present investigation these parameters are calculated by the Cohen and Reshotko method for seven blunt bodies of revolution flying at supersonic speeds. A comparison of the results of the stability theory with transition points determined from heat-transfer distributions obtained for these bodies by previous investigators then shows that when transition occurred it took place even though the boundary layer was computed to be very stable for the entire region between the stagnation and the transition point. It is suggested that in these cases transition probably was not caused by the growth of the small two-dimensional wave-like disturbances imposed at one instant as assumed in the stability theory used in the present investigation.

In every case transition occurred at a larger boundary-layer Reynolds number than the estimated minimum Reynolds number for transition. Consequently, no contradiction of the assumption that there is a minimum transition Reynolds number and no disagreement with the results of the method for estimating this Reynolds number was found.

A plot of the calculated boundary-layer Reynolds number at transition against the calculated maximum roughness Reynolds number ahead of transition for the five of the seven sets of data for which transition data were available apparently showed a connection. A further examination indicated, however, that the scatter of these data is too large to allow the conclusion to be drawn from only five sets of data that there really is a connection. The conclusion seems to be only that the likelihood of obtaining large regions of laminar flow increases as the body is made smoother. It is remarked that the dependence of the boundary-layer Reynolds number at transition on the wall temperature ratio at transition was very much weaker than on the maximum roughness Reynolds number.

REFERENCES

(1) Lin, C. C., "The Theory of Hydrodynamic Stability," Cambridge University Press, 1955

(2) Tetervin, Neal, "An Estimate of the Minimum Reynolds Number for Transition from Laminar to Turbulent Boundary-Layer Flow by Means of Energy Considerations," NAVORD Report 6854, 1960

(3) Cohen, Clarence B. and Reshotko, G., "The Compressible Laminar Boundary Layer with Heat Transfer and Arbitrary Pressure Gradient," NACA TR 1294, 1956

(4) Handbook of Supersonic Aerodynamics, NAVORD Report 1488 (Vol. 1), 1950

(5) Feldman, Saul, "Hypersonic Gas Dynamic Charts for Equilibrium Air," Research Report No. 40, AVCO Research Laboratory, 1957

(6) Ames Research Staff, "Equations, Tables, and Charts for Compressible Flow," NACA TR 1135, 1953

(7) Hansen, C. Frederick, "Approximations for the Thermodynamic and Transport Properties of High-Temperature Air," NASA TR R-50, 1959

(8) Milne, W. E., "Numerical Calculus," Princeton University Press, 1949

(9) Buglia, J. James, "Heat Transfer and Boundary-Layer Transition on a Highly Polished Hemisphere-Cone in Free Flight at Mach Numbers up to 3.14 and Reynolds Numbers up to 24 x 10^6," NASA TN D-955, 1961

(10) Chauvin, L. T. and Speegle, K. C., "Boundary-Layer Transition and Heat Transfer Measurements from Flight Tests of Blunt and Sharp 50° Cones at Mach Numbers from 1.7 to 4.7," NACA RM L57D04, 1957

(11) Krasnican, M. J. and Wisniewski, R. J., "Free-Flight Determination of Boundary-Layer Transition and Heat Transfer for a Hemisphere-Cylinder at Mach Numbers to 5.6," NACA RM E57F10, 1957

(12) Garland, B. J., Swanson, A. G., and Speegle, K. C., "Aerodynamic Heating and Boundary-Layer Transition on a 1/10-Power Nose Shape in Free Flight at Mach Numbers up to 6.7 and Free-Stream Reynolds Numbers up to 16 x 10^6," NACA RM L57E14a, 1957

(13) Rumsey, C. B. and Lee, D. B., "Heat-Transfer Measurements in Free Flight at Mach Numbers up to 14.6 on a Flat-Faced Conical Nose with a Total Angle of 29°," NACA RM L57L03, 1958

(14) Rumsey, C. B. and Lee, D. B., "Heat-Transfer Measurements on a Blunt Spherical-Segment Nose to a Mach Number of 15.1 and Flight Performance of the Rocket-Propelled Model to a Mach Number of 17.8," NASA TMX-77, 1959

(15) Lockheed Technical Memorandum S2-60-11, "Preliminary Flight Test Analysis for the 3-204-1 Flight Test Vehicle," September 1957

(16) Lockheed Polaris Missile System, FTV3 Series, Special Test Vehicles, Missile Final Test Report, August 1958

(17) Tetervin, Neal, "Charts and Tables for Estimating the Stability of the Compressible Laminar Boundary Layer with Heat Transfer and Arbitrary Pressure Gradient," NASA Memo 5-4-59L, 1959

(18) Butler, John F., "A Fortran II (IBM-704) Subroutine for the Solution of Ordinary Differential Equations with Automatic Linkage, Termination and Output Features," NAVORD Report 6701, October 1959

(19) Jones, Jim J., "Experimental Investigation of the Heat-Transfer Rate to a Series of 20° Cones of Various Surface Finishes at a Mach Number of 4.95," NASA Memo 6-10-59L, 1959

(20) Jack, John R., Wisniewski, Richard J., and Diaconis, N. S., "Effects of Extreme Surface Cooling on Boundary-Layer Transition," NACA TN 4094, 1957

(21) Wisniewski, Richard J. and Jack, John R., "Recent Studies on the Effect of Cooling on Boundary-Layer Transition at Mach 4," Jour. Aero/Space Sci., Vol. 28, No. 3, pp. 250-251, March 1961

(22) Schlichting, H., "Boundary Layer Theory," McGraw-Hill Book Co., New York, 1960

(23) Elder, J. W., "An Experimental Investigation of Turbulent Spots and Breakdown to Turbulence," Jour. Fluid Mech., 9, 2, pp. 235-246, October 1960

(24) Eckert, Ernst R. G., "Survey on Heat Transfer at High Speeds," Aero. Res. Lab., WADC Technical Report 54-70 (Contract AF 33(616)-2214), 1954

(25) Smith, A. M. O. and Clutter, D. W., "The Smallest Height of Roughness Capable of Affecting Boundary Layer Transition," Jour. Aero. Sci., Vol. 26, No. 4, pp. 229-245, April 1959

(26) Feindt, E. G., "Untersuchungen uber die Abhangigkeit des Umschlages laminar-turbulent von der Oberflachenrauhigkeit und der Druckverteilung," Jahrbuch 1956 der Schiffbautechnischen Gesellschaft, 50, pp. 180-203, 1957

(27) Bandettini, Angelo and Isler, Walter E., "Boundary-Layer-Transition Measurements on Hemispheres of Various Surface Roughnesses in a Wind Tunnel at Mach Numbers from 2.48 to 3.55," NASA Memo 12-25-58A, 1959

(28) Freund, John E., "Modern Elementary Statistics," Prentice-Hall, New York, 1952

(29) Wilkens, M. E. and Darsow, J. F., "Finishing and Inspection of Model Surfaces for Boundary-Layer-Transition Tests," NASA Memo 1-19-59A, 1959

(30) Stoney, William E., Jr. and Swanson, Andrew G., "Heat Transfer Measured on a Flat-Face Cylinder in Free Flight at Mach Numbers up to 13.9," NACA RM L57E13, 1957

(31) Wagner, Richard D., Jr., "Some Aspects of the Modified Newtonian and Prandtl-Meyer-Expansion Method for Axisymmetric Blunt Bodies at Zero Angle of Attack," Jour. Aero/Space Sci., pp. 851-852, December 1959

Table 1

BODY AND FLIGHT PARAMETERS

Body	M_∞	Re_∞	Re_L	L feet	T_∞ °R	$\bar{\rho}_\infty$ slugs/cu ft	$\frac{T_o}{T_\infty}$	$\frac{p_o}{p_\infty}$	H_o, BTU/slug	γ_E	$\frac{T_{wo}}{T_o}$	d	Pr_w	$H\sqrt{Re_L}$ o	$\left(\frac{d^2 \frac{C_p}{C_{p_o}}}{dx^2}\right)_o$	Reference
29° Hemisphere-Cone	2.32	7.094×10^6	2.081×10^7	.5415	500.7	18.88×10^{-4}	2.076	7.413	8035	1.4	.700	1	.75	.3951	-2.000	9
	2.47	7.470×10^6	2.141×10^7	.5415	500.0	18.60×10^{-4}	2.220	8.333	8580	1.4	.670	1	.75	.3990	-2.000	9
	2.63	7.850×10^6	2.194×10^7	.5415	499.0	18.31×10^{-4}	2.383	9.382	9181	1.4	.630	1	.75	.4047	-2.000	9
	2.80	8.231×10^6	2.231×10^7	.5415	497.9	19.00×10^{-4}	2.569	10.57	9870	1.4	.602	1	.75	.4098	-2.000	9
	2.97	8.610×10^6	2.265×10^7	.5415	496.6	17.67×10^{-4}	2.765	11.83	10,610	1.4	.580	1	.75	.4136	-2.000	9
	3.14	8.935×10^6	2.281×10^7	.5415	495.0	17.34×10^{-4}	2.972	13.17	11,360	1.4	.566	1	.75	.4163	-2.000	9
50° Hemisphere Cone	2.5	4.920×10^6	1.405×10^7	.3700	507.0	17.70×10^{-4}	2.250	8.525	8820	1.4	.6632	1	.76	.4000	-2.000	10
	3.0	5.770×10^6	1.515×10^7	.3700	502.0	17.00×10^{-4}	2.800	12.06	10,860	1.4	.5731	1	.76	.4151	-2.000	10
	3.5	6.515×10^6	1.619×10^7	.3700	497.0	16.40×10^{-4}	3.446	16.24	13,260	1.4	.5171	1	.76	.4269	-2.000	10
	4.0	7.180×10^6	1.573×10^7	.3700	491.0	15.80×10^{-4}	4.200	21.06	15,940	1.4	.4812	1	.76	.4366	-2.000	10
	4.7	8.030×10^6	1.558×10^7	.3700	487.0	15.00×10^{-4}	5.417	28.91	20,400	1.4	.4600	1	.76	.4444	-2.000	10
Hemisphere-Cylinder	3.0	4.875×10^6	1.270×10^7	.3750	472.0	14.09×10^{-4}	2.797	12.06	10,210	1.4	.3902	1	.76	.4504	-2.000	11
	4.0	6.675×10^6	1.568×10^7	.3750	475.0	14.36×10^{-4}	4.000	21.06	15,410	1.4	.2790	.9525	.76	.4870	-2.000	11
	4.6	7.875×10^6	1.701×10^7	.3750	478.0	14.76×10^{-4}	4.920	27.71	19,310	1.4	.2550	.9420	.76	.5022	-2.000	11
	5.2	9.112×10^6	1.848×10^7	.3750	480.0	15.25×10^{-4}	5.900	35.29	23,780	1.38	.2414	.9210	.76	.5186	-2.000	11
	5.5	9.750×10^6	1.937×10^7	.3750	482.0	15.49×10^{-4}	6.930	39.42	26,260	1.37	.2387	.9068	.76	.5252	-2.000	11
"1/10th-Power" Nose Cylinder	1.72	2.875×10^6	$.9090\times10^7$	.2500	519.0	22.20×10^{-4}	1.591	4.310	6381	1.4	.6525	1	.75	.6627	-.2980	12
	2.33	3.750×10^6	1.103×10^7	.2500	517.0	21.60×10^{-4}	2.087	7.474	8330	1.4	.5119	1	.75	.7087	-.2640	12
	2.71	4.150×10^6	1.150×10^7	.2500	512.0	20.30×10^{-4}	2.469	9.930	9770	1.4	.5042	1	.75	.7164	-.2560	12
	3.18	4.575×10^6	1.164×10^7	.2500	502.0	19.10×10^{-4}	3.022	13.50	11,730	1.4	.4528	1	.75	.7409	-.2480	12
	4.25	5.900×10^6	1.236×10^7	.2500	495.0	18.40×10^{-4}	4.612	23.72	17,650	1.4	.3469	1	.75	.8042	-.2400	12
	5.14	6.900×10^6	1.313×10^7	.2500	491.0	17.60×10^{-4}	6.085	34.48	23,840	1.377	.3093	.9685	.75	.8525	-.2360	12
	6.10	7.750×10^6	1.466×10^7	.2500	490.0	16.70×10^{-4}	7.300	48.38	31,970	1.342	.3009	.8640	.75	.9040	-.2340	12
	6.68	8.150×10^6	1.520×10^7	.2500	488.0	16.00×10^{-4}	8.000	55.01	37,410	1.305	.3233	.8020	.76	.9275	-.2340	12
Flat-Face Cone-Cylinder	10.0	$.3230\times10^6$	$.04875\times10^7$	.10858	395.5	$.9080\times10^{-4}$	15.00	130.0	64,200	1.172	.1311	.7200	.740	1.291	-.1882	13
	13.0	$.6050\times10^6$	$.09490\times10^7$	.10858	388.8	1.300×10^{-4}	19.72	221.0	104,550	1.145	.1672	.5812	.747	1.300	-.1877	13
	14.5	$.8210\times10^6$	$.1236\times10^7$	.10858	383.8	1.587×10^{-4}	22.60	274.0	127,700	1.138	.1833	.5447	.750	1.296	-.1875	13
Spherical-Segment-Nose Cylinder	8.4	$.3600\times10^6$	$.0578\times10^7$	.4875	423.8	$.2760\times10^{-4}$	12.4	97.0	49,500	1.303	.1375	.8200	.742	.5530	-3.275	14
	10.8	$.5288\times10^6$	$.0899\times10^7$	.4875	420.2	$.3180\times10^{-4}$	16.0	163.0	79,050	1.245	.1258	.6572	.742	.5982	-3.259	14
	15.1	$.8550\times10^6$	$.1322\times10^7$	.4875	417.0	$.3690\times10^{-4}$	24.4	320.0	150,000	1.215	.1180	.5335	.748	.6402	-3.249	14
Elliptical-Nose Cylinder	13.29	4.690×10^6	$.6990\times10^7$	.2983	392.4	3.610×10^{-4}	21.2	233.0	110,100	1.226	.1852	.6020	.77	.7540	-1.064	15, 16

Table 2

BODY PRESSURE DISTRIBUTION, WALL TEMPERATURE DISTRIBUTION, AND RADIUS DISTRIBUTION DATA

Body	Pressure Distribution	Wall Temperature Distribution	Radius Distribution
29° Hemisphere-Cone reference (9)	$0 \le x \le .8$ $C_p/C_{p_o} = \cos^2 x$ $x \ge .8$ From dashed line of figure 8 of reference (9)	Tabular representation of $\bar{t}_w, \bar{t}_e$. Obtained from reference (9).	$0 \le x \le 1.31772$ R=sin x $x \ge 1.31772$ R= sin 75.5° (x-1.31772)sin 14.5
50° Hemisphere-Cone reference (10)	$C_p/C_{p_o} = \cos^2 x$	Tabular representation of $\bar{t}_w$. Obtained from reference (10).	R=sin x
Hemisphere Cylinder reference (11)	$C_p/C_{p_o} = \cos^2 x$	Tabular representation of $\bar{t}_w$. Obtained from reference (11).	R=sin x
"1/10th-Power" Nose Shape reference (12)	Tabular representation of $\bar{p}_e/\bar{p}_o$ from "measured" curve of figure 9 of reference (12)	Tabular representation of $\bar{t}_w$. Obtained from reference (12).	Tabular representation obtained from $R = A x_a^{\frac{1}{10}} + B x_a$ where $A = .79750(3^{\frac{1}{10}})$ $B = .062349$ and $x = \int_0^r \sqrt{1+\left(\frac{dx_a}{dR}\right)^2}\, dR$
Flat-Face Cone-Cylinder reference (13)	$0 < x < .9800$ Tabular representation of $\bar{p}_e/\bar{p}_o$ from "measured" curve (M_∞=2) of figure 15 of reference (30). $.9800 < x < 1.411$, fairing between end $\bar{p}_e/\bar{p}_o$ values. $1.411 < x < 4.361$, $\bar{p}_e/\bar{p}_o$ equal to value for sharp cone. $4.361 < x < 4.711$, fairing between end $\bar{p}_e/\bar{p}_o$ values. $x > 4.711$, $\bar{p}_e/\bar{p}_o$ equal to $\bar{p}_\infty/\bar{p}_o$	Tabular representation of $\bar{t}_w$. Obtained from reference (13).	$0 < x < 1$, R=x $1 < x \le 1.1264$, $R = 1 + .09592 \sin\left(\frac{x-1}{.09592}\right)$ $1.1264 < x < 4.607$, $R = 1.0928 + .2504(x-1.1264)$ $x > 4.607$, R=1.968
Spherical-Segment-Nose Cylinder reference (14)	$0 < x < .46$ Tabular representation of $\bar{p}_e/\bar{p}_o$ from figure 17 of reference (14). $.46 \le x \le .5210$, fairing between end $\bar{p}_e/\bar{p}_o$ values. $x > .5210$, $\bar{p}_e/\bar{p}_o$ equal to $\bar{p}_\infty/\bar{p}_o$	Tabular representation of $\bar{t}_w$. Obtained from reference (14).	$0 \le x \le .46$ R=sin x $x > .46$ R=.4444
Elliptical-Nose Cylinder references (15) and (16)	$0 < x < 1.1147$ C_p/C_{p_o} obtained from reference (31). $x > 1.1147$, $\bar{p}_e/\bar{p}_o$ from curve faired through data of figure 15 of reference (15), with $\bar{p}_e/\bar{p}_o = .0491$ at x=1.1147	Tabular representation of $\bar{t}_w$. Obtained from reference (15).	$0 < x < 1.1147$ Tabular representation obtained from $x = \int_0^{\sin^{-1}R} \sqrt{1-B^2\sin^2\nu}\, d\nu$ $B^2 = 1 - \left(\frac{1.2}{3.58}\right)^2$ $x > 1.1147$ R = 1 Also, $\frac{\left(x_a - \frac{1.2}{3.58}\right)^2}{\left(\frac{1.2}{3.58}\right)^2} + R^2 = 1$

Table 3

SURFACE ROUGHNESS DATA

Body	Surface Roughness (m, microinches)	Method of Measurement	Roughness Height to Calculate Re_k
29° Hemisphere-Cone reference (9)	2 to 3 m on hemispherical portion of nose. 3 to 5 m on conical portion.	Interferometer microscope	$0 \leq x \leq 1.326$ 3 m $x > 1.326$ 5 m
50° Hemisphere-Cone reference (10)	Approximately 25 m rms before surface oxidation to stabilize emissivity.	Profilometer	70.7 m
Hemisphere Cylinder reference (11)	3 to 5 m in vicinity of stagnation point; 5 m aft of stagnation region on hemisphere-cylinder forebody. Scratches of order of 15 m aft of stagnation region.	Interferometer microscope on a sample of nickel polished in a manner similar to that used on the polished nose section.	5 m
"1/10th-Power" Nose Shape reference (12)	Average of 6 to 8 m Maximum of 15 m	Surface finish attained with No. 600 paper	15 m
Flat-Face Cone-Cylinder reference (13)	15 to 20 m; several fine scratches much deeper than 20 m	Interferometer microscope	20 m
Spherical-Segment-Nose Cylinder reference (14)	15 to 20 m; several fine scratches much deeper than 20 m.	Interferometer microscope	20 m
Elliptical-Nose Cylinder references (15) and (16)	1/2 m rms along meridian ABCEA' Patch of 45 m rms along meridian ALM for $x > .3491$ 11 individual surface defects with depth greater than 20 m. Deepest pit 70 m deep and 800 m in diameter at position E.* Remainder of pits less than 40 m deep. * ($x = 1.181$)	Individual surface defects by electronic microscope	1.415 m along ABCEA' 127.3 m along ALM for $x > .3491$, 1.415 m for $x < .3491$

Table 4a

CALCULATED BOUNDARY-LAYER PARAMETERS

29^{o} Hemisphere-Cone

$M_\infty = 2.32$

x	S_w	M_e	$\frac{Re_k}{k^2 Re_L^{3/2}}$	Re_θ	St_∞ x10^3	$\frac{d\left(\frac{C_p}{C_{p_o}}\right)}{dx}$	$Re_{\theta,c}$ x10^{-4}	$Re_{\theta,m}$
0.	-.2999	0.	0.	0.	0.7379	0.	2.2	53.8
0.04497	-.3006	0.0500	0.04535	40.31	0.7366	-0.04132	2.2	53.9
0.1450	-.3019	0.1615	0.1426	130.6	0.7202	-0.2658	2.2	54.0
0.2450	-.3048	0.2742	0.2310	219.7	0.7024	-0.4717	2.3	54.4
0.3450	-.3094	0.3887	0.3050	307.1	0.6761	-0.6357	2.4	55.0
0.4450	-.3153	0.5058	0.3604	392.4	0.6415	-0.7753	2.6	55.9
0.5450	-.3224	0.6266	0.3939	474.8	0.5994	-0.8842	2.8	57.0
0.6450	-.3305	0.7519	0.4044	554.1	0.5506	-0.9592	3.2	58.4
0.7450	-.3385	0.8827	0.3918	629.8	0.4960	-1.015	4.0	60.2
0.8450	-.3444	1.025	0.3635	700.7	0.4300	-1.063	7.0	62.9
0.9450	-.3612	1.188	0.3300	767.3	0.3621	-1.109	57.0	66.2
1.045	-.3921	1.386	0.2891	834.4	0.2908	-1.108	99.0	70.8
1.145	-.4079	1.605	0.1996	902.6	0.2335	-0.8056	∞	74.6
1.245	-.4132	1.764	0.1192	971.4	0.2163	-0.3538	∞	73.7
1.345	-.4040	1.825	0.07277	1044.	0.2161	-0.08052	∞	65.0
1.445	-.3957	1.829	0.05052	1121.	0.2047	-0.03477	3.9	52.2
1.545	-.3926	1.811	0.03832	1196.	0.1972	-0.08448	0.044	39.9
1.645	-.3866	1.780	0.03259	1274.	0.1951	-0.1016	0.0080	17.8
1.745	-.3777	1.747	0.03225	1352.	0.1927	+0.09353	0.0081	19.0
1.845	-.3699	1.722	0.03524	1421.	0.1853	+0.07064	0.028	38.6
1.945	-.3648	1.707	0.03978	1481.	0.1751	+0.04030	0.35	46.5
2.045	-.3616	1.701	0.04315	1532.	0.1662	+0.01460	5.4	52.6
2.145	-.3578	1.699	0.04317	1578.	0.1594	+0.00264	23.0	55.4

Table 4a

CALCULATED BOUNDARY-LAYER PARAMETERS

29° Hemisphere-Cone

$M_\infty = 2.32$ (cont'd)

x	S_w	M_e	$\frac{Re_k}{k^2 Re_L{}^{3/2}}$	Re_θ	St_∞ x10^3	$\frac{d\left(\frac{C_p}{C_{p_o}}\right)}{dx}$	$Re_{\theta,c}$ x10^{-4}	$Re_{\theta,m}$
2.245	-.3517	1.698	0.04134	1620.	0.1545	0.	28.0	56.0
2.345	-.3425	1.698	0.03889	1658.	0.1504	-0.00013	23.0	56.0
2.445	-.3306	1.698	0.03624	1693.	0.1465	-0.00003	17.0	56.0
2.545	-.3169	1.698	0.03364	1726.	0.1429	0.	12.0	56.0
2.645	-.3042	1.698	0.03142	1758.	0.1396	0.	8.6	56.0
2.745	-.2940	1.698	0.02968	1789.	0.1366	0.	6.6	56.0

Laminar at x = 2.100
Turbulent at x = 2.822

Table 4a

CALCULATED BOUNDARY-LAYER PARAMETERS

29° Hemisphere-Cone

$M_\infty = 2.47$

x	S_w	M_e	$\frac{Re_k}{k^2 Re_L^{3/2}}$	Re_θ	St_∞ x10^3	$\frac{d\left(\frac{C_p}{C_{p_o}}\right)}{dx}$	$Re_{\theta,c}$ x10^{-4}	$Re_{\theta,m}$
0.	-.3300	0.	0.	0.	0.7502	0.	2.5	53.7
0.04458	-.3303	0.0500	0.04999	41.28	0.7488	-0.04097	2.5	53.8
0.1446	-.3333	0.1625	0.1591	134.5	0.7336	-0.2649	2.7	54.1
0.2446	-.3384	0.2762	0.2599	226.6	0.7158	-0.4710	2.8	54.6
0.3446	-.3452	0.3918	0.3460	317.1	0.6891	-0.6351	2.9	55.2
0.4446	-.3536	0.5102	0.4122	405.4	0.6540	-0.7748	3.2	56.1
0.5446	-.3625	0.6325	0.4530	490.9	0.6108	-0.8838	3.6	57.2
0.6446	-.3720	0.7597	0.4668	573.0	0.5607	-0.9590	4.1	58.6
0.7446	-.3818	0.8928	0.4541	651.5	0.5047	-1.015	5.3	60.4
0.8446	-.3910	1.038	0.4242	725.4	0.4380	-1.063	11.0	63.1
0.9446	-.4005	1.206	0.3724	793.7	0.3655	-1.109	∞	66.6
1.045	-.4127	1.411	0.3011	860.0	0.2861	-1.109	∞	71.4
1.145	-.4253	1.643	0.2011	928.6	0.2242	-0.8071	∞	75.7
1.245	-.4246	1.816	0.1139	996.0	0.2030	-0.3555	∞	75.4
1.345	-.4237	1.883	0.07249	1067.	0.2054	-0.08132	∞	66.6
1.445	-.4286	1.888	0.04998	1143.	0.1943	+0.03445	3.8	52.3
1.545	-.4297	1.868	0.03654	1213.	0.1801	+0.08433	0.045	35.9
1.645	-.4253	1.834	0.03039	1285.	0.1731	+0.1016	0.0090	3.76
1.745	-.4189	1.798	0.03108	1358.	0.1719	+0.09358	0.0094	7.74
1.845	-.4131	1.770	0.03589	1422.	0.1710	+0.07074	0.035	34.6
1.945	-.4087	1.754	0.04254	1479.	0.1685	+0.04042	0.52	46.6
2.045	-.4047	1.747	0.04735	1529.	0.1646	+0.01468	11.0	53.0

Table 4a

CALCULATED BOUNDARY-LAYER PARAMETERS

29° Hemisphere-Cone

M_{∞} = 2.47 (cont'd)

x	S_w	M_e	$\frac{Re_k}{k^2 Re_L^{3/2}}$	Re_θ	St_∞ x10^3	$\frac{d\left(\frac{C_p}{C_{p_o}}\right)}{dx}$	$Re_{\theta,c}$ x10^{-4}	$Re_{\theta,m}$
2.145	-.3990	1.745	0.04740	1576.	0.1594	+0.00267	63.0	55.9
2.245	-.3915	1.744	0.04511	1618.	0.1546	0.	80.0	56.6
2.345	-.3828	1.744	0.04237	1658.	0.1503	-0.00009	64.0	56.6
2.445	-.3716	1.744	0.03945	1694.	0.1463	0.	48.0	56.6
2.545	-.3593	1.744	0.03668	1728.	0.1426	0.	35.0	56.6
2.645	-.3453	1.744	0.03396	1761.	0.1392	0.	24.0	56.6
2.745	-.3276	1.744	0.03107	1790.	0.1358	0.	15.0	56.6

Laminar at x = 2.100
Turbulent at x = 2.822

Table 4a

CALCULATED BOUNDARY-LAYER PARAMETERS

29° Hemisphere-Cone

$M_\infty = 2.63$

x	S_w	M_e	$\frac{Re_k}{k^2 Re_L^{3/2}}$	Re_θ	St_∞ x10^3	$\frac{d\left(\frac{C_p}{C_{p_o}}\right)}{dx}$	$Re_{\theta,c}$ x10^{-4}	$Re_{\theta,m}$
0.	-.3678	0.	0.	0.	0.7640	0.	3.2	53.9
0.04425	-.3684	0.0500	0.05697	42.39	0.7626	-0.04066	3.2	53.9
0.1442	-.3706	0.1634	0.1820	138.6	0.7489	-0.2641	3.3	54.2
0.2442	-.3740	0.2779	0.2959	233.5	0.7303	-0.4704	3.4	54.6
0.3442	-.3780	0.3946	0.3900	326.6	0.7023	-0.6346	3.5	55.3
0.4442	-.3827	0.5142	0.4583	417.0	0.6656	-0.7743	3.8	56.2
0.5442	-.3887	0.6378	0.4979	504.4	0.6209	-0.8835	4.1	57.3
0.6442	-.3961	0.7667	0.5084	588.1	0.5691	-0.9588	4.7	58.7
0.7442	-.4049	0.9019	0.4915	668.0	0.5115	-1.015	6.2	60.5
0.8442	-.4153	1.050	0.4592	743.4	0.4435	-1.063	15.0	63.4
0.9442	-.4296	1.222	0.4079	814.0	0.3701	-1.109	∞	66.8
1.044	-.4492	1.435	0.3356	883.9	0.2893	-1.109	∞	71.9
1.144	-.4694	1.679	0.2269	957.5	0.2232	-0.8085	∞	76.4
1.244	-.4772	1.865	0.1300	1029.	0.1958	-0.3569	∞	76.8
1.344	-.4680	1.940	0.07596	1098.	0.1956	-0.0820	∞	68.4

Laminar at x = 1.049
In transition at x = 1.326

Table 4a

CALCULATED BOUNDARY-LAYER PARAMETERS

29° Hemisphere-Cone

$M_\infty = 2.80$

x	S_w	M_e	$\frac{Re_k}{k^2 Re_L^{3/2}}$	Re_θ	St_∞ x10^3	$\frac{d\left(\frac{C_p}{C_{p_o}}\right)}{dx}$	$Re_{\theta,c}$ x10^{-4}	$Re_{\theta,m}$
0.	-.3990	0.	0.	0.	0.7774	0.	3.8	54.0
0.04395	-.3992	0.0500	0.06360	43.28	0.7759	-0.04039	3.8	54.1
0.1440	-.4003	0.1641	0.2035	141.8	0.7634	-0.2634	3.9	54.3
0.2440	-.4026	0.2795	0.3296	239.1	0.7442	-0.4698	4.0	54.7
0.3440	-.4051	0.3970	0.4321	343.3	0.7154	-0.6341	4.2	55.4
0.4440	-.4083	0.5177	0.5044	426.8	0.6775	-0.7739	4.5	56.3
0.5440	-.4132	0.6426	0.5452	515.8	0.6315	-0.8832	4.9	57.4
0.6440	-.4193	0.7729	0.5531	601.0	0.5782	-0.9586	5.6	58.9
0.7440	-.4265	0.9101	0.5300	682.0	0.5186	-1.015	7.3	60.7
0.8440	-.4352	1.061	0.4899	758.2	0.4486	-1.063	19.0	63.5
0.9440	-.4482	1.237	0.4301	829.4	0.3727	-1.109	∞	67.2
1.044	-.4681	1.456	0.3504	900.5	0.2892	-1.109	∞	72.4
1.144	-.4884	1.713	0.2325	976.1	0.2186	-0.8097	∞	77.0

Laminar at x = .7850
In transition at x = 1.049

Table 4a

CALCULATED BOUNDARY-LAYER PARAMETERS

29° Hemisphere-Cone

$M_{\infty} = 2.97$

x	S_w	M_e	$\frac{Re_k}{k^2 Re_L^{3/2}}$	Re_θ	St_∞ x10^3	$\frac{d\left(\frac{C_p}{C_{p_o}}\right)}{dx}$	$Re_{\theta,c}$ x10^{-4}	$Re_{\theta,m}$
0.	-.4200	0.	0.	0.	0.7898	0.	4.5	54.1
0.04371	-.4202	0.0500	0.06868	44.01	0.7884	-0.04016	4.5	54.2
0.1437	-.4232	0.1648	0.2224	144.7	0.7771	-0.2628	4.7	54.4
0.2437	-.4280	0.2808	0.3641	244.3	0.7578	-0.4694	4.9	54.8
0.3437	-.4330	0.3991	0.4820	342.0	0.7287	-0.6338	5.2	55.5
0.4437	-.4380	0.5206	0.5667	436.8	0.6902	-0.7736	5.7	56.4
0.5437	-.4430	0.646[illegible]	0.6123	528.1	0.6430	-0.8829	6.2	57.5
0.6437	-.4486	0.7782	0.6189	615.2	0.5881	-0.9584	7.1	58.9
0.7437	-.4544	0.9170	0.5885	697.6	0.5268	-1.014	8.9	60.8
0.8437	-.4616	1.070	0.5385	775.0	0.4551	-1.063	23.0	63.7

Laminar at x = .6632
In transition at x = .7850

Table 4a

CALCULATED BOUNDARY-LAYER PARAMETERS

29° Hemisphere-Cone

$M_{\infty} = 3.14$

x	S_w	M_e	$\frac{Re_k}{k^2 Re_L{}^{3/2}}$	Re_θ	St_∞ x10^3	$\frac{d\left(\frac{C_p}{C_{p_o}}\right)}{dx}$	$Re_{\theta,c}$ x10^{-4}	$Re_{\theta,m}$
0.	-.4340	0.	0.	0.	0.8039	[illegible]	5.1	54.1
0.04351	-.4343	0.0500	0.07226	44.46	0.8025	-0.03998	5.1	54.2
0.1435	-.4368	0.1653	0.2344	146.5	0.7917	-0.2623	5.2	54.4
0.2435	-.4412	0.2820	0.3834	247.4	0.7719	-0.4690	5.5	54.8
0.3435	-.4478	0.4009	0.5110	346.6	0.7425	-0.6334	5.9	55.5
0.4435	-.4551	0.5231	0.6065	443.0	0.7034	-0.7734	6.5	56.4
0.5435	-.4627	0.6499	0.6621	536.0	0.6555	-0.8827	7.3	57.6
0.6435	-.4714	0.7826	0.6778	625.0	0.5998	-0.9583	8.4	59.0
0.7435	-.4799	0.9229	0.6509	709.4	0.5372	-1.014	11.0	60.9
0.8435	-.4854	1.078	0.5890	787.8	0.4632	-1.062	28.0	63.8

Laminar at x = .6632
In transition at x = .7850

Table 4b

CALCULATED BOUNDARY-LAYER PARAMETERS

50° Hemisphere-Cone

$M_\infty = 2.5$

x	S_w	M_e	$\frac{Re_k}{k^2 Re_L^{3/2}}$	Re_θ	St_∞ x10^{-3}	$\frac{d\left(\frac{C_p}{C_{p_o}}\right)}{dx}$	$Re_{\theta,c}$ x10^{4}	$Re_{\theta,m}$
0.	-.3364	0.	0.	0.	0.9238	0.	2.6	53.7
0.04452	-.3362	0.0500	0.05091	33.53	0.9220	-0.08891	2.6	53.8
0.1445	-.3354	0.1627	0.1601	109.2	0.9028	-0.2850	2.7	54.1
0.2445	-.3330	0.2765	0.2549	183.5	0.8792	-0.4698	2.7	54.5
0.3445	-.3264	0.3923	0.3239	255.8	0.8430	-0.6358	2.6	55.1
0.4445	-.3129	0.5110	0.3579	324.8	0.7940	-0.7765	2.5	56.0
0.5445	-.2917	0.6336	0.3558	389.5	0.7328	-0.8862	2.4	57.1

Laminar at x = .3379
In transition at x = .5222

CONFIDENTIAL
NOLTR 62-25

Table 4b

CALCULATED BOUNDARY-LAYER PARAMETERS

50° Hemisphere-Cone

$M_\infty = 3.0$

x	S_w	M_e	$\frac{Re_k}{k^2 Re_L^{3/2}}$	Re_θ	St_∞ x10-3	$\frac{d\left(\frac{C_p}{C_{p_o}}\right)}{dx}$	$Re_{\theta,c}$ x10^{-4}	$Re_{\theta,m}$
0.	-.4273	0.	0.	0.	0.9639	0.	4.8	54.1
0.04367	-.4284	0.0500	0.07079	36.14	0.9624	-0.08723	4.8	54.1
0.1437	-.4290	0.1649	0.2272	118.8	0.9684	-0.2834	4.9	54.4
0.2437	-.4253	0.2810	0.3594	200.0	0.9231	-0.4683	4.8	54.8
0.3437	-.4137	0.3994	0.4452	278.4	0.8839	-0.6345	4.5	55.4
0.4437	-.3930	0.5211	0.4734	352.6	0.8309	-0.7754	4.0	56.3
0.5437	-.3631	0.6472	0.4497	421.2	0.7646	-0.8854	3.6	57.5

Laminar at x = .3379
In transition at x = .5222

Table 4b

CALCULATED BOUNDARY-LAYER PARAMETERS

50° Hemisphere-Cone

$M_\infty = 3.5$

x	S_w	M_e	$\frac{Re_k}{k^2 Re_L^{3/2}}$	Re_θ	St_∞ x10-3	$\frac{d\left(\frac{C_p}{C_{p_o}}\right)}{dx}$	$Re_{\theta,c}$ x10-4	$Re_{\theta,m}$
0.	-.4821	0.	0.	0.	1.022	0.	7.5	54.2
0.04314	-.4842	0.0500	0.08809	38.43	1.020	-0.08624	7.7	54.3
0.1432	-.4878	0.1662	0.2893	127.1	1.010	-0.2824	7.9	54.5
0.2432	-.4840	0.2838	0.4566	214.2	0.9823	-0.4674	7.8	54.9
0.3432	-.4680	0.4038	0.5510	297.8	0.9389	-0.6337	6.9	55.6
0.4432	-.4227	0.5273	0.5248	374.1	0.8744	-0.7748	5.0	56.5
0.5432	-.3647	0.6556	0.4476	441.5	0.7960	-0.8849	3.7	57.7

Laminar at x = .3379
In transition at x = .5222

Table 4b

CALCULATED BOUNDARY-LAYER PARAMETERS

50° Hemisphere-Cone

$M_\infty = 4.0$

x	S_w	M_e	$\frac{Re_k}{k^2 Re_L^{3/2}}$	Re_θ	St_∞ x10-3	$\frac{d\left(\frac{C_p}{C_{p_o}}\right)}{dx}$	Re_θ $\times 10^{-4}$	$Re_{\theta,m}$
0.	-.5190	0.	0.	0.	1.044	0.	10.0	54.3
0.04285	-.5193	0.0500	0.1016	38.72	1.042	-0.08560	10.0	54.3
0.1428	-.5203	0.1671	0.3318	128.3	1.034	-0.2818	10.0	54.5
0.2428	-.5185	0.2856	0.5286	216.6	1.006	-0.4668	10.0	55.0
0.3428	-.5043	0.4067	0.6393	301.2	0.9613	-0.6332	9.3	55.6
0.4428	-.4497	0.5314	0.5779	376.7	0.8909	-0.7744	6.2	56.6
0.5428	-.3809	0.6611	0.4691	442.0	0.8070	-0.8846	4.1	57.8

Laminar at x = .3379
In transition at x = .5222

Table 4b

CALCULATED BOUNDARY-LAYER PARAMETERS

50° Hemisphere-Cone

$M_\infty = 4.7$

x	S_w	M_e	$\frac{Re_k}{k^2 Re_L^{3/2}}$	Re_θ	St_∞ x10-3	$\frac{d\left(\frac{C_p}{C_{p_o}}\right)}{dx}$	$Re_{\theta,c}$ x10^{-4}	$Re_{\theta,m}$
0.	-.5403	0.	0.	0.	1.095	0.	12.0	54.3
0.04256	-.5415	0.0500	0.1104	39.24	1.093	-0.08503	12.0	54.3
0.1426	-.5430	0.1679	0.3634	130.5	1.086	-0.2813	12.0	54.5
0.2426	-.5415	0.2873	0.5794	220.5	1.056	-0.4663	12.0	55.0
0.3426	-.5312	0.4093	0.7122	306.9	1.010	-0.6328	12.0	55.7
0.4426	-.4835	0.5351	0.6550	384.2	0.9360	-0.7740	8.2	56.7
0.5426	-.4093	0.6661	0.5125	449.2	0.8435	-0.8844	4.9	57.9

Laminar at x = .3379
In transition at x = .5222

Table 4c

HEMISPHERE-CYLINDER

$M_\infty = 3.0$

x	S_w	M_e	$\frac{Re_k}{k^2 {Re_L}^{3/2}}$	Re_θ	St_∞ x10-3	$\frac{d\left(\frac{C_p}{C_{p_o}}\right)}{dx}$	$Re_{\theta,c}$ x10-4	$Re_{\theta,m}$
0.	-.6100	0.	0.	0.	1.057	0.	21.0	54.3
0.04367	-.6064	0.0500	0.1742	35.85	1.054	-0.08723	21.0	54.3
0.1437	-.5881	0.1649	0.5004	116.0	1.049	-0.2834	18.0	54.5
0.2437	-.5701	0.2810	0.7226	194.0	1.020	-0.4683	16.0	55.0

Transition ahead of x = .2008

Table 4c

HEMISPHERE-CYLINDER

$M_\infty = 4.0$

x	S_w	M_e	$\frac{Re_k}{k^2 Re_L^{3/2}}$	Re_θ	St_∞ x10-3	$\frac{d\left(\frac{C_p}{C_{p_o}}\right)}{dx}$	$Re_{\theta,c}$ x10-4	$Re_{\theta,m}$
0.	-.7210	0.	0.	0.	1.124	0.	53.0	54.0
0.04285	-.7146	0.0500	0.3600	43.0	1.120	-0.08560	50.0	54.1
0.1428	-.6869	0.1671	0.9306	139.7	1.108	-0.2818	40.0	54.3
0.2428	-.6536	0.2856	1.164	231.8	1.071	-0.4668	31.0	54.9

Transition ahead of x = .2008

Table 4c

HEMISPHERE-CYLINDER

$M_\infty = 4.6$

x	S_w	M_e	$\frac{Re_k}{k^2 Re_L{}^{3/2}}$	Re_θ	St_∞ x10-3	$\frac{d\left(\frac{C_p}{C_{p_o}}\right)}{dx}$	$Re_{\theta,c}$ x10-4	$Re_{\theta,m}$
0.	-.7449	0.	0.	0.	1.152	0.	64.0	54.0
0.04260	-.7384	0.0500	0.4252	46.15	1.146	-0.08509	61.0	54.0
0.1426	-.7105	0.1678	1.082	150.2	1.130	-0.2814	48.0	54.3
0.2426	-.6733	0.2871	1.294	248.4	1.088	-0.4664	36.0	54.8

Transition ahead of x = .2008

Table 4c

HEMISPHERE-CYLINDER

$M_{\infty} = 5.2$

x	S_w	M_e	$\frac{Re_k}{k^2 Re_L{}^{3/2}}$	Re_θ	St_∞ x10-3	$\frac{d\left(\frac{C_p}{C_{p_o}}\right)}{dx}$	$Re_{\theta,c}$ x10-4	$Re_{\theta,m}$
0.	-.7584	0.	0.	0.	1.165	0.	71.0	53.9
0.04212	-.7541	0.0500	0.4583	48.5	1.160	-0.08415	69.0	54.0
0.1421	-.7150	0.1691	1.053	157.8	1.134	-0.2804	50.0	54.3
0.2421	-.6636	0.2898	1.140	258.1	1.084	-0.4655	33.0	54.9

Transition ahead of x = .2008

Table 4c

HEMISPHERE-CYLINDER

$M_\infty = 5.5$

x	S_w	M_e	$\frac{Re_k}{k^2 Re_L{}^{3/2}}$	Re_θ	St_∞ x10-3	$\frac{d\left(\frac{C_p}{C_{p_o}}\right)}{dx}$	$Re_{\theta,c}$ x10-4	$Re_{\theta,m}$
0.	-.7611	0.	0.	0.	1.169	0.	73.0	53.9
0.04191	-.7548	0.0500	0.4447	49.51	1.163	-0.08372	69.0	54.0
0.1419	-.7049	0.1698	0.9395	160.6	1.128	-0.2800	46.0	54.3
0.2419	-.6461	0.2910	0.9861	261.2	1.078	-0.4652	29.0	54.9

Table 4d

"1/10-POWER" NOSE SHAPE

$M_\infty = 1.72$

x	S_w	M_e	$\frac{Re_k}{k^2 Re_L^{3/2}}$	Re_θ	St_∞ x10^3	$\frac{d\left(\frac{C_p}{C_{p_o}}\right)}{dx}$	$Re_{\theta,c}$ x10^{-4}	$Re_{\theta,m}$
0.	-.3475	0.	0.	0.	0.6018	0.	2.8	53.8
0.1615	-.3476	0.08185	0.06436	62.15	0.6940	-0.09095	2.9	54.5
0.2115	-.3474	0.1144	0.09311	84.09	0.7072	-0.1410	3.0	54.9
0.3115	-.3466	0.1903	0.1671	127.3	0.7554	-0.2931	3.0	55.5
0.4115	-.3464	0.2890	0.2834	171.0	0.7926	-0.6469	3.2	57.2
0.5115	-.3478	0.4698	0.5268	214.7	0.8887	-1.789	3.5	59.4
0.6115	-.3443	0.7957	0.6824	276.2	0.8880	-3.283	4.2	62.2
0.7115	-.3382	1.230	0.4503	350.8	0.6488	-2.937	59.0	67.9
0.8115	-.3561	1.592	0.2098	427.0	0.4756	-1.186	∞	71.7
0.9115	-.3673	1.730	0.1112	501.4	0.4285	-0.2428	63.0	64.9
1.012	-.3682	1.756	0.08026	573.8	0.3757	-0.04048	47.0	59.1
1.112	-.3687	1.761	0.06791	640.8	0.3350	-0.02854	44.0	56.8
1.212	-.3692	1.763	0.06179	701.6	0.3059	+0.00259	38.0	56.5
1.312	-.3678	1.764	0.05694	756.9	0.2828	+0.00001	43.0	56.8
1.412	-.3656	1.766	0.05256	808.9	0.2639	-0.00008	41.0	56.9
1.512	-.3638	1.768	0.04938	851.5	0.2502	0.	39.0	56.9
1.612	-.3619	1.770	0.04840	857.8	0.2478	0.	37.0	56.9
1.712	-.3601	1.770	0.04684	878.3	0.2417	0	36.0	56.9
1.812	-.3586	1.772	0.04415	921.8	0.2297	0.	34.0	56.9
1.895	-.3584	1.774	0.04230	958.0	0.2207	0.	34.0	57.0

Laminar at x = 1.920

2

Table 4d

"1/10-POWER" NOSE SHAPE

$M_\infty = 2.33$

x	S_w	M_e	$\frac{Re_k}{k^2 Re_L{}^{3/2}}$	Re_θ	St_∞ x10^3	$\frac{d\left(\frac{C_p}{C_{p_o}}\right)}{dx}$	$Re_{\theta,c}$ x10^{-4}	$Re_{\theta,m}$
0.	-.4881	0.	0.	0.	0.6191	0.	7.9	54.2
0.1615	-.4871	0.08186	0.1092	73.60	0.7144	-0.07923	7.9	54.8
0.2115	-.4861	0.1144	0.1583	98.90	0.7346	-0.1250	7.9	55.2
0.3115	-.4833	0.1903	0.2808	149.4	0.7890	-0.2598	7.7	55.6
0.4115	-.4787	0.2890	0.4630	200.8	0.8370	-0.5732	7.7	57.2
0.5115	-.4712	0.4699	0.8200	253.2	0.9434	-1.584	7.7	59.2
0.6115	-.4616	0.7958	1.026	325.3	0.9417	-2.903	8.3	62.0
0.7115	-.4579	1.230	0.6798	411.9	0.6921	-2.612	∞	67.8
0.8115	-.4753	1.592	0.3250	498.4	0.4910	-1.074	∞	71.9
0.9115	-.4900	1.730	0.1813	579.8	0.4302	-0.2206	∞	65.5
1.012	-.4925	1.757	0.1344	658.0	0.3837	-0.03687	∞	59.2
1.112	-.4815	1.761	0.1085	729.4	0.3452	-0.00242	∞	57.0
1.212	-.4691	1.763	0.09246	793.8	0.3150	+0.00171	89.0	56.6
1.312	-.4632	1.764	0.08349	853.2	0.2920	+0.00014	99.0	56.8
1.412	-.4611	1.766	0.0772	909.8	0.2731	-0.00006	∞	56.9

Laminar at x = .910
In transition at x = 1.340

Table 4d

"1/10-POWER" NOSE SHAPE

$M_\infty = 2.71$

x	S_w	M_e	$\frac{Re_k}{k^2 Re_L^{3/2}}$	Re_θ	St_∞ x10^3	$\frac{d\left(\frac{C_p}{C_{p_o}}\right)}{dx}$	$Re_{\theta,c}$ x10^{-4}	$Re_{\theta,m}$
0.	-.4960	0.	0.	0.	0.6436	0.	8.4	54.2
0.1615	-.4952	0.08185	0.1040	80.00	0.7092	-0.06557	8.4	54.5
0.2115	-.4944	0.1144	0.1542	106.4	0.7326	-0.1110	8.4	55.2
0.3115	-.4917	0.1903	0.2813	156.6	0.8067	-0.2454	8.3	55.7
0.4115	-.4853	0.2890	0.4632	208.7	0.8627	-0.5481	8.1	57.2
0.5115	-.4728	0.4698	0.8065	261.1	0.9756	-1.530	7.8	59.2
0.6115	-.4626	0.7957	1.010	333.8	0.9772	-2.811	8.4	62.0
0.7115	-.4670	1.230	0.6918	422.1	0.7231	-2.523	∞	67.8
0.8115	-.4911	1.592	0.3402	510.6	0.5142	-1.027	∞	71.8
0.9115	-.5072	1.730	0.1921	593.6	0.4479	-0.2086	∞	65.3
1.012	-.5110	1.756	0.1437	673.6	0.4001	-0.03253	∞	59.0
1.112	-.4992	1.761	0.1160	746.3	0.3598	-0.00264	∞	57.0
1.212	-.4759	1.763	0.09342	810.3	0.3270	+0.00117	92.0	56.7
1.312	-.4503	1.764	0.07652	867.8	0.3011	+0.00016	99.0	56.8

Laminar at x = .742
In transition at x = .910

Table 4d

"1/10-POWER" NOSE SHAPE

$M_\infty = 3.18$

x	S_w	M_e	$\frac{Re_k}{k^2 Re_L{}^{3/2}}$	Re_θ	St_∞ x10^3	$\frac{d\left(\frac{C_p}{C_{p_o}}\right)}{dx}$	$Re_{\theta,c}$ x10^{-4}	$Re_{\theta,m}$
0.	-.5472	0.	0.	0.	0.6760	0.	13.0	54.3
0.1615	-.5458	0.08184	0.1388	78.73	0.7834	-0.0751	13.0	54.9
0.2115	-.5444	0.1144	0.2013	105.4	0.8088	-0.1194	13.0	55.2
0.3115	-.5384	0.1903	0.3486	159.3	0.8687	-0.2439	12.0	55.6
0.4115	-.5241	0.2890	0.5430	214.5	0.9164	-0.5370	11.0	57.2
0.5115	-.5068	0.4698	0.9205	267.6	1.038	-1.510	10.0	59.2
0.6115	-.5009	0.7957	1.152	344.5	1.043	-2.654	11.0	61.8
0.7115	-.5125	1.230	0.8053	438.2	0.7756	-2.305	∞	67.3
0.8115	-.5388	1.592	0.4110	526.9	0.5461	-0.9655	∞	71.6
0.9115	-.5523	1.730	0.2368	610.3	0.4673	-0.2118	∞	65.7
1.012	-.5503	1.757	0.1728	690.1	0.4193	-0.03652	∞	59.4
1.112	-.5359	1.761	0.1365	762.4	0.3783	-0.00331	∞	57.1

Laminar at x = .742
In transition at x = .910

Table 4d

"1/10-POWER" NOSE SHAPE

$M_\infty = 4.25$

x	S_w	M_e	$\frac{Re_k}{k^2 Re_L{}^{3/2}}$	Re_θ	St_∞ x10^3	$\frac{d\left(\frac{C_p}{C_{p_o}}\right)}{dx}$	$Re_{\theta,c}$ x10^{-4}	$Re_{\theta,m}$
0.	-.6531	0.	0.	0.	0.7217	0.	30.0	54.2
0.1615	-.6517	0.08186	0.2388	89.29	0.8279	-0.06901	30.0	54.7
0.2115	-.6506	0.1144	0.3460	119.6	0.8550	-0.1104	30.0	55.1
0.3115	-.6459	0.1903	0.6013	180.2	0.9208	-0.2303	29.0	55.6
0.4115	-.6345	0.2590	0.9346	241.1	0.9834	-0.5168	27.0	57.2
0.5115	-.6200	0.4699	1.550	302.4	1.121	-1.442	24.0	59.1
0.6115	-.6130	0.7958	1.933	386.9	1.126	-2.642	25.0	61.8
0.7115	-.6249	1.230	1.386	488.9	0.8409	-2.368	∞	67.4
0.8115	-.6513	1.592	0.7350	588.4	0.5829	-0.9621	∞	71.7
0.9115	-.6649	1.730	0.4409	676.9	0.4951	-0.1963	∞	65.6
1.012	-.6634	1.757	0.3275	759.7	0.4506	-0.02910	∞	59.0
1.112	-.6465	1.761	0.2506	833.4	0.4083	-0.00072	∞	56.9

Laminar at x = .742
In transition at x = .910

Table 4d

"1/10-POWER" NOSE SHAPE

$M_{\infty} = 5.14$

x	S_w	M_e	$\frac{Re_k}{k^2 Re_L^{3/2}}$	Re_θ	St_∞ x10^3	$\frac{d\left(\frac{C_p}{C_{p_o}}\right)}{dx}$	$Re_{\theta,c}$ x10^{-4}	$Re_{\theta,m}$
0.	-.7005	0.	0.	0.	0.7600	0.	44.0	54.1
0.1610	-.6994	0.08214	0.3168	93.47	0.8860	-0.07068	44.0	54.6
0.2110	-.6980	0.1149	0.4549	126.0	0.9111	-0.1110	44.0	55.0
0.3110	-.6931	0.1914	0.7801	191.1	0.9748	-0.2283	42.0	55.5
0.4110	-.6828	0.2906	1.200	256.8	1.038	-0.5070	39.0	57.0
0.5110	-.6658	0.4720	1.920	322.4	1.178	-1.413	35.0	59.0
0.6110	-.6524	0.7990	2.281	410.9	1.179	-2.589	34.0	61.8
0.7110	-.6565	1.235	1.573	514.4	0.8804	-2.343	∞	67.4
0.8110	-.6815	1.597	0.8433	615.1	0.6097	-0.9617	∞	71.8
0.9110	-.6996	1.735	0.5320	706.2	0.5193	-0.1941	∞	65.7
1.011	-.7001	1.762	0.4048	791.1	0.4743	-0.03032	∞	59.2
1.111	-.6842	1.766	0.3090	865.9	0.4301	-0.00159	∞	57.0

Laminar at x = .742
In transition at x = .910

Table 4d

"1/10-POWER" NOSE SHAPE

$M_\infty = 6.10$

x	S_w	M_e	$\frac{Re_k}{k^2 Re_L^{3/2}}$	Re_θ	St_∞ x10^3	$\frac{d\left(\frac{C_p}{C_{p_o}}\right)}{dx}$	$Re_{\theta,c}$ x10^{-4}	$Re_{\theta,m}$
0.	-.7399	0.	0.	0.	0.7981	0.	61.0	54.0
0.1602	-.7376	0.08260	0.3985	100.1	0.9324	-0.06923	60.0	54.5
0.2102	-.7353	0.1157	0.5622	136.0	0.9516	-0.1064	59.0	54.8
0.3102	-.7271	0.1930	0.9367	206.3	1.013	-0.2248	55.0	55.5
0.4102	-.7078	0.2931	1.323	274.6	1.077	-0.4943	48.0	57.0
0.5102	-.6773	0.4754	1.908	341.2	1.212	-1.402	38.0	59.1
0.6102	-.6514	0.8043	2.109	427.3	1.216	-2.602	34.0	61.9
0.7102	-.6437	1.242	1.352	528.0	0.9063	-2.323	∞	67.5
0.8102	-.6674	1.605	0.7110	625.4	0.6315	-0.9472	∞	71.9
0.9102	-.6971	1.743	0.4881	720.2	0.5417	-0.1968	∞	65.8
1.010	-.7104	1.769	0.4137	812.1	0.4978	-0.03272	∞	59.4

Laminar at x = .416
In transition at x = .611

Table 4d

"1/10-POWER" NOSE SHAPE

$M_\infty = 6.68$

x	S_w	M_e	$\frac{Re_k}{k^2 Re_L^{3/2}}$	Re_θ	St_∞ x10^3	$\frac{d\left(\frac{C_p}{C_{p_o}}\right)}{dx}$	$Re_{\theta,c}$ x10^{-4}	$Re_{\theta,m}$
0.	-.7394	0.	0.	0.	0.7950	0.	61.0	54.0
0.1593	-.7380	0.08308	0.3628	100.4	0.9186	-0.06745	60.0	54.5
0.2093	-.7358	0.1166	0.5188	135.6	0.9450	-0.1070	59.0	54.9
0.3093	-.7260	0.1948	0.8551	204.7	1.011	-0.2239	55.0	55.4
0.4093	-.7040	0.2957	1.184	272.7	1.069	-0.4914	46.0	57.0
0.5093	-.6623	0.4788	1.583	336.7	1.193	-1.370	34.0	59.1
0.6093	-.6106	0.8096	1.527	416.1	1.175	-2.547	25.0	62.1
0.7093	-.5936	1.248	0.9532	505.2	0.8802	-2.323	∞	67.7

Laminar at x = .416
In transition at x = .611

Table 4e

FLAT-FACE CONE-CYLINDER

$M_\infty = 10.0$

x	g_w	M_e	$\frac{Re_k}{k^2 Re_L^{3/2}}$	Re_θ	St_∞ x10^3	$\frac{d\left(\frac{C_p}{C_{p_o}}\right)}{dx}$	$Re_{\theta,c}$ x10^{-4}	$Re_{\theta,m}$
0.	-.8690	0.	0.	0.	5.236	0.	* >100	53.6
0.1000	-.8689	0.03314	0.3335	9.988	4.607	-0.01108	>100	53.2
0.2130	-.8683	0.06174	0.5736	19.77	4.330	-0.01434	>100	53.1
0.3130	-.8677	0.08885	0.8616	27.64	4.380	-0.03413	>100	54.5
0.4130	-.8672	0.1262	1.314	36.22	4.698	-0.06910	>100	55.0
0.5130	-.8666	0.1692	1.802	45.95	4.935	-0.08574	>100	54.8
0.6130	-.8660	0.2137	2.286	56.10	5.037	-0.1167	>100	55.1
0.7130	-.8655	0.2674	2.986	66.10	5.213	-0.1878	>100	56.2
0.8130	-.8666	0.3378	3.968	71.22	5.543	-0.2643	>100	56.4
0.9130	-.8688	0.4010	5.016	88.31	5.514	-0.4150	>100	58.2
1.013	-.8714	0.6442	11.42	93.45	6.869	-2.780	>100	62.3
1.113	-.8739	1.328	9.727	112.7	5.764	-4.088	∞	70.4
1.213	-.8763	2.126	1.708	139.8	2.123	-1.091	∞	85.3
1.413	-.8803	2.286	0.6059	169.2	1.606	-0.03998	∞	73.9
1.613	-.8824	2.286	0.5348	181.8	1.571	0.	∞	64.3
1.813	-.8824	2.286	0.5067	192.1	1.487	0.	∞	64.3
2.013	-.8814	2.286	0.4728	201.3	1.416	0.	∞	64.3
2.213	-.8810	2.286	0.4487	209.8	1.357	0.	∞	64.3
2.413	-.8817	2.286	0.4393	217.8	1.310	0.	∞	64.3
2.613	-.8823	2.286	0.4312	225.2	1.268	0.	∞	64.3
2.813	-.8830	2.286	0.4248	232.3	1.232	0.	∞	64.3
3.013	-.8833	2.286	0.4158	238.9	1.198	0.	∞	64.3
3.213	-.8830	2.286	0.4025	245.0	1.168	0.	∞	64.3
3.413	-.8828	2.286	0.3914	250.9	1.140	0.	∞	64.3

2

Table 4e

FLAT-FACE CONE-CYLINDER

M_∞ = 10.0 (cont'd)

x	S_w	M_e	$\frac{Re_k}{k^2 Re_L^{3/2}}$	Re_θ	St_∞ x10^3	$\frac{d\left(\frac{C_p}{C_{p_o}}\right)}{dx}$	$Re_{\theta,c}$ x10^{-4}	$Re_{\theta,m}$
3.613	-.8826	2.286	0.3814	256.6	1.114	0.	∞	64.3
3.813	-.8825	2.286	0.3726	262.0	1.091	0.	∞	64.3
4.013	-.8829	2.286	0.3681	267.3	1.070	0.	∞	64.3
4.213	-.8830	2.286	0.3646	272.4	1.051	0.	∞	64.3
4.413	-.8837	2.286	0.3853	277.5	1.003	-0.00924	∞	70.7
4.613	-.8854	2.751	0.6982	342.8	0.3811	-0.4401	∞	98.8
4.813	-.8879	3.482	0.00325	631.2	0.06862	0.	∞	84.3
5.013	-.8894	3.482	0.00337	633.0	0.06870	0.	∞	84.3
5.213	-.8903	3.482	0.00343	634.4	0.06869	0.	∞	84.3
5.295	-.8904	3.482	0.00344	634.8	0.06866	0.	∞	84.3

Flow laminar at x = 4.493
Flow not laminar at x = 4.906

*> means $Re_{\theta,c}$ greater than 10^6 but not ∞

Table 4e

FLAT-FACE CONE-CYLINDER

$M_\infty = 13.0$

x	S_w	M_e	$\frac{Re_k}{k^2 Re_L^{3/2}}$	Re_θ	St_∞ x10^3	$\frac{d\left(\frac{C_p}{C_{p_o}}\right)}{dx}$	$Re_{\theta,c}$ x10^{-4}	$Re_{\theta,m}$
0.	-.8327	0.	0.	0.	4.238	0.	*>100	53.7
0.1000	-.8327	0.03353	0.1568	13.06	3.726	-0.01105	>100	53.3
0.2107	-.8327	0.06188	0.2705	25.58	3.513	-0.01736	>100	53.1
0.3107	-.8327	0.08906	0.4114	35.82	3.552	-0.03344	>100	54.5
0.4107	-.8329	0.1266	0.6375	46.97	3.817	-0.06009	>100	55.0
0.5107	-.8331	0.1702	0.8886	59.69	4.018	-0.08495	>100	54.9
0.6107	-.8332	0.2150	1.143	73.02	4.107	-0.1151	>100	55.1
0.7107	-.8335	0.2690	1.513	86.10	4.252	-0.1849	>100	56.2
0.8107	-.8355	0.3398	2.041	100.1	4.530	-0.2649	>100	56.4
0.9107	-.8396	0.4036	2.593	115.6	4.531	-0.3826	>100	57.8
1.011	-.8447	0.6366	6.173	121.6	5.614	-2.708	>100	62.3
1.111	-.8498	1.326	5.643	145.8	4.829	-4.182	∞	70.3
1.211	-.8548	2.160	0.9632	178.1	1.695	-1.141	∞	85.2
1.411	-.8647	2.320	0.3164	218.3	1.341	-0.00480	∞	66.8
1.611	-.8739	2.320	0.3493	234.9	1.285	0.	∞	64.9
1.811	-.8798	2.320	0.3740	249.6	1.229	0.	∞	64.9
2.011	-.8794	2.320	0.3532	261.7	1.170	0.	∞	64.9
2.211	-.8795	2.320	0.3393	272.9	1.123	0.	∞	64.9
2.411	-.8804	2.320	0.3335	283.5	1.084	0.	∞	64.9
2.611	-.8814	2.320	0.3293	293.4	1.050	0.	∞	64.9
2.811	-.8824	2.320	0.3265	302.8	1.020	0.	∞	64.9
3.011	-.8835	2.320	0.3252	311.7	0.9938	0.	∞	64.9
3.211	-.8850	2.320	0.3276	320.3	0.9710	0.	∞	64.9
3.411	-.8864	2.320	0.3302	328.6	0.9503	0.	∞	64.9

Table 4e

FLAT-FACE CONE-CYLINDER

$M_\infty = 13.0$ (cont'd)

x	S_w	M_e	$\frac{Re_k}{k^2 Re_L^{3/2}}$	Re_θ	St_∞ x10^3	$\frac{d\left(\frac{C_p}{C_{p_o}}\right)}{dx}$	$Re_{\theta,c}$ x10^{-4}	$Re_{\theta,m}$
3.611	-.8878	2.320	0.3337	336.5	0.9316	0.	∞	64.9
3.811	-.8894	2.320	0.3380	344.2	0.9146	0.	∞	64.9
4.011	-.8916	2.320	0.3496	352.0	0.9001	0.	∞	64.9
4.211	-.8937	2.320	0.3610	359.5	0.8867	0.	∞	64.9
4.411	-.8958	2.320	0.3814	366.9	0.8664	-0.00277	∞	67.5
4.611	-.8984	2.726	0.7514	439.3	0.3664	-0.4529	∞	97.5
4.811	-.9012	3.678	0.00120	1049.	0.03051	0.	∞	88.0
5.011	-.9034	3.678	0.00128	1052.	0.03063	0.	∞	88.0
5.211	-.9050	3.678	0.00133	1054.	0.03071	0.	∞	88.0
5.295	-.9054	3.678	0.00134	1055.	0.03073	0.	∞	88.0

Flow laminar at x = 4.493
Flow not laminar at x = 4.906

*> means $Re_{\theta,c}$ greater than 10^6 but not ∞

Table 4e

FLAT-FACE CONE-CYLINDER

M_∞ = 14.5

x	S_w	M_e	$\frac{Re_k}{k^2 Re_L^{3/2}}$	Re_θ	St_∞ x10^3	$\frac{d\left(\frac{C_p}{C_{p_o}}\right)}{dx}$	$Re_{\theta,c}$ x10^{-4}	$Re_{\theta,m}$
0.	-.8167	0.	0.	0.	3.752	0.	*>100	53.7
0.1000	-.8167	0.03363	0.1203	14.54	3.297	-0.01104	>100	53.4
0.2101	-.8168	0.06192	0.2071	28.40	3.111	-0.01729	>100	53.2
0.3101	-.8169	0.08912	0.3158	39.78	3.156	-0.03326	>100	54.5
0.4101	-.8157	0.1268	0.4817	52.09	3.376	-0.05988	>100	55.1
0.5101	-.8127	0.1704	0.6451	66.00	3.541	-0.08474	>100	54.9
0.6101	-.8092	0.2154	0.7936	80.42	3.604	-0.1147	>100	55.2
0.7101	-.8055	0.2694	1.004	94.38	3.716	-0.1841	>100	56.2
0.8101	-.8051	0.3403	1.310	109.3	3.952	-0.2650	>100	56.5
0.9101	-.8115	0.4044	1.693	126.3	3.972	-0.3752	>100	57.7
1.010	-.8213	0.6348	4.276	132.8	4.937	-2.685	>100	62.2
1.110	-.8312	1.323	4.164	159.5	4.306	-4.192	∞	70.3
1.210	-.8414	2.159	0.7595	192.1	1.537	-1.157	∞	85.2
1.410	-.8573	2.323	0.2683	237.9	1.222	-0.00639	∞	67.2
1.610	-.8667	2.323	0.2912	257.4	1.169	0.	∞	64.9
1.810	-.8733	2.323	0.3123	274.5	1.116	0.	∞	64.9
2.010	-.8728	2.323	0.2943	288.6	1.060	0.	∞	64.9
2.210	-.8733	2.323	0.2841	301.7	1.015	C.	∞	64.9
2.410	-.8756	2.323	0.2865	314.3	0.9807	0.	∞	64.9
2.610	-.8779	2.323	0.2901	326.1	0.9512	0.	∞	64.9
2.810	-.8802	2.323	0.2952	337.3	0.9255	0.	∞	64.9
3.010	-.8823	2.323	0.2996	348.0	0.9025	0.	∞	64.9
3.210	-.8839	2.323	0.3019	358.0	0.8813	0.	∞	64.9
3.410	-.8854	2.323	0.3048	367.6	0.8621	0.	∞	64.9

Table 4e

FLAT-FACE CONE-CYLINDER

M_∞ = 14.5 (cont'd)

x	S_w	M_e	$\frac{Re_k}{k^2 Re_L{}^{3/2}}$	Re_θ	St_∞ x10^3	$\frac{d\left(\frac{C_p}{C_{p_o}}\right)}{dx}$	$Re_{\theta,c}$ x10^{-4}	$Re_{\theta,m}$
3.610	-.8870	2.323	0.3086	376.8	0.8449	0.	∞	64.9
3.810	-.8889	2.323	0.3150	385.9	0.8296	0.	∞	64.9
4.010	-.8912	2.323	0.3256	394.8	0.8164	0.	∞	64.9
4.210	-.8935	2.323	0.3373	403.6	0.8042	0.	∞	64.9
4.410	-.8957	2.323	0.3580	412.2	0.7848	-0.00322	∞	68.0
4.610	-.8982	2.730	0.6985	493.1	0.3294	-0.4562	∞	97.7
4.810	-.9010	3.760	0.00067	1342.	0.02016	0.	∞	89.5
5.010	-.9056	3.760	0.00076	1349.	0.02036	0.	∞	89.5
5.210	-.9115	3.760	0.00090	1357.	0.02062	0.	∞	89.5
5.295	-.9140	3.760	0.00097	1361.	0.02073	0.	∞	89.5

Flow laminar at x = 4.493
Flow not laminar at x = 4.906

* means $Re_{\theta,c}$ greater than 10^6 but not ∞

Table 4f

SPHERICAL-SEGMENT NOSE

$M_\infty = 8.4$

x	S_w	M_e	$\frac{Re_k}{k^2 Re_L^{3/2}}$	Re_θ	St_∞ x10^3	$\frac{d\left(\frac{C_p}{C_{p_o}}\right)}{dx}$	$Re_{\theta,c}$ x10^{-4}	$Re_{\theta,m}$
0.	-.8624	0.	0.	0.	10.16	0.	*>100	53.6
0.07184	-.8624	0.1173	3.510	19.83	9.855	-0.1844	>100	52.7
0.1218	-.8621	0.1743	4.827	31.13	9.204	-0.2504	>100	53.0
0.2218	-.8631	0.2968	7.999	52.50	8.882	-0.4874	>100	54.4
0.3218	-.8651	0.4430	11.62	74.09	8.730	-0.8377	>100	56.0
0.4218	-.8645	0.6463	17.32	92.20	8.239	-3.408	>100	62.2
0.5218	-.8641	3.539	0.09132	42.07	1.677	0.	∞	85.4
0.6218	-.8641	3.539	0.06669	57.63	1.224	0.	∞	85.4
0.7218	-.8641	3.539	0.05506	69.80	1.011	0.	∞	85.4

Flow laminar at x = .7165

*> means $Re_{\theta,c}$ greater than 10^6 but not ∞

Table 4f

SPHERICAL-SEGMENT NOSE

$M_\infty = 10.8$

x	S_w	M_e	$\frac{Re_k}{k^2 Re_L^{3/2}}$	Re_θ	St_∞ x10^3	$\frac{d\left(\frac{C_p}{C_{p_o}}\right)}{dx}$	$Re_{\theta,c}$ x10^{-4}	$Re_{\theta,m}$
0.	-.8743	0.	0.	0.	9.844	0.	* >100	53.6
0.07087	-.8748	0.1189	3.652	24.34	9.568	-0.1822	>100	52.6
0.1209	-.8746	0.1773	5.038	38.39	8.927	-0.2479	>100	53.0
0.2209	-.8779	0.3022	8.768	65.08	8.645	-0.4829	>100	54.4
0.3209	-.8807	0.4511	13.00	92.11	8.502	-0.8299	>100	56.0
0.4209	-.8775	0.6555	18.11	114.5	7.953	-3.297	>100	62.2
0.5209	-.8773	3.752	0.05976	33.02	1.556	0.	∞	89.4
0.6209	-.8783	3.752	0.04059	49.71	1.036	0.	∞	89.4
0.7209	-.8794	3.752	0.03324	62.10	0.8317	0.	∞	89.4

Flow laminar at x = .7165

*> means $Re_{\theta,c}$ greater than 10^6 but not ∞

Table 4f

SPHERICAL-SEGMENT NOSE

$M_\infty = 15.1$

x	S_w	M_e	$\frac{Re_k}{k^2 Re_L{}^{3/2}}$	Re_θ	St_∞ x10^3	$\frac{d\left(\frac{C_p}{C_{p_o}}\right)}{dx}$	$Re_{\theta,c}$ x10^{-4}	$Re_{\theta,m}$
0.	-.8821	0.	0.	0.	9.317	0.	*>100	53.6
0.07037	-.8807	0.1197	3.459	29.71	9.031	-0.1810	>100	52.6
0.1204	-.8800	0.1789	4.735	46.92	8.418	-0.2465	>100	53.0
0.2204	-.8881	0.3052	9.137	80.18	8.243	-0.4802	>100	54.4
0.3204	-.8961	0.4555	15.29	114.7	8.188	-0.8252	>100	56.0
0.4204	-.8896	0.6604	19.41	142.3	7.540	-3.234	>100	62.2
0.5204	-.8911	4.064	0.03186	25.28	1.295	0.	∞	95.4
0.6204	-.8961	4.064	0.02157	42.34	0.7857	0.	∞	95.4
0.7204	-.9013	4.064	0.01916	54.59	0.6201	0.	∞	95.4

Flow laminar at $x = .7165$

*> means $Re_{\theta,c}$ greater than 10^6 but not ∞

Table 4g

ELLIPTICAL-NOSE CYLINDER

Section ABCEA'

x	S_w	M_e	$\frac{Re_k}{k^2 Re_L{}^{3/2}}$	Re_θ	$St_\infty \times 10^3$	$\frac{d\left(\frac{C_p}{C_{p_o}}\right)}{dx}$	$Re_{\theta,c} \times 10^{-4}$	$Re_{\theta,m}$
0.	-.8149	0.	0.	0.	2.148	0.	*>100	53.7
0.1080	-.8149	0.06740	0.4119	61.16	1.910	-0.02400	>100	51.1
0.1580	-.8149	0.08007	0.4438	80.57	1.714	-0.02502	>100	51.4
0.2580	-.8149	0.1110	0.6510	112.7	1.640	-0.06012	>100	54.6
0.3580	-.8149	0.1649	1.071	149.9	1.808	-0.1169	>100	55.2
0.4580	-.8149	0.2248	1.486	194.7	1.885	-0.1656	>100	55.1
0.5580	-.8146	0.2912	1.954	239.2	1.924	-0.2488	>100	55.8
0.6580	-.8152	0.3732	2.570	285.9	1.986	-0.3804	>100	56.8
0.7580	-.8228	0.4750	3.610	335.7	2.065	-0.5875	>100	55.0
0.8580	-.8264	0.6236	5.084	381.8	2.126	-1.286	>100	60.8
0.9580	-.8280	0.9686	6.334	433.4	2.046	-3.091	>100	65.4
1.058	-.8449	1.656	3.631	514.8	1.224	-2.954	∞	75.9
1.158	-.8652	2.541	0.5932	775.3	0.3007	-0.5908	∞	93.6
1.258	-.8735	2.685	0.1484	871.9	0.2478	-0.01249	∞	83.2
1.458	-.8739	2.618	0.1597	1010.	0.2344	-0.01225	∞	82.6
1.658	-.8747	2.648	0.1449	1048.	0.2154	-0.01201	∞	84.0
1.858	-.8739	2.672	0.1294	1091..	0.1984	-0.01177	∞	86.0

Flow in early portion of transition at x = 1.815

***> means $Re_{\theta,c}$ greater than 10^6 but not ∞**

Table 4g

ELLIPTICAL-NOSE CYLINDER

Section ALM

x	S_w	M_e	$\frac{Re_k}{k^2 Re_L^{3/2}}$	Re_θ	St_∞ x10^3	$\frac{d\left(\frac{C_p}{C_{p_o}}\right)}{dx}$	$Re_{\theta,c}$ x10^{-4}	$Re_{\theta,m}$
0.	-.8149	0.	0.	0.	2.148	0.	*>100.	53.7
0.1080	-.8149	0.06740	0.4119	61.16	1.910	-0.02400	>100.	51.1
0.1580	-.8149	0.08007	0.4438	80.57	1.714	-0.02502	>100.	51.4
0.2580	-.8149	0.1110	0.6512	112.7	1.640	-0.06012	>100.	54.6
0.3580	-.8149	0.1649	1.071	149.9	1.808	-0.1169	>100.	55.2
0.4580	-.8140	0.2248	1.469	193.5	1.883	-0.1656	>100.	55.1
0.5580	-.8130	0.2912	1.916	238.8	1.920	-0.2488	>100.	55.8
0.6580	-.8100	0.3732	2.409	284.6	1.972	-0.3804	>100.	56.8
0.7580	-.7877	0.4750	2.372	325.9	1.970	-0.5875	90.8	58.3

Flow laminar at x = .4190
In transition at x = .6290

45-microinch roughness begins at x = .3491

*> means $Re_{\theta,c}$ greater than 10^6 but not ∞

Table 5

CALCULATED VALUES OF $Re_{\theta,T}$, $Re_{k,M}$, AND $\left(\frac{\bar{t}w}{\bar{t}e}\right)_T$ FOR FIVE OF THE SEVEN BLUNT BODIES OF REVOLUTION

$Re_{\theta,T}$	$Re_{k,M}$	$\left(\frac{\bar{t}w}{\bar{t}e}\right)_T$	
1557	.008195	1.011	
1555	.009850	.9634	
888	.01115	.7802	29° Hemisphere-Cone
713	.01243	.6776	
632	.01426	.6282	
642	.01573	.5959	
251	4.270	.6934	
274	6.600	.6038	
293	9.060	.5472	50° Hemisphere-Cone
297	10.06	.5108	
303	11.02	.4838	
579	.9400	.8148	
449	.9840	.7143	
465	1.144	.6516	
519	2.100	.4988	"1/10-Power" Nose Shape
546	2.717	.4495	
278	1.898	.3542	
277	1.790	.3949	
304	1.055	.1675	
397	1.610	.1464	Flat-Face Cone-Cylinder
446	1.710	.1417	
1082	.01825	.2271	Elliptical-Nose Cylinder
177	30.80	.1866	

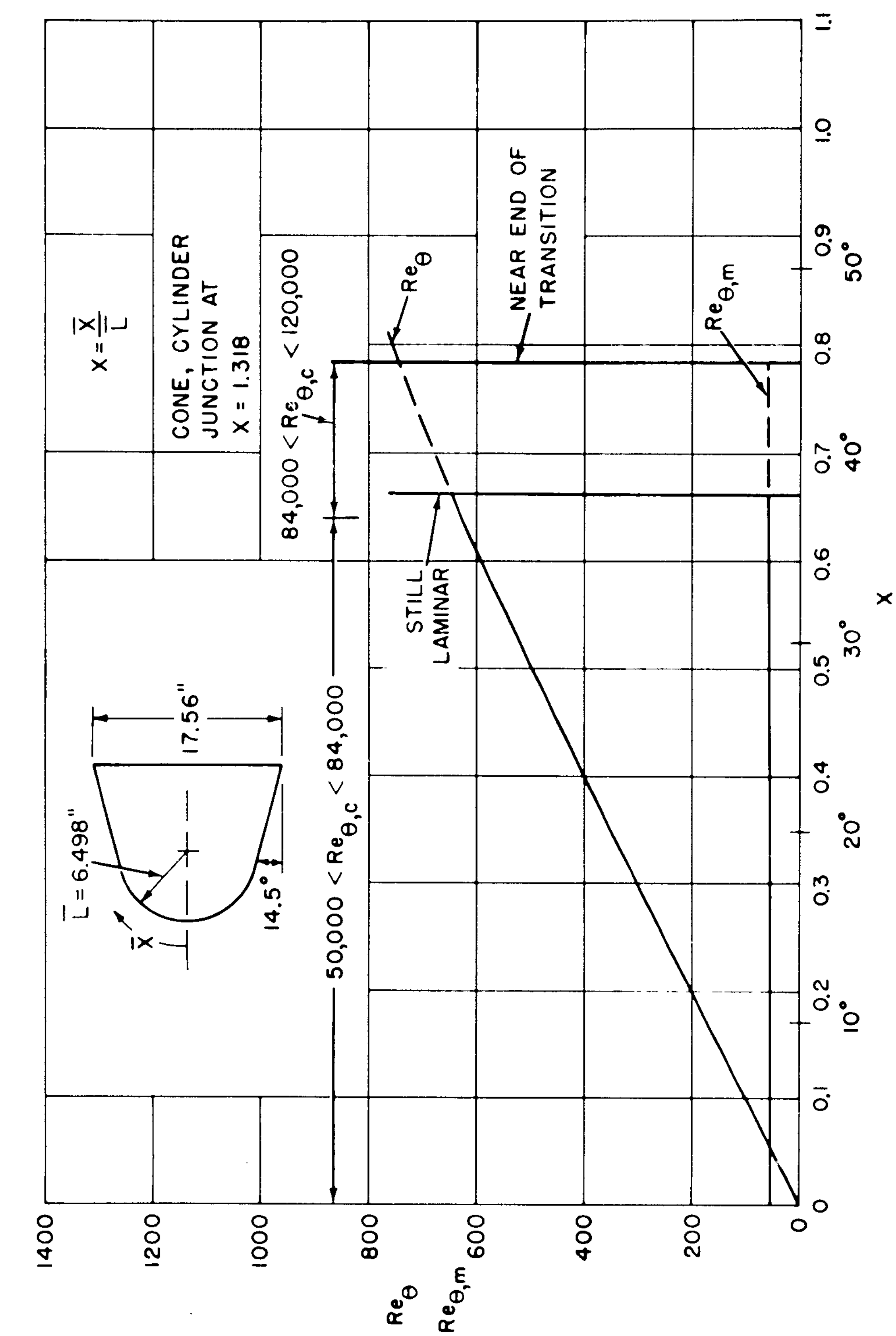

(a) BOUNDARY LAYER REYNOLDS NUMBERS

FIG. 1 29° HEMISPHERE - CONE IN FLIGHT AT A MACH NUMBER OF 3.14 AND A REYNOLDS NUMBER, Re_∞, OF 8.94×10^6

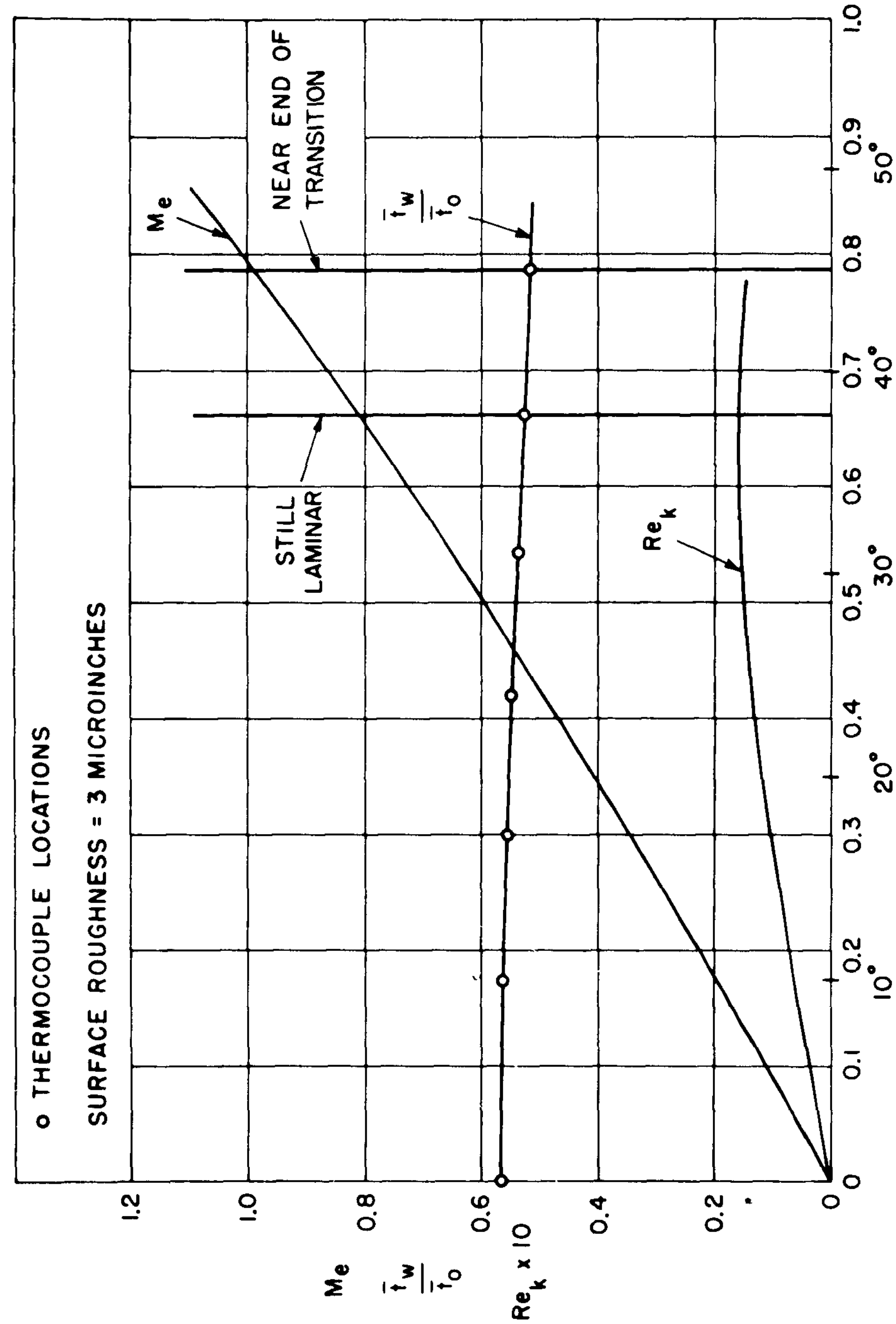

(b) LOCAL MACH NUMBER, LOCAL WALL TEMPERATURE RATIO, AND LOCAL ROUGHNESS REYNOLDS NUMBER

FIG. 1 CONCLUDED

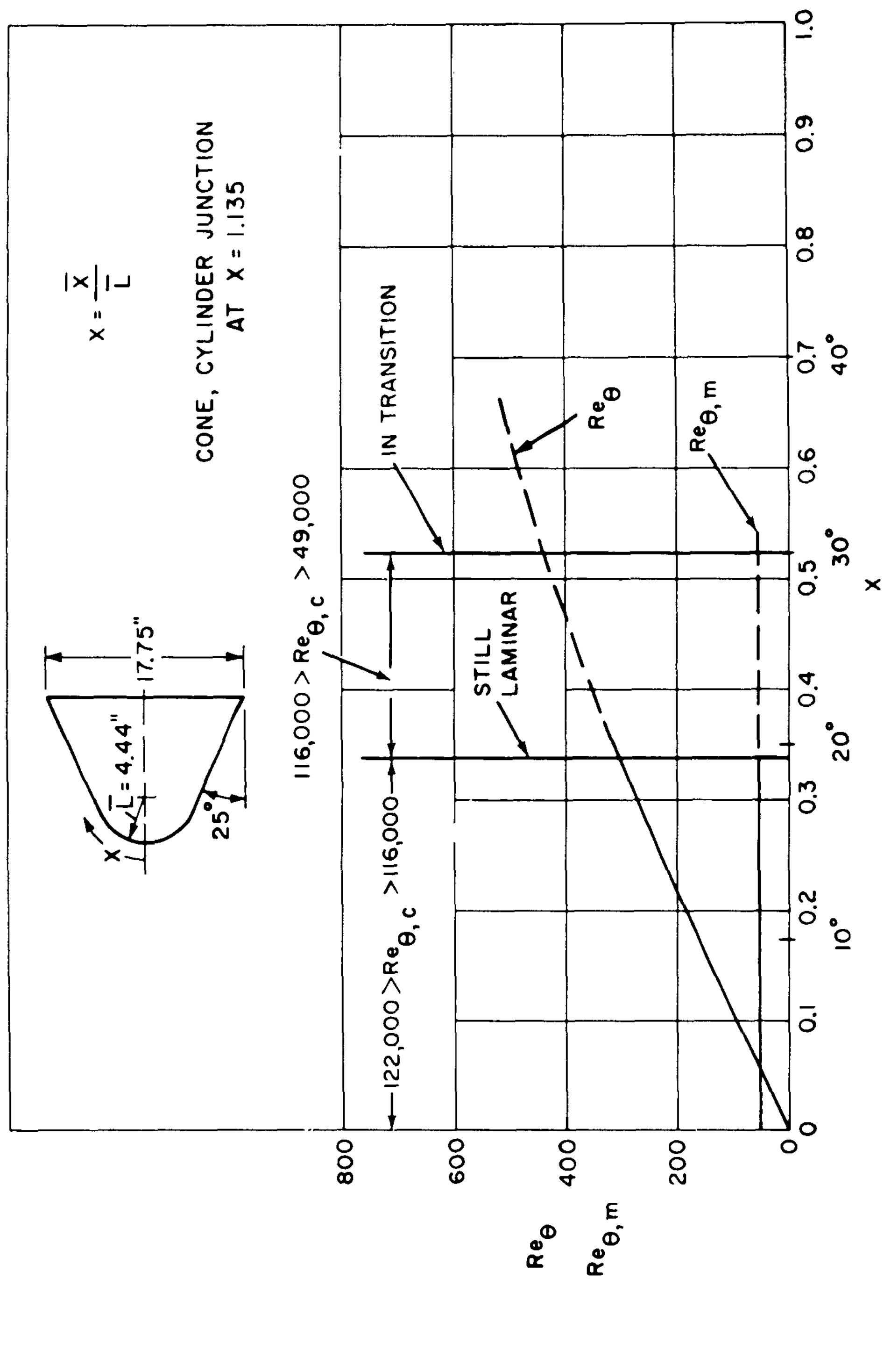

(a) BOUNDARY LAYER REYNOLDS NUMBERS

FIG. 2 50° HEMISPHERE-CONE IN FLIGHT AT A MACH NUMBER OF 4.7 AND A REYNOLDS NUMBER, Re_∞, OF 8.03×10^6

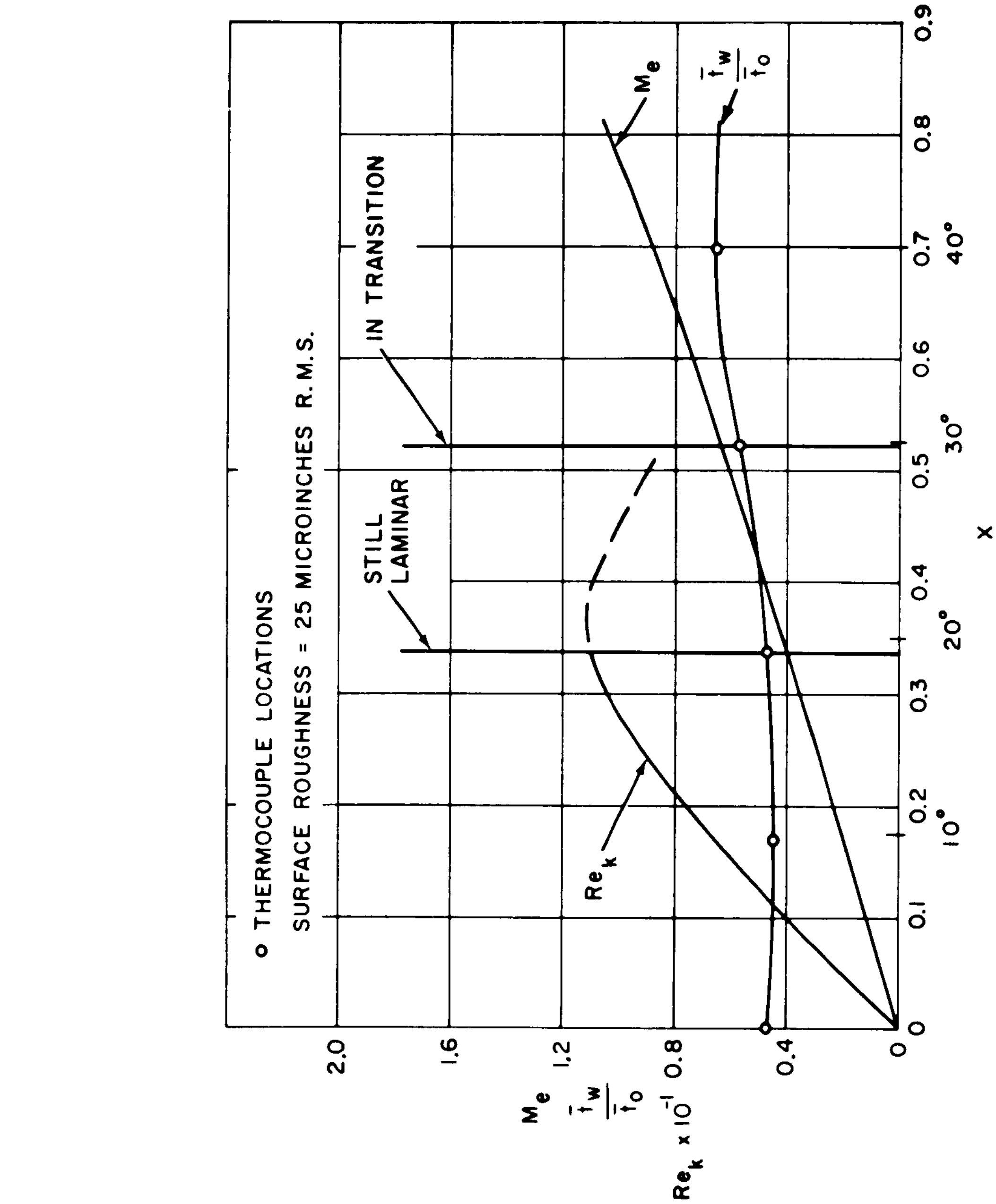

(b) LOCAL MACH NUMBER, LOCAL WALL TEMPERATURE RATIO, AND LOCAL ROUGHNESS REYNOLDS NUMBER

FIG. 2 CONCLUDED

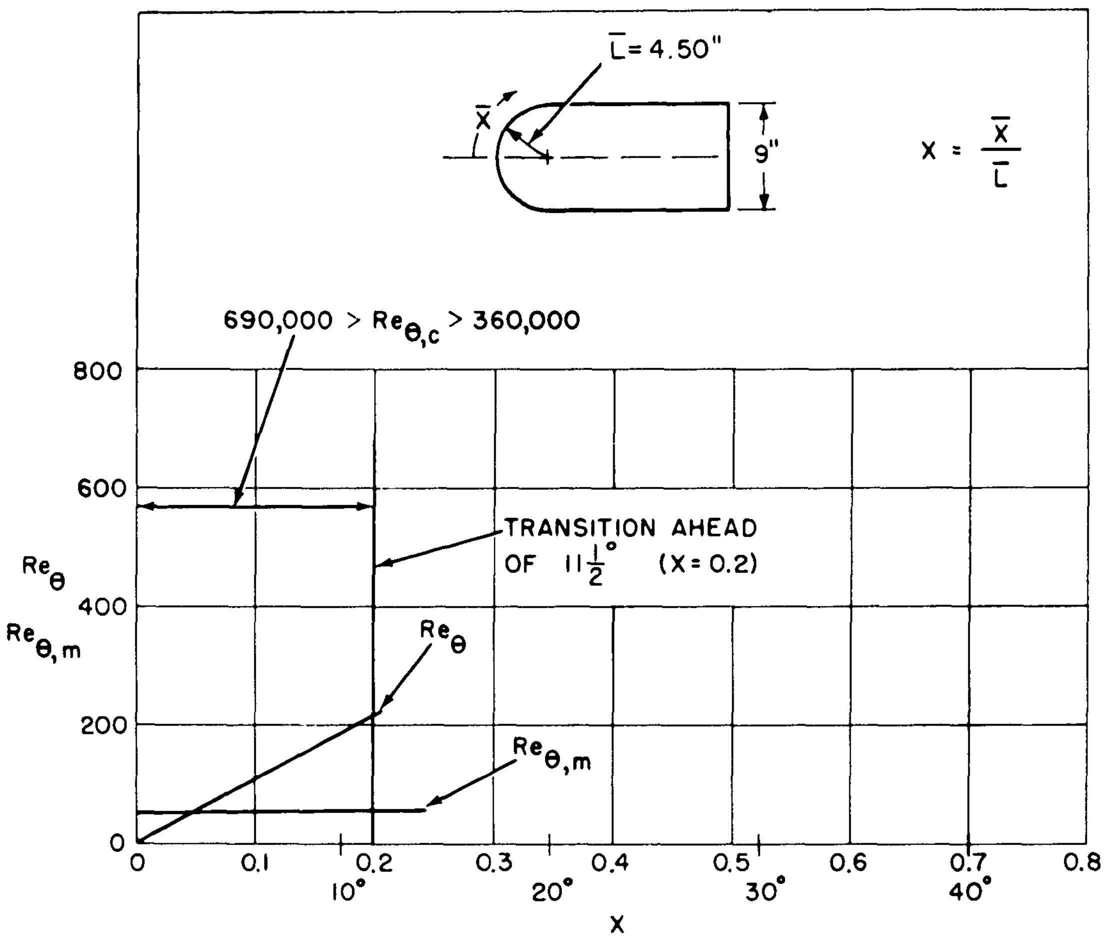

(a) BOUNDARY LAYER REYNOLDS NUMBERS

FIG. 3 HEMISPHERE-CYLINDER IN FLIGHT AT A MACH NUMBER OF 5.50 AND A REYNOLDS NUMBER, Re_∞, OF 9.75×10^6

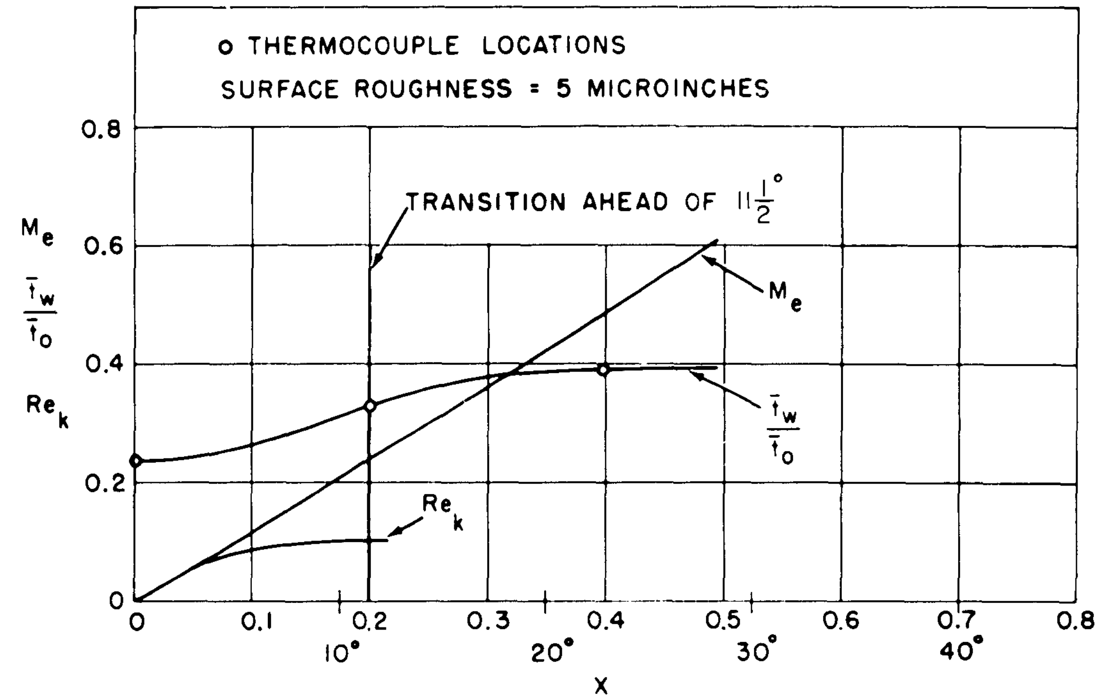

(b) LOCAL MACH NUMBER, LOCAL WALL TEMPERATURE RATIO, AND LOCAL ROUGHNESS REYNOLDS NUMBER

FIG. 3 CONCLUDED

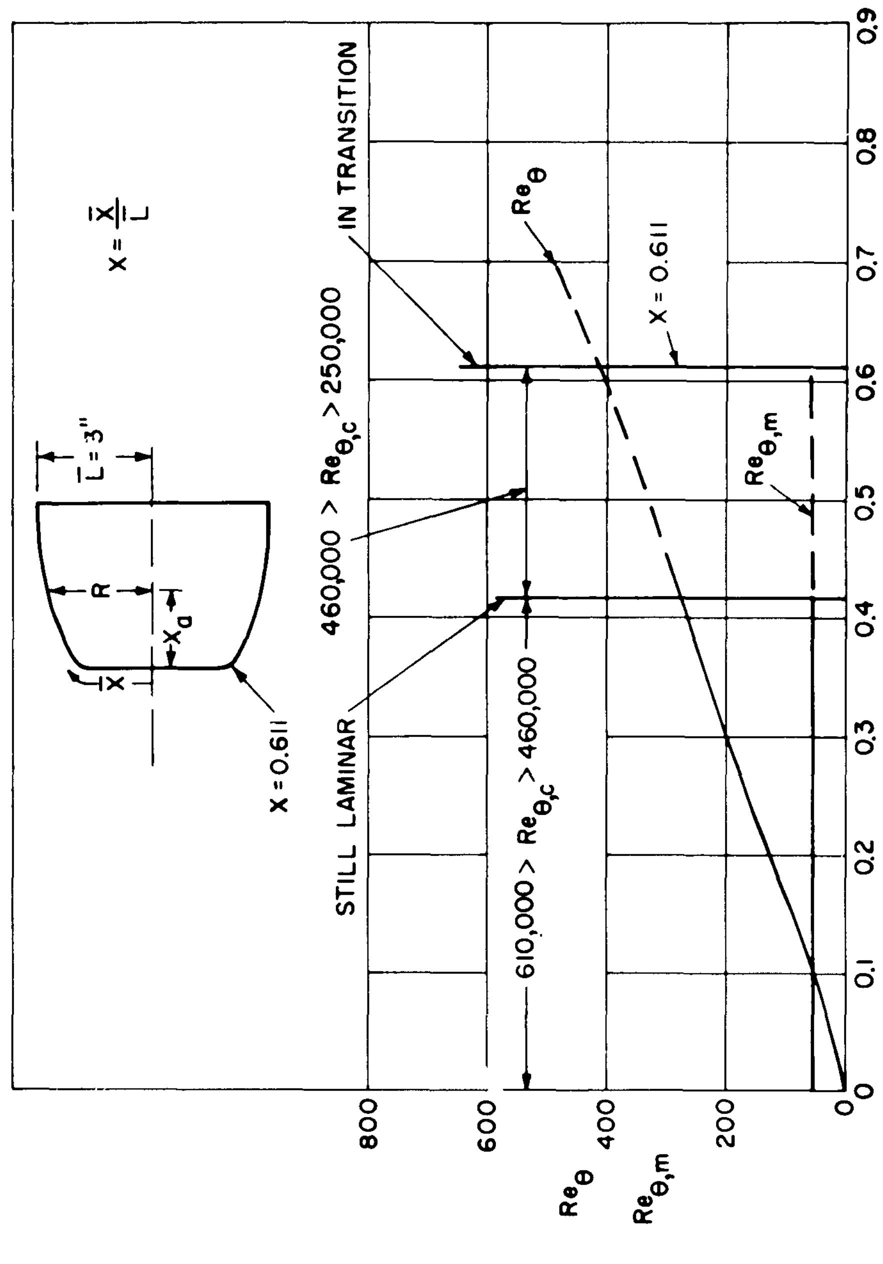

(a) BOUNDARY LAYER REYNOLDS NUMBERS

FIG. 4 "1/10 POWER" NOSE SHAPE IN FLIGHT AT A MACH NUMBER OF 6.68 AND A REYNOLDS NUMBER, Re_∞, OF 8.15×10^6

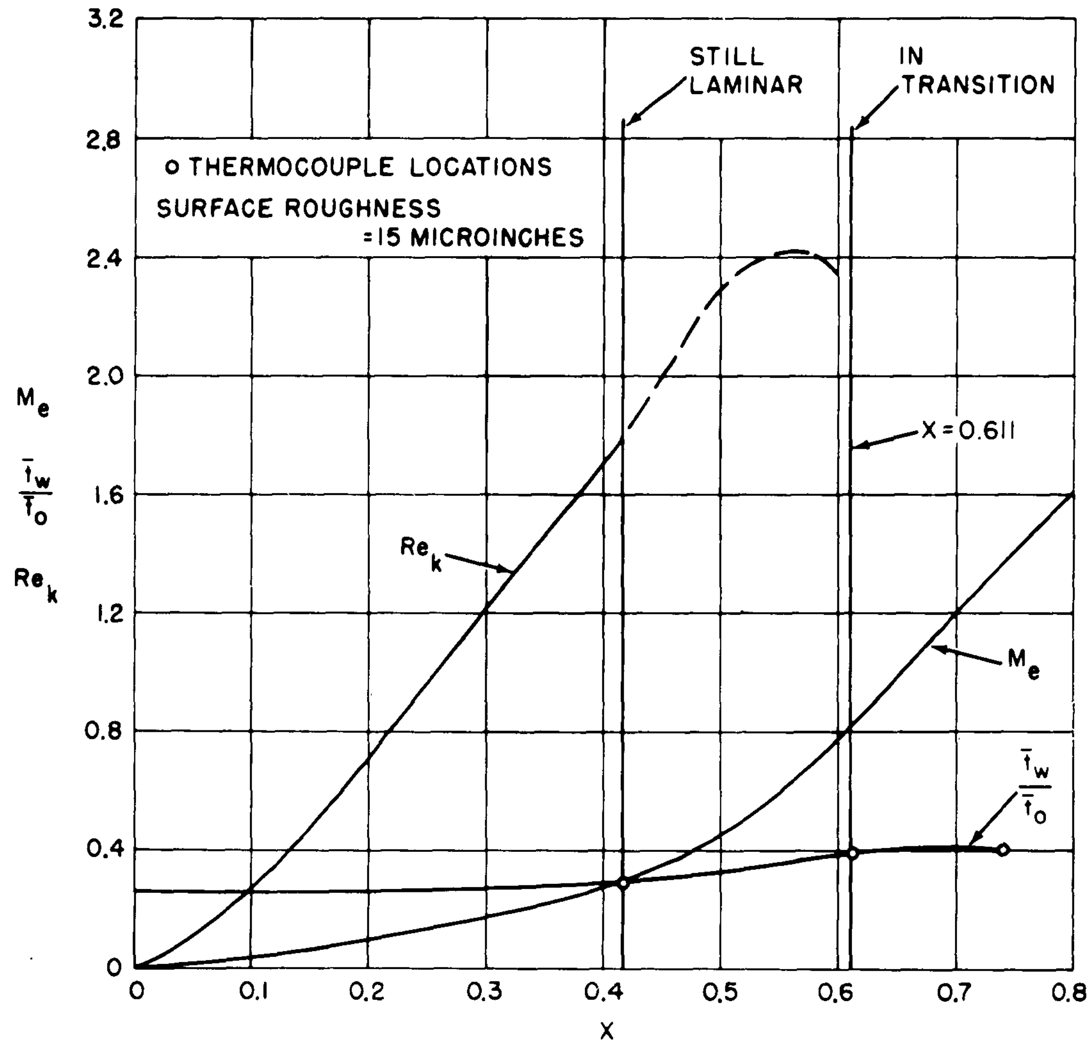

(b) LOCAL MACH NUMBER, LOCAL WALL TEMPERATURE RATIO, AND LOCAL REYNOLDS NUMBER

FIG. 4 CONCLUDED

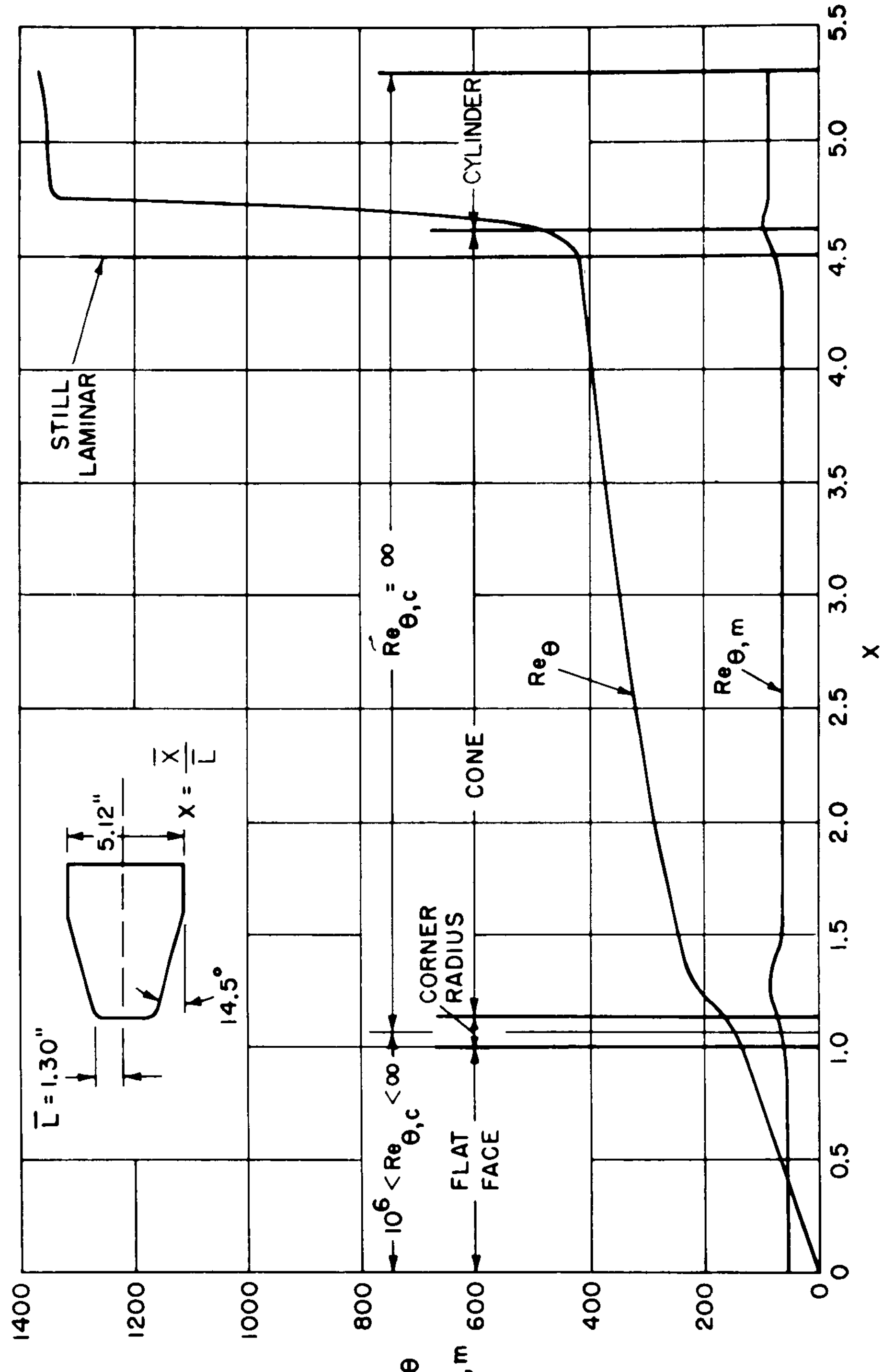

(a) BOUNDARY LAYER REYNOLDS NUMBER

FIG. 5 FLAT-FACE CONE-CYLINDER IN FLIGHT AT A MACH NUMBER OF 14.5 AND A REYNOLDS NUMBER, Re_∞, OF 0.821 x 10^6

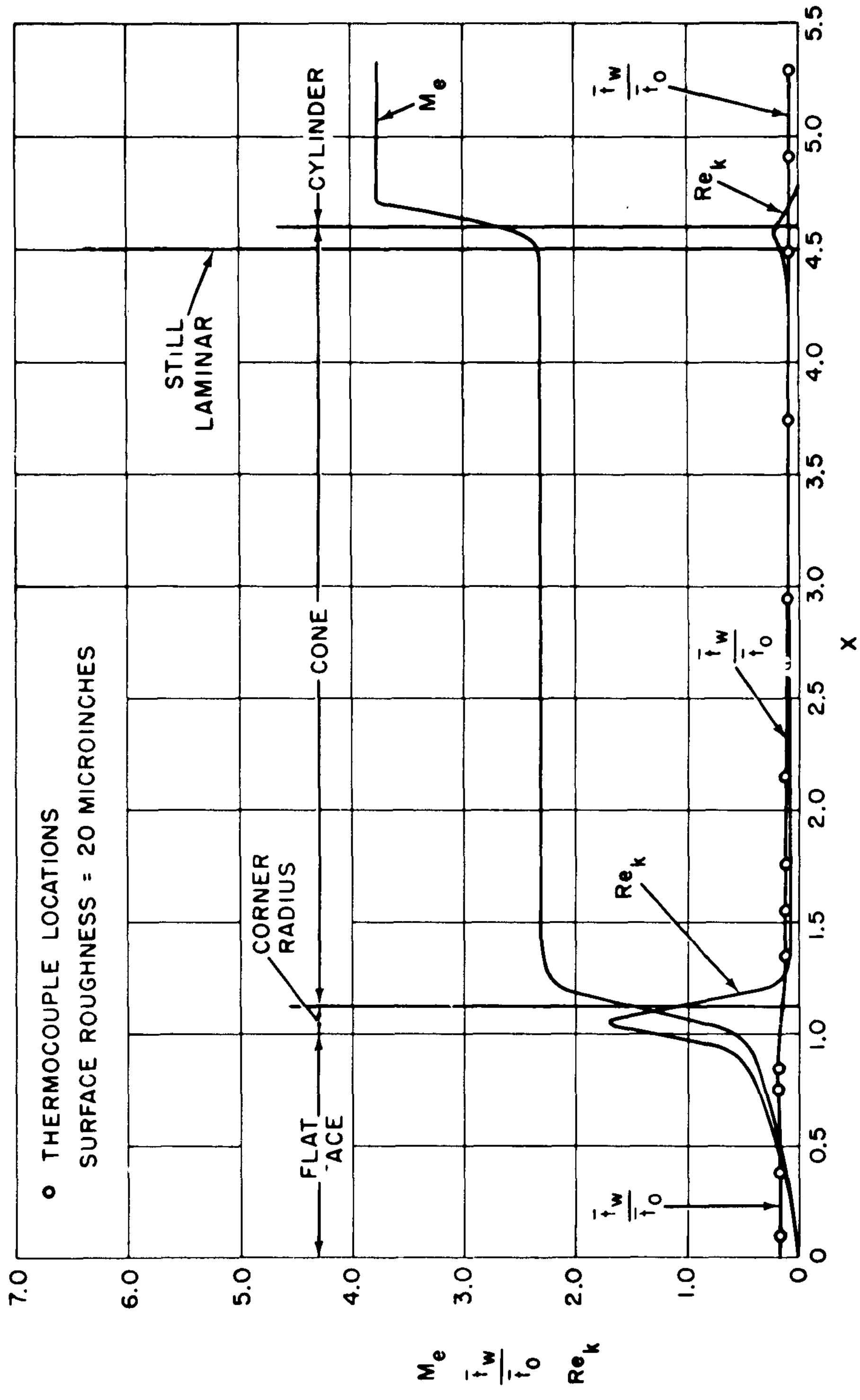

(b) LOCAL MACH NUMBER, LOCAL WALL TEMPERATURE RATIO AND LOCAL ROUGHNESS REYNOLDS NUMBER

FIG. 5 CONCLUDED

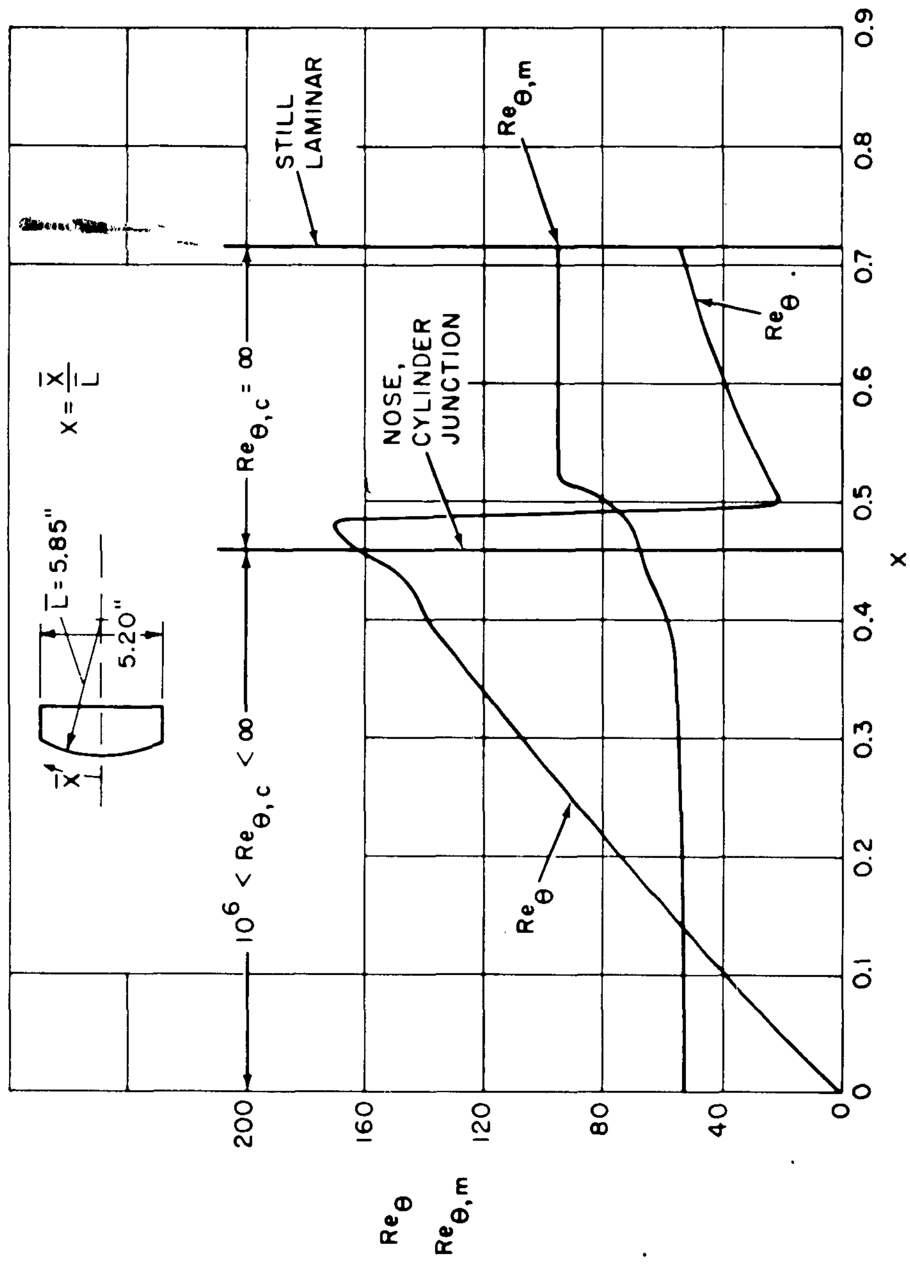

(a) BOUNDARY LAYER REYNOLDS NUMBERS

FIG. 6 SPHERICAL-SEGMENT-NOSE CYLINDER IN FLIGHT AT A MACH NUMBER OF 15.1 AND A REYNOLDS NUMBER, Re_∞, OF 0.855×10^6

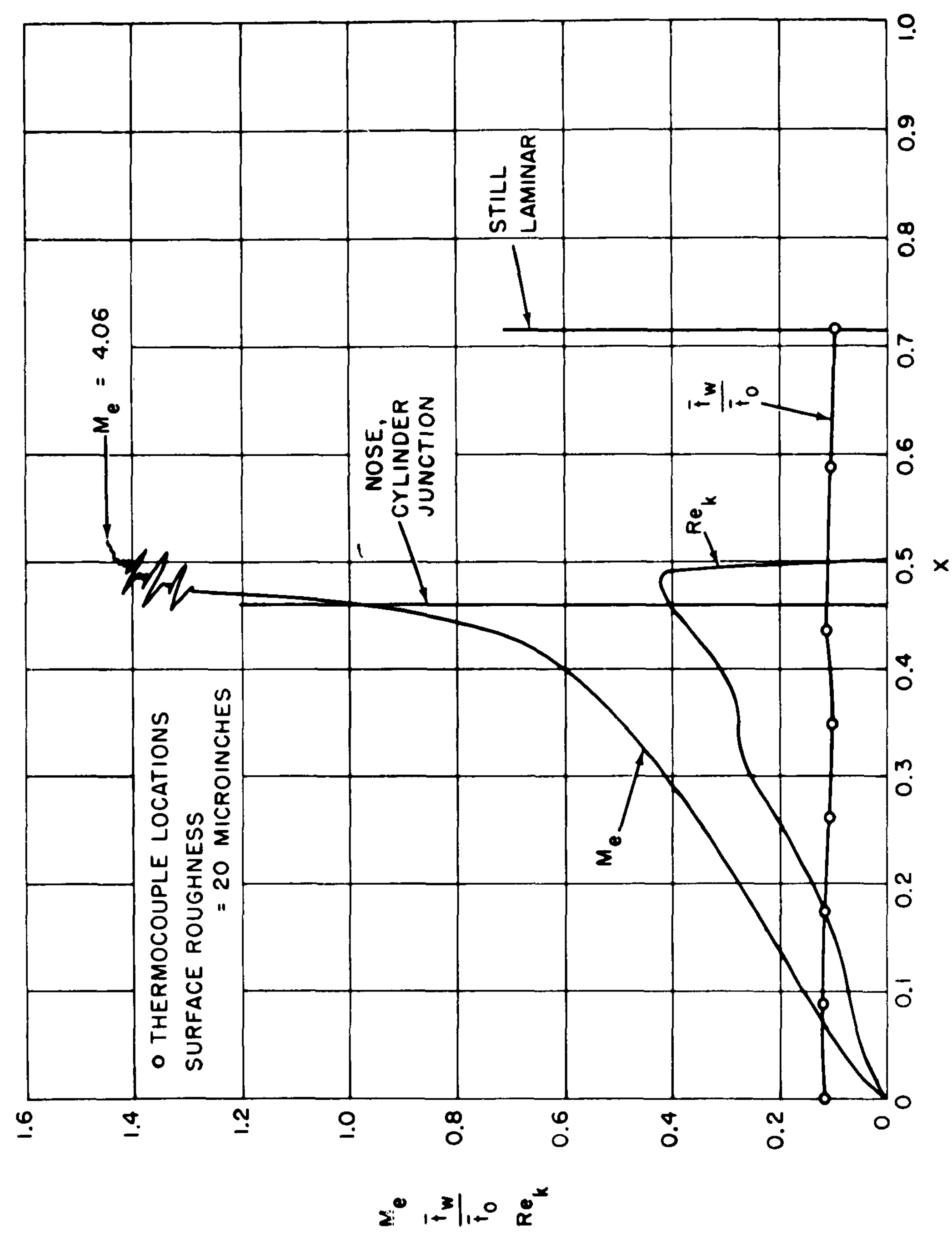

(b) LOCAL MACH NUMBER, LOCAL WALL TEMPERATURE RATIO, AND LOCAL ROUGHNESS REYNOLDS NUMBER

FIG. 6 CONCLUDED

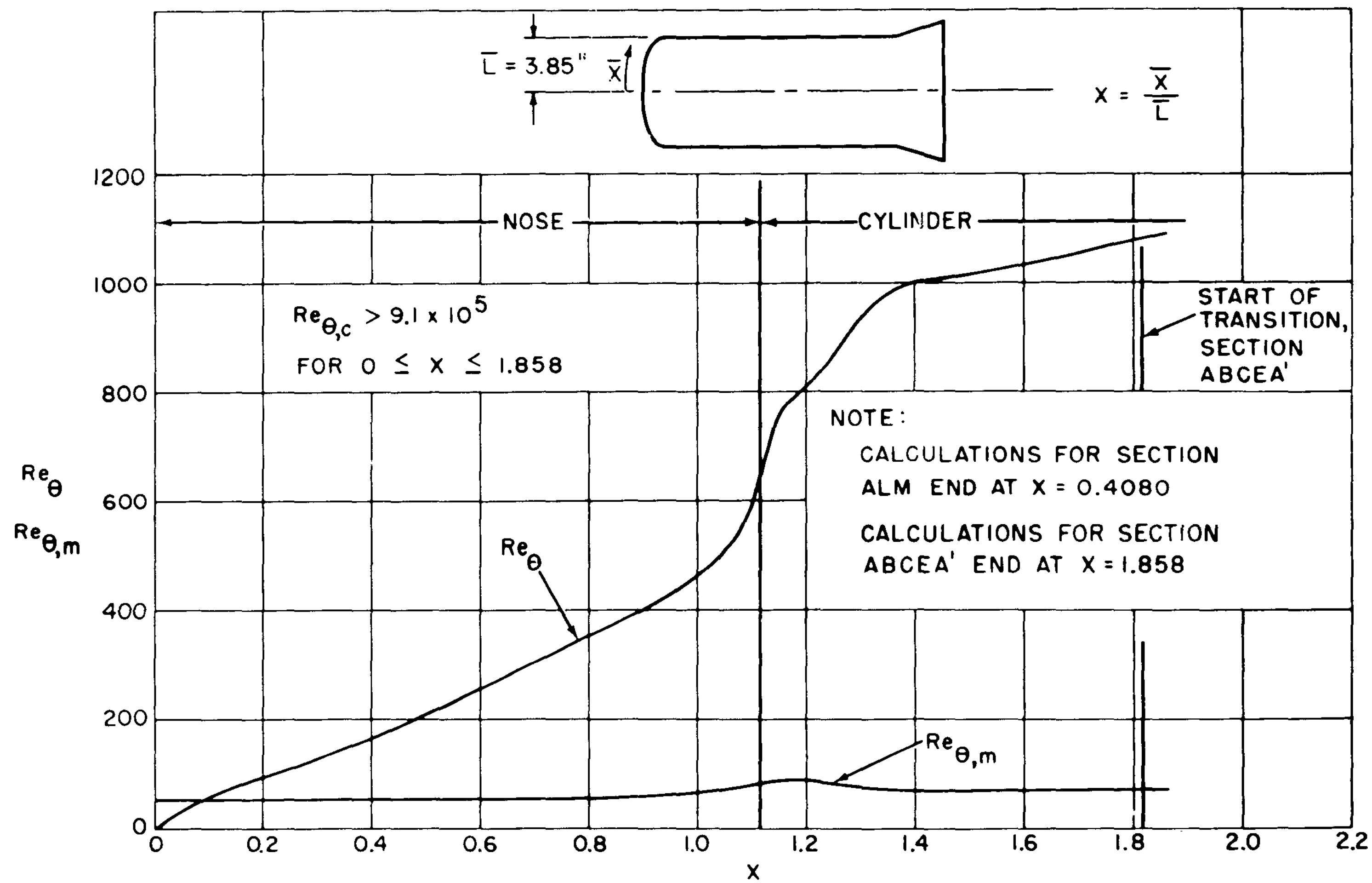

(a) BOUNDARY LAYER REYNOLDS NUMBERS, SECTIONS ABCEA' AND ALM

FIG. 7 ELLIPTICAL-NOSE CYLINDER IN FLIGHT AT A MACH NUMBER OF 13.29 AND A REYNOLDS NUMBER, Re_∞, OF 4.69×10^6

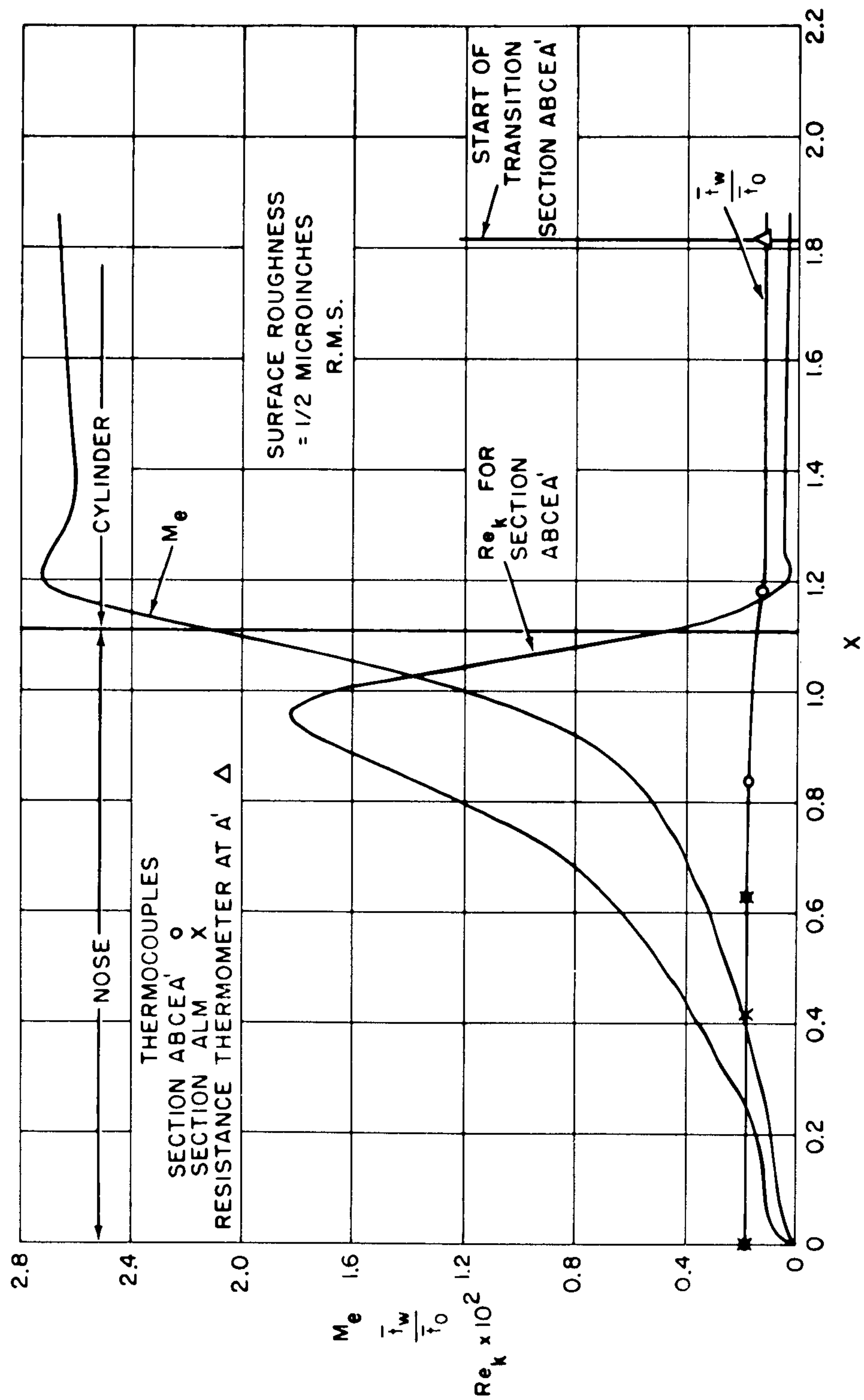

(b) LOCAL MACH NUMBER, LOCAL WALL TEMPERATURE RATIO, AND LOCAL ROUGHNESS REYNOLDS NUMBER

FIG. 7

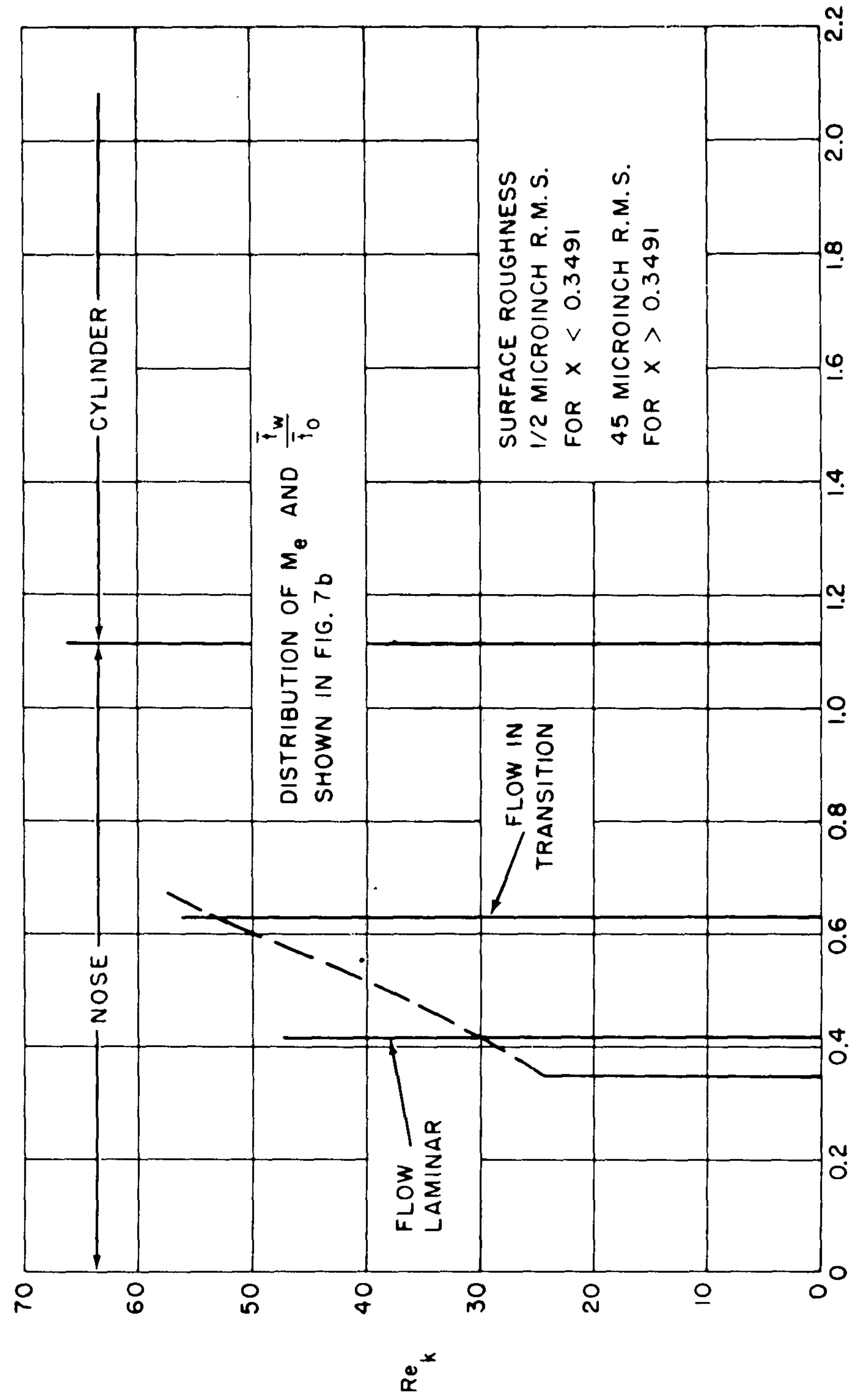

(c) LOCAL ROUGHNESS REYNOLDS NUMBER FOR SECTION ALM

FIG. 7 CONCLUDED

C

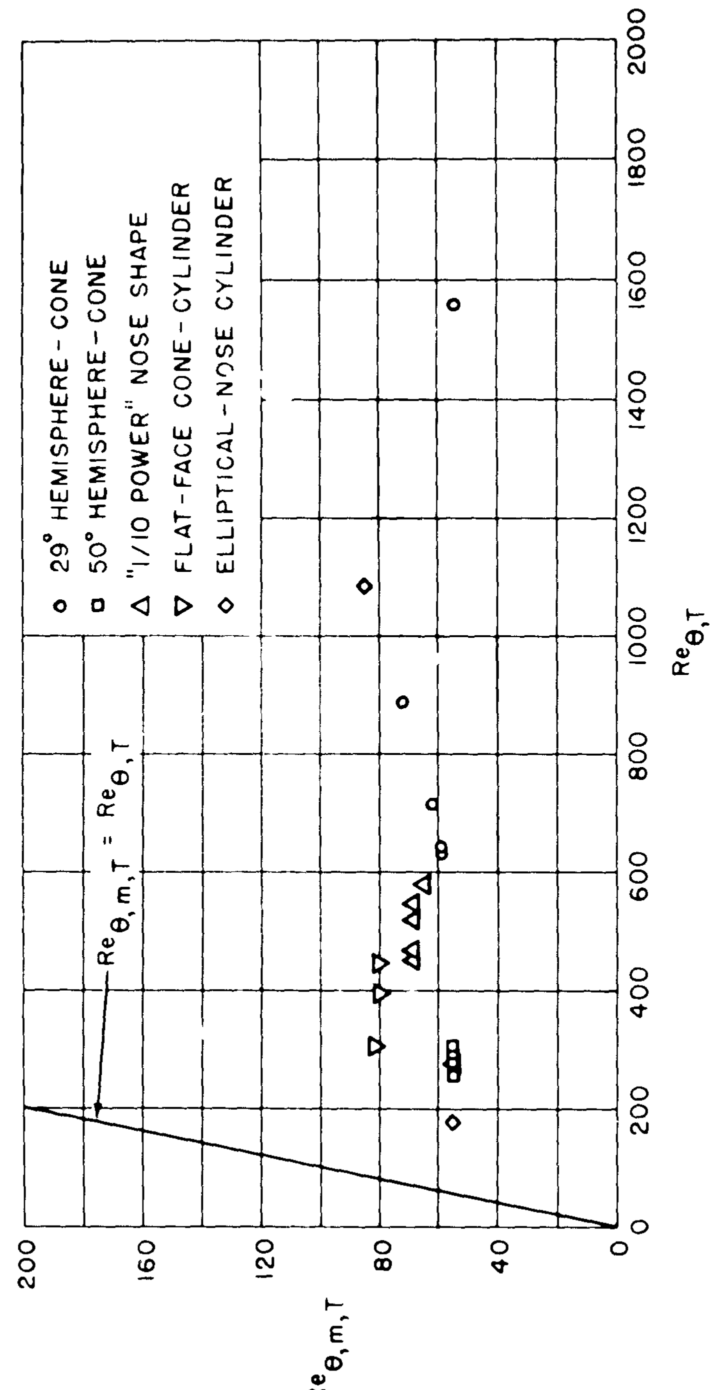

FIG. 8 COMPARISON BETWEEN TRANSITION REYNOLDS NUMBER, $Re_{\theta,T}$ AND VALUE OF MINIMUM TRANSITION REYNOLDS NUMBER AT TRANSITION, $Re_{\theta,m,T}$

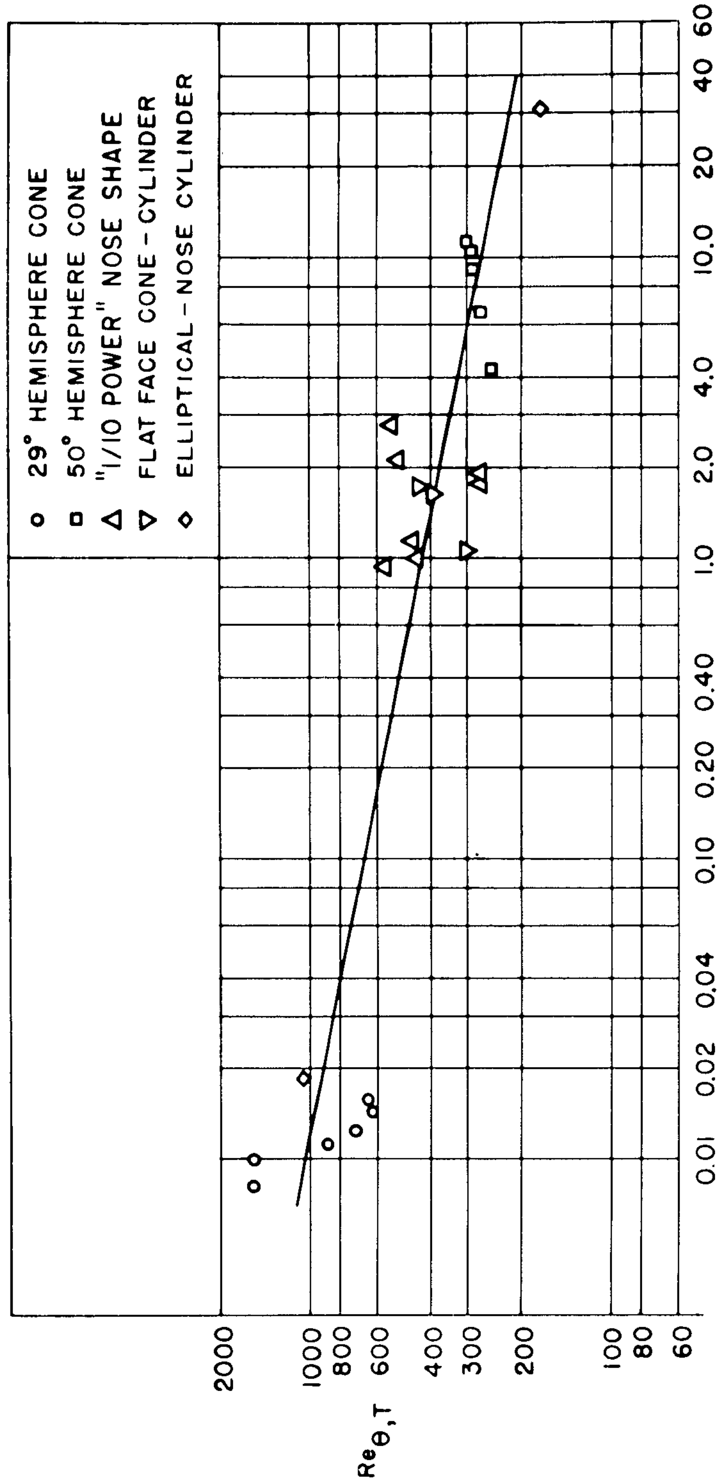

FIG. 9 TRANSITION REYNOLDS NUMBER $Re_{\theta,T}$ AND MAXIMUM ROUGHNESS REYNOLDS NUMBER AHEAD OF TRANSITION, $Re_{k,M}$

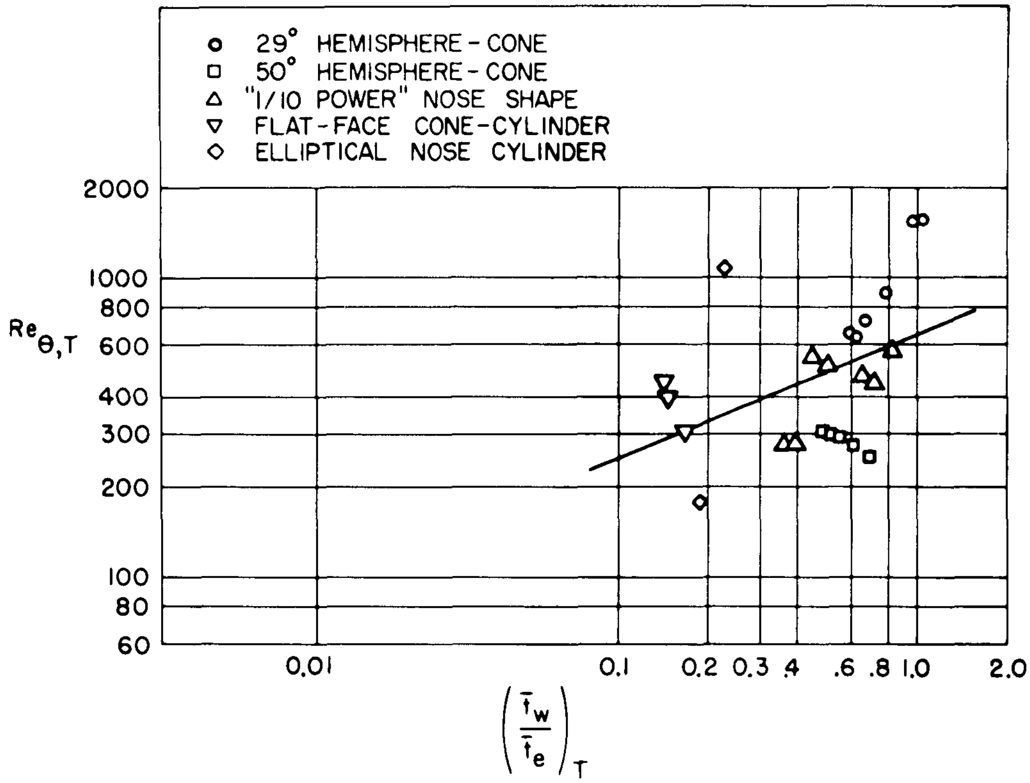

FIG. 10 TRANSITION REYNOLDS NUMBER $Re_{\theta,T}$ AND WALL TEMPERATURE RATIO AT TRANSITION $\left(\frac{\bar{t}_w}{\bar{t}_e}\right)_T$

AERODYNAMICS DEPARTMENT
EXTERNAL DISTRIBUTION LIST (SP1)

	No. of Copies
Director, Special Projects Department of the Navy Washington 25, D. C.	
Attn: SP-20	4
Attn: SP-27	2
Attn: SP-272	2
Chief, Bureau of Naval Weapons	
Attn: RRMA	1
Attn: RMGA	1
Bureau of Naval Weapons Representative (Special Projects Office) P. O. Box 504 Sunnyvale, California	
Attn: SpL-314	2
Office of Naval Research Washington 25, D. C.	1
Atomic Energy Commission Engineering Development Branch Division of Reactor Development Headquarters, US AEC Washington 25, D. C.	
Attn: Mr. J. M. Simmons	1
Attn: Mr. M. J. Whitman	1
Attn: Mr. J. Conners	1
U. S. Atomic Energy Commission P. O. Box 62 Oak Ridge, Tennessee	
Attn: TRI:NLP:ATL:10-7	1
Director Naval Research Laboratory Washington 25, D. C.	
Attn: Mr. Edward Chapin, Code 6310	1
Commander Wright Air Development Division Wright-Patterson Air Force Base, Ohio	1
National Aeronautics and Space Administration George C. Marshall Space Flight Center Huntsville, Alabama	
Attn: M-S&M-PT (Mr. H. A. Connell)	2
Attn: M-SFM-M (Dr. W. R. Lucas)	1

AERODYNAMICS DEPARTMENT
EXTERNAL DISTRIBUTION LIST (SP1)

	No. of Copies
National Aeronautics and Space Administration 1520 H Street, N. W. Washington, D. C.	5
NASA, Langley Research Center Langley Field Virginia Attn: Mr. Roger W. Peters (Structures Res. Division)	1
Attn: Mr. Russell Hopko, PARD	1
NASA, Lewis Research Center 21000 Brookpark Road Cleveland 35, Ohio Attn: Mr. George Mandel, Chief, Library	2
ASTIA Arlington Hall Station Arlington 12, Virginia Attn: TIPDR	10
Commander Air Force Ballistic Missile Division Air Research and Development Command P. O. Box 262 Inglewood, California Attn: WDTVR	2
Aerospace Corporation El Segundo, California Attn: Dr. Bitondo	1
Applied Physics Laboratory The Johns Hopkins University Silver Spring, Maryland Attn: Librarian	2
AVCO Manufacturing Corporation Research and Advanced Development Division 201 Lowell Street Wilmington, Massachusetts Attn: Dr. B. D. Henshall (Aerodynamics Section)	1
AVCO Manufacturing Corporation Everett, Massachusetts Attn: Dr. Kantrowitz	1

AERODYNAMICS DEPARTMENT
EXTERNAL DISTRIBUTION LIST (SP1)

	No. of Copies
Defense Metals Information Center Battelle Memorial Institute 505 King Avenue Columbus 1, Ohio	1
General Applied Science Laboratories, Inc. Merrick and Stewart Avenues East Meadow, New York	
Attn: Mr. Robert Byrne	1
General Electric Company Space Vehicle and Missiles Department 201 South 12th Street Philadelphia, Pennsylvania	
Attn: Dr. J. Stewart	1
Attn: Mr. Otto Klima	1
General Electric Research Laboratory 3198 Chestnut Street Philadelphia, Pennsylvania	
Attn: Dr. Leo Steg	1
Attn: Mr. E. J. Nolan	1
Attn: Mr. L. McCreight	1
Institute for Defense Analyses Advanced Research Projects Agency Washington 25, D. C.	
Attn: Mr. W. G. May, General Sciences Br.	1
Jet Propulsion Laboratory 4800 Oak Grove Drive Pasadena 3, California	
Attn: I. R. Kowlan, Chief, Reports Group	1
Attn: Dr. L. Jeffee	2
Kaman Aircraft Corporation Nuclear Division Colorado Springs, Colorado	
Attn: Dr. A. P. Bridges	1
Lawrence Radiation Laboratory P. O. Box 808 Livermore, California	
Attn: Mr. W. M. Wells, Propulsion Div.	1
Attn: Mr. Carl Kline	1
Lockheed Missiles and Space Company P. O. Box 504 Sunnyvale, California	
Attn: Dr. L. H. Wilson Via: BUWEPSREP, Sunnyvale	2

AERODYNAMICS DEPARTMENT
EXTERNAL DISTRIBUTION LIST (SP1)

	No. of Copies
Los Alamos Scientific Laboratory P. O. Box 1663 Los Alamos, New Mexico Attn: Dr. Donald F. MacMillan (N-L Group Leader)	1
Oak Ridge National Laboratory P. O. Box E Oak Ridge, Tennessee Attn: Mr. W. D. Manly	1
Polytechnic Institute of Brooklyn 527 Atlantic Avenue Freeport, New York Attn: Dr. Paul A. Libby Via: Commanding Officer Officer of Naval Research Branch Office 346 Broadway, New York 13, New York	1
Sandia Corporation Livermore Laboratory P. O. Box 969 Livermore, California	1
Sandia Corporation Sandia Base Albuquerque, New Mexico Attn: Mr. Alan Pope	1
United Aircraft Corporation Research Laboratories East Hartford 8, Connecticut Attn: Mr. H. J. Charette	1
NASA Ames Research Center Moffett Field, California Attn: Librarian	1

CATALOGING INFORMATION FOR LIBRARY USE

BIBLIOGRAPHIC INFORMATION

	DESCRIPTORS	CODES		DESCRIPTORS	CODES
SOURCE	NOL Technical report	NOLTR	SECURITY CLASSIFICATION AND CODE COUNT	Confidential	C025
REPORT NUMBER	62-25	620025	CIRCULATION LIMITATION		
REPORT DATE	16 August 1962	0862	CIRCULATION LIMITATION OR BIBLIOGRAPHIC		
			BIBLIOGRAPHIC (SUPPL., VOL., ETC.)		

SUBJECT ANALYSIS OF REPORT

DESCRIPTORS	CODES	DESCRIPTORS	CODES	DESCRIPTORS	CODES
Transition	TRNI	Theory	THEY	Ratio	RATI
Blunt	BLUN	Laminar	LAMI		
Bodies	BODY	Flow	FLOW		
Flight	FLIG	Comparison	CMRI		
Minimum	MINM	Locations	LOCT		
Critical	CRIT	Heat-transfer	HEAF		
Roughness	ROUG	Distributions	DISR		
Reynolds number	REYN	Maximum	MAXM		
Configuration	COFI	Point	POIN		
Supersonic	SUPR	Local	LOCA		
Boundary layer	BOUL	Wall	WALL		
Stability	STBI	Temperature	TEMP		

PRNC-NOL-5070/28 (5-62)

Naval Ordnance Laboratory, White Oak, Md.
(NOL technical report 62-25)
TRANSITION, MINIMUM CRITICAL, MINIMUM TRANSITION, AND ROUGHNESS REYNOLDS NUMBERS, FOR SEVEN BLUNT BODIES OF REVOLUTION IN FLIGHT BETWEEN MACH NUMBERS OF 1.72 and 15.1 (U), by Neal Tetervin. 16 August 1962. 36p. charts, tables. (Aerodynomics research report 173) Task NOL-363

CONFIDENTIAL

Transition occurred in boundary layers calculated to be very stable with respect to small disturbances in region between stagnation and transition point. Transition never occurred below estimated minimum boundary layer transition Reynolds number. Although data indicate relation between boundary layer transition Reynolds number and maximum roughness Reynolds number ahead of transition, too little data are considered to conclude a connection exists.
Abstract card is unclassified

1. Bodies - Oscillations
2. Bodies - Boundary layer
3. Bodies - Heat transfer
4. Bodies - Flow
5. Reynolds number

I. Title
II. Tetervin, Neal
III. Series
IV. Project

Naval Ordnance Laboratory, White Oak, Md.
(NOL technical report 62-25)
TRANSITION, MINIMUM CRITICAL, MINIMUM TRANSITION, AND ROUGHNESS REYNOLDS NUMBERS, FOR SEVEN BLUNT BODIES OF REVOLUTION IN FLIGHT BETWEEN MACH NUMBERS OF 1.72 and 15.1 (U), by Neal Tetervin. 16 August 1962. 36p. charts, tables. (Aerodynomics research report 173) Task NOL-363

CONFIDENTIAL

Transition occurred in boundary layers calculated to be very stable with respect to small disturbances in region between stagnation and transition point. Transition never occurred below estimated minimum boundary layer transition Reynolds number. Although data indicate relation between boundary layer transition Reynolds number and maximum roughness Reynolds number ahead of transition, too little data are considered to conclude a connection exists.
Abstract card is unclassified

1. Bodies - Oscillations
2. Bodies - Boundary layer
3. Bodies - Heat transfer
4. Bodies - Flow
5. Reynolds number

I. Title
II. Tetervin, Neal
III. Series
IV. Project

Naval Orinance Laboratory, White Oak, Md.
(NOL technical report 62-25)
TRANSITION, MINIMUM CRITICAL, MINIMUM TRANSITION, AND ROUGHNESS REYNOLDS NUMBERS, FOR SEVEN BLUNT BODIES OF REVOLUTION IN FLIGHT BETWEEN MACH NUMBERS OF 1.72 and 15.1 (U), by Neal Tetervin. 16 August 1962. 36p. charts, tables. (Aerodynomics research report 173) Task NOL-363

CONFIDENTIAL

Transition occurred in boundary layers calculated to be very stable with respect to small disturbances in region between stagnation and transition point. Transition never occurred below estimated minimum boundary layer transition Reynolds number. Although data indicate relation between boundary layer transition Reynolds number and maximum roughness Reynolds number ahead of transition, too little data are considered to conclude a connection exists.
Abstract card is unclassified

1. Bodies - Oscillations
2. Bodies - Boundary layer
3. Bodies - Heat transfer
4. Bodies - Flow
5. Reynolds number

I. Title
II. Tetervin, Neal
III. Series
IV. Project

Naval Ordnance Laboratory, White Oak, Md.
(NOL technical report 62-25)
TRANSITION, MINIMUM CRITICAL, MINIMUM TRANSITION, AND ROUGHNESS REYNOLDS NUMBERS, FOR SEVEN BLUNT BODIES OF REVOLUTION IN FLIGHT BETWEEN MACH NUMBERS OF 1.72 and 15.1 (U), by Neal Tetervin. 16 August 1962. 36p. charts, tables. (Aerodynomics research report 173) Task NOL-363

CONFIDENTIAL

Transition occurred in boundary layers calculated to be very stable with respect to small disturbances in region between stagnation and transition point. Transition never occurred below estimated minimum boundary layer transition Reynolds number. Although data indicate relation between boundary layer transition Reynolds number and maximum roughness Reynolds number ahead of transition, too little data are considered to conclude a connection exists.
Abstract card is unclassified

1. Bodies - Oscillations
2. Bodies - Boundary layer
3. Bodies - Heat transfer
4. Bodies - Flow
5. Reynolds number

I. Title
II. Tetervin, Neal
III. Series
IV. Project